THE REPUBLIC OF ARMENIA

MINISTRY OF EDUCATION AND SCIENCE

YEREVAN STATE UNIVERSITY

GRIGORYAN ARMINE PAPIN

THE STUDY OF THE PECULIARITIES OF SPECTRAL COMPRESSION AND SELF-COMPRESSION OF REGULAR AND RANDOMLY MODULATED PULSES

Dissertation on scientific degree of Doctor of Philosophy (Ph.D) in Physics and Mathematics in specialty 01.04.21 Laser Physics

Scientific supervisor:

Doctor of science,

Professor R. S. Hakobyan

YEREVAN– 2018

CONTENTS

INTRODUCTION

The progress in the technology of manufacturing of silica optical fibers leads to not only a revolution in the field of optical communications, but also to the formation of a new direction in science – nonlinear fiber optics.

Although silica glass is not a material with strong nonlinearity, the large length of the fiber with low optical losses and small dimensions of cross-section of the fibers significantly reduce the threshold of occurrence of various nonlinear phenomena. On the other hand, the study of the femtosecond range of durations of optical pulses [1-3] leads to the possibility of propagation of radiation with high intensity in optical fibers and observed nonlinear phenomena which are observed rare in the field of large pulse durations[4].

All this leads to a wide interest in nonlinear fiber optics and many interesting results have been obtained which are applied in optical communications, laser technology, technology of information processing, optical computing machines, optical sensors of various physical quantities, etc. The transition to the new femtosecond time scale brought new physical and technical challenges related to self-interaction and interaction of powerful impulses with extremely short duration in optical fibers [5], their synthesis, control, transmission, and registration. For the solution of these problems in femtosecond time scale, particularly it is used methods of nonlinear and adaptive optics, Fourier-optics and holography, spectral interferometry. The pulse compression based on the nonlinear process of self-phase modulation (SPM) of radiation in fiber and subsequent dispersive delay line (DDL) allows reach 10^3 times compression and the formation of extremely short pulses for optical range with the durations of units femtoseconds [6-8].

At the end of last century, the development of fiber optics and the creation of a new special fibers led to the creation of fiber lasers which have attracted attention as prospective, reliable and compact sources of ultrashort pulses. The well-known disadvantage of the fiber laser is a pulse with relatively low power, however it is worth to mention that recently the active research related to the generation of pulse with high powers by using multimode fibers, single-mode fibers with large core radius, and also photonic crystal single-mode fibers was implemented.

Along with the intensive research of the process of soliton-formation and soliton regime of pulse propagation in the fiber, by obtaining pulse with duration in the femtosecond range, creating

fiber laser and so on, a new field of research aimed on the solution of problems of parameter registration of ultrashort pulses and their control was created [4]. The processes of self-interaction and interaction of optical pulses in standard and amplified fiber with different dispersive characteristics serve as a foundation for a new and promising approach for analysis-synthesis problems in femtosecond time range. So, within the problems of soliton formation, the self similarity phenomenon has raised interest in optics, particularly, in similaritons which maintain only their functional form as oppose to the solitons which maintain all their characteristics [9,10]. The methods of similarity have wide range of applications in various fields of physics, particularly, in hydrodynamics, mechanics and plasma physics [11]. The interests in these methods in optics are mainly stimulated by the applications of similaritons in the analysis-synthesis problems in ultrafast optics. The important property of similaritons is the following: it is formed in the active fiber from arbitrary initial pulses, additionally the duration, spectral width, and the chirp of the formed similariton does not depend on the form, duration and phase of initial pulse but rather by its energy and the characteristics of the fiber. The parabolic similaritons have wide range practical interest for problems of ultrafast optics and photonics due to their temporal, spectral parabolic forms, and phase. It is worth to mention that at the current stage of investigation in this field, there are number of important unsolved problems[10]. Particularly, despite the large interest in the formation and propagation of optical similaritons, the complete analysis of opportunities of similariton formation in conventional silica fibers is missing. The impact of such nonlinear and dispersive phenomena, such as nonstationary wave, the inertia of nonlinear response, high-order dispersion (higher than second) has not been sufficiently studied. A special attention on the research of potential application of similaritons in problems of registration and the measurement of characteristics of ultrashort pulses, and also in problems of signal synthesis in the processes of temporal and spectral compression (SC) is required. Presently, the number of experimental realizations of similaritons and their research is relatively small, especially for the experiments in the femtosecond time scale and for similaritons with wide spectrum. However, such studies are very significant from the point of view of similariton application in femtosecond optics. One of the most significant and functional applications of similariton is the pulse compression (PC) conditioned by the parabolic phase of similariton [12,13].

Along with the important directions, the spectral compression has demonstrated the potential applications in the analysis-synthesis problems in ultrafast optics [14,15]. Generally, the spectral compressor has dispersive delay line and a nonlinear fiber as its members [16,17]. Lately, the spectral self-compression was numerically [18] and experimentally [19] implemented in a single-mode fiber (SMF) with anomalous dispersion.

Although there is a wide research in the directions mentioned above, numerous unsolved problems existed until now. The research of spectral self-compression was at a premature level, and in order to achieve a more holistic physical pattern of the process, a detailed study was necessary for all the values of system parameters. The peculiarities of spectral compression and self-compression were studied only for the initial regular pulses.

The aim of the dissertation is to fill in the gaps in the research introduced above. The study of the characteristics of spectral compression and self-compression is done not only for the regular pulses but also for the randomly modulated pulses by examining the impact of coherency on the process. In addition, via the method of the compensation of third-order dispersion by initial pulse asymmetry we increase the effectiveness of pulse compression. In order to obtain needed asymmetry and random pulses, the use of liquid crystal spatial light modulators (LC-SLMs) is offered.

Such LC-SLMs can independently control the amplitude and the phase of the transmitted light by electrical fields giving possibility to programmable generate pulses with practically arbitrary (within physical limits) shaping and are now commercially available. The commercial LC-SLMs most often have a twisted nematic structure, and the amplitude and the phase of the transmitted light are coupled in a specific manner. In this thesis we proposed new type of LC-SLMs that allows using very low electrical fields to control desired pulse shaping. These LC-SLMs are based on the cell of twist nematic with cholesteric mixture (TNCM) and with homeotropic boundaries. Near the critical cell thickness this system becomes sensitive to the external fields and at a very low electrical voltage a transition of the Fréedericksz type takes place from a stable twisted distribution to a stable homogeneous homeotropic distribution. We developed the relevant mode extraction method for the calculation of mask patterns which can generate multiple pulse sequences with arbitrary relative amplitudes and phases. By the choosing relevant distribution of the electric field voltages (lower than 1V) across the mask with TNCM SLM we get very different pulse shaping. This method could

allow us to generate much type of desired waveforms: square pulses, double pulses, triple pulses, multiple pulses, pulses train, symmetric and asymmetric pulses and random pulses.

The relevance and the pragmatic value of the research fields presented above and the further observation of unresolved problems determine the **aim** and scope of this dissertation. Particularly:

- The studies of pulse self-interaction in a fiber with anomalous dispersion in order to detect the opportunity to realize the soliton spectral self-compression in standard silica fiber.
- The studies of analogue between soliton spectral self-compression and soliton-effect self-compression.
- The studies of high-order effects preventing the effective regime pulse compression and possibilities to optimize the pulse compression process.
- To study the characterizations of spatial light modulators based on twist nematics with cholesteric mixtures and with homeotropic boundary conditions for ultrashort pulse shaping and to develop the relevant mode extraction method.

The contents of the work are listed below*:*

Introduction, four chapters, summary, and the list of the literature. The work consists of 107 pages, and contains 66 figures, the bibliography including 211 names.

In the introduction, the urgency and the objective of the thesis are presented. The content of dissertation, scientific novelty, the practical significance and defending statements.

In chapter 1, the review of the literature related to the dissertation is introduced.

Chapter 2 is dedicated to the research of soliton spectral self-compression process for ultrashort pulses in a single-mode fiber with anomalous dispersion, when the dispersive length is less than the nonlinearity length ($L_D < L_{NL}$ .i.e. R<1). The behavior of pulse and spectrum for different initial pulses, particularly, for Gaussian, secant-hyperbolic and super-Gaussian pulses in the case of different values of fiber length is investigated. The research shows that the soliton spectral self-compression has periodical character: in the first step of propagation, we have spectral compression which leads to the reduction of the impact of dispersion, resulting in the decline of the value of dispersive length L_D and consequently the nonlinearity parameter R. When the $R > 1$ ($L_D > L_{NL}$) condition is satisfied, the pulse is compressed. Afterwards, the spectrum is stretched within pulse compression. This leads to the gradually increase of dispersion role causing the

reduction of L_D and R. When $R<1$, the $L_D < L_{NL}$ condition is satisfied, and spectrum is again compressed.

The research is done for the different values of nonlinearity parameter. The dependence of the process periodicity on the nonlinearity parameter is studied: the approximations of the curve introducing nonlinearity parameter dependent frequency (the frequency of the spectral compression and stretching) are introduced.

In chapter 3, the possibility for improving pulse compression via third-order dispersion compensation by asymmetry of the initial pulse is demonstrated.

The spectral compression for randomly modulated pulses is studied. Our numerical investigations of the spectral compression process are carried out for the additive noise model for initial pulses with different coherence time. The impact of randomly modulated pulse coherency on the spectral compression process based on numerical solution of nonlinear Schrödinger equation is introduced.

Our numerical studies show the possibility of the spectral self-compression for randomly modulated pulses in a single-mode fiber with negative dispersion: the characteristics of the process are carried out in the case of different values of the fiber length and the nonlinearity parameter.

In chapter 4 the properties of a TNCM SLM with homeotropic boundary conditions are theoretically characterized. The relevant mode extraction method for the calculation of mask patterns is offered. By the choosing relevant distribution of the electric field voltages (lower than 1V) across the mask with TNCM SLM we get very different pulse shaping. The generation of different number of pulses and intensity ratio of them are introduced by altering the amplitude of the electric field voltages distribution. The possibility of the generation of numerous types of wanted waveforms (square pulses, double pulses, triple pulses, multiple pulses, pulses train, symmetric and asymmetric pulses and random pulses) is offered.

Summary states the main results of the thesis.

Scientific novelty:

Through detailed studies and innovative investigations the following unprecedented results have been obtained:

- We demonstrate the soliton spectral self-compression process, realized in the fiber "directly", without dispersive delay line, and reveal the characteristics and regularity on the basis of the physical pattern of the process.
- We show that there is an analogue between the processes of soliton-effect self-compression and soliton spectral self-compression which is implemented in a single - mode fiber with Kerr-nonlinearity and anomalous dispersion. The studies are done not only for the transform-limited pulses but also for pre-chirped pulses.
- Through detailed investigations, we study the evolution of the pulse and the spectrum of transform-limited pulses during the propagation in the fiber and it is shown that the soliton spectral self-compression is implemented for various initial pulses: the main difference is the periodicity of the process. The approximation curves which show the frequency of the soliton spectral self-compression and stretching dependence on nonlinearity parameter are studied.
- Through numerical study, we show that it is possible to compensate the third-order dispersion by initial pulse asymmetry manipulation. This opportunity is conditioned by the fact that the phase which is obtained during the propagation in the fiber depends on the initial pulse shape.
- Via the method of the compensation of third-order dispersion by initial pulse asymmetry we increase the effectiveness of pulse compression as compared to the compression of regular pulses. The pulse compression with a ratio corresponding to the pulse spectral broadening in the fiber is obtained.
- The spectral compression for randomly modulated pulses in view of the noise nonlinear suppression and filtering is studied. The impact of coherency on the process efficiency is demonstrated. The study shows that the spectral compression ratio decreases as coherence time of the initial randomly modulated optical signals increases.
- Our numerical studies show the possibility of the spectral self-compression for randomly modulated signals in a single - mode fiber with negative dispersion. The study is implemented for the additive noise model. The characteristic features of the spectral self-

compression for various values of the fiber length and the nonlinearity parameter are studied.

- We developed the relevant mode extraction method for the calculation of mask patterns which can generate multiple pulse sequences with arbitrary relative amplitudes and phases. As the mask we used liquid crystal spatial light modulator based on the cell with twist structure of nematic and cholesteric mixture and with homeotropic boundary conditions on the walls.
- By the choosing relevant distribution of the electric field voltages (≈ 0.1V) across the mask with SLM we get very different pulse shaping. This approach allows to control of the relative amplitudes of different pulse within pulse train. By varying the modulation depth (by altering the amplitude of the electric field voltages distribution), we generate different number of pulses and intensity ratio of them.

Practical significance

The results introduced in the thesis can be used as a base for the improvement of productive methods in ultrafast optics and laser physics. They have potential applications in analysis-synthesis problems in ultrafast optics, in problems of registration and the measurement of characteristics of ultrashort pulses, in nonlinear optical filtering of noise, etc.

Pulse shaping technique is a widely used for applications such as pulse compression and dispersion control, coherent control of quantum systems, laser control of matter, telecommunications, optical metrology, bio-imaging, microscopy and multidimensional spectroscopy.

Defending statements:

1. The soliton spectral self-compression implemented due to the self-interaction of pulse in the fiber with anomalous dispersion when the dispersive length in the fiber is shorter than the nonlinearity length is a spectral analogue of soliton-effect self-compression. In the range of values of nonlinearity parameter for 0.25 to 1 and fiber lengths of 1 to 20000, up to 30 times soliton spectral self-compression is possible to obtain.
2. In the pulse compression process, the third-order dispersion preventing the process efficiency can be compensated via shaping of asymmetric pulses at the system input. This approach improves the effectiveness of pulse compression as compared to the compression

of regular pulses: an effective pulse compression is achieved, with a ratio corresponding to the pulse spectral broadening in fiber.

3. The mask patterns with the structure based on twist nematic with cholesteric mixture with homeotropic boundary conditions can be used for the effective shaping of ultrashort pulses.
4. The ultrashort pulse shaping is possible to realize by very low fields (≈ 0.1V) in the cell of twist nematic with cholesteric mixture with the homeotropic boundary conditions due to the effect of Fréedericksz transition without an external field.

The main results of dissertation are published in [20-34] works.

The works presented in the dissertation are performed at Chair of Optics of Physics Department at Yerevan State University. The scientific supervisor of the thesis is Doctor of science, Professor R. S. Hakobyan.

CHAPTER 1. REVIEW OF THE LITERATURE

§1.1 Fiber - optics technology

At the end of seventies years of last century fiber-optics technologies lead to the wide integration of silica optical fiber in the current science and technology. The interest of researchers in fibers was related with problems of optical communications [35].

The fiber optic transfer of ultrashort pulses is interesting thanks to numerous reasons. Fiber delivery allows pulse to transmit such places, which is difficult to reach, applying lenses and conservative mirrors such as it is shown [35, 36] work for endoscopic multiphoton microscopy, which is a new medical diagnostic device [37]. The main challenge in the fiber optic delivery is the dispersion and nonlinearity (for Ti:Sapphire femtosecond lasers) which is characteristic to the fiber technology[35].

The normal group-velocity dispersion and nonlinear features of conventional fibers (at 800 nm wave length) limit fiber transfer, for pulses with 100fs duration to energies ~20 pJ. For the conventional Ti:sapphire laser, it is even less than 1% of the initial pulse energy because of that it is unusably for several applications[35]. A pulse with 1nJ energy is strongly deformed after passing through fiber with length of one meter. The dispersive length is $L_D = \tau_o^2 / |k_2|$ (where k_2 is the coefficient of second - order dispersion, and τ_0 is the initial pulse duration. As the pulse stretching is conditioned by the different spectral components which are moved with dissimilar phase speeds, so it is valuable to mention that $L_D \sim 1/\Delta\omega^2$ where $\Delta\omega$ is the width of pulse. The dispersive effects have greater impact for greater pulse width [35].

For pulses with 100fs duration, which are propagated in conventional fiber single mode fiber (SMF), at 800 nm wave length), the dispersive length is approximately nine cm [35]. $L_{NL} = (k_0 n_2 I_0)^{-1}$ is the nonlinearity length, where n_2 and I_0 are the Kerr index of silica and the peak intensity of pulse, respectively. The nonlinearity length is the $L_{NL} \sim 1.3cm$ in the case of pulses with

100fs duration and 1nJ energy (at 800 nm wave length). As we see, $L_D / L_{NL} \sim 7$, therefore it can be said that firstly the nonlinear effect predominates[35].

The spectrum substantially stretches during initial propagation trough fiber (almost few cm), furtherly group-velocity dispersion dominates the nonlinearity. The pulse stretches, and the peak power decreases correspondingly. As a result, the pulse is stretched spectrally and temporally after fiber (with a meter length) and has parabolic phase[35].

Until now, it has created the best product for fiber transmission mostly circumventing the nonlinear effect (for radiation with 100fs duration, Ti:sapphire lasers) [35]. Via DDL, the pulse obtains a negative linear chirp, due to that the width of pulse becomes larger. The pulse returns to approximately the initial duration after fiber with normal group-velocity dispersion; it is not needed for the compensation of nonlinearity. The pre-chirping method is practically good in the case of small energy, yet in the case of 20pJ energy the significant deformation takes place because of inevitable nonlinearity, and finally we again have pulse compression at some amount. After the propagation of pulse with negative chirp in the environment with positive refraction index of nonlinearity, the spectrum is compressed due to SPM, therefore pulse becomes larger [35,2].

There are numerous methods of fiber transmission which have been introduced in previously. The first method reference to the fiber with normal dispersion for example traditional large mode area fibers (Fig. 1.1.1), [38], microstructured unending single mode large mode area fibers, and high-order-mode fibers [35, 39].

Air-guiding fibers possessing a low n_2 aimed to decrease the nonlinearity effects and to allow work with great powers, are the next class of fiber transmission. They are named as hollow core PBG fiber, which has the negative dispersion [40] and CPBG fiber [41]. In addition to the advantages both fibers have there are also disadvantages: a large positive dispersion slope and high transmission loss are instances of such weaknesses.

It was effectively shown, the application of single-mode fiber and single-mode PCF in the imaging system (Fig. 1.1.2, [42]). In the single-mode fibers, the fs pulses, which are near-infrared, are stretched many times due to the chromatic dispersion and, in mainly, nonlinear effects having power dependence: they become substantial when energy get close to 0.1nJ [43]. However, for the effective multiphoton excitation, it is needed that the pulses have tiny duration and great peak-

power. Besides, for the saving of spatial beam form corresponding for the diffraction-limited focusing, the single mode propagation is required. Nevertheless, the restriction of step index single-mode fiber core width is almost five micrometer for the performing the single-mode state[35].

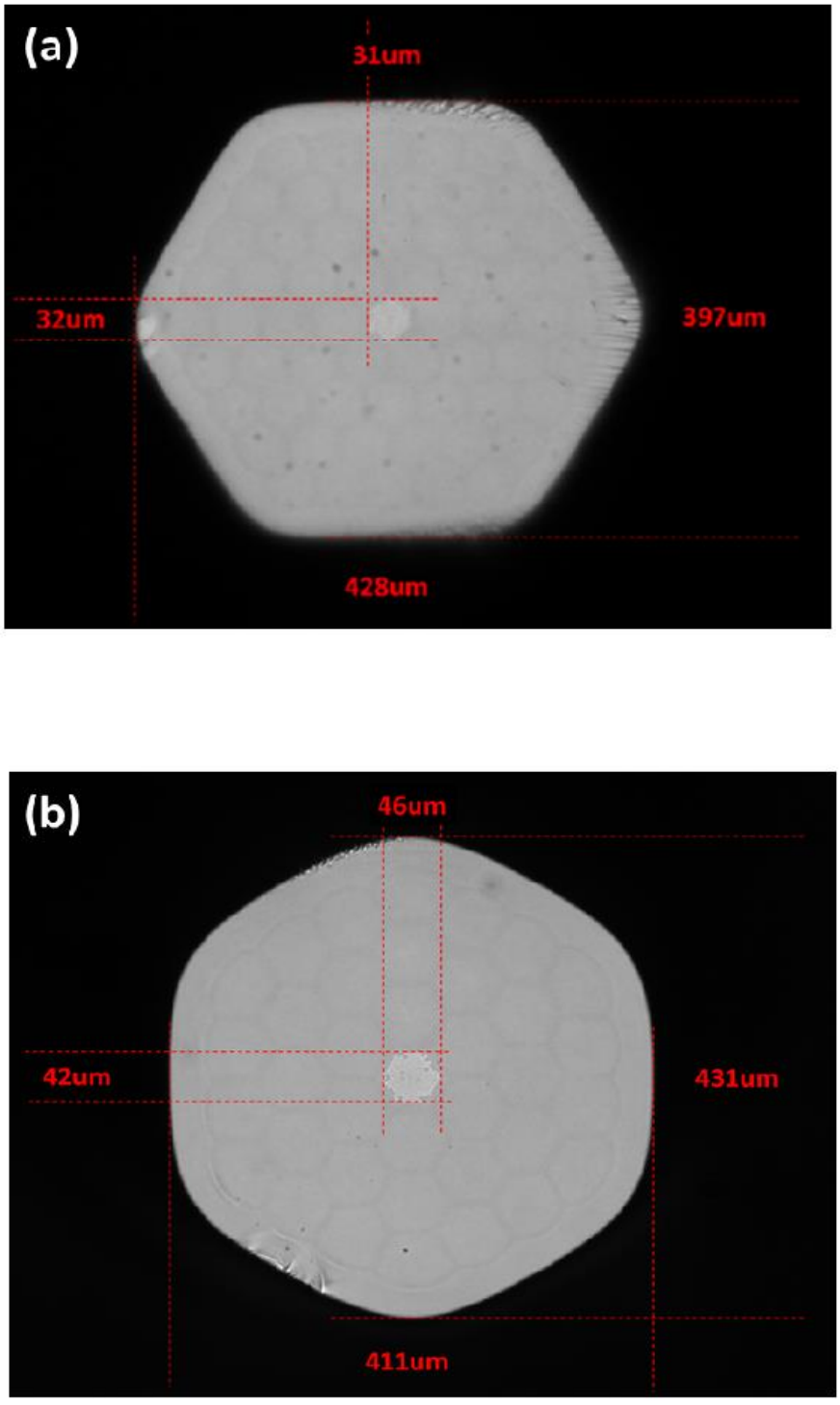

Fig. 1.1.1. *The cross section photos of the large mode area fibers [39].*

Due to the core with tiny diameter of single-mode fiber, it becomes receptive for providing nonlinearity, such as self-phase modulation, which can reform the initial pulse spectrum.

Initially, the single-mode fibers were used in 2-photon endoscopy, however, it was shown that the signal is weak in the case of such scheme which is conditioned by several effects [44]. Because of the high peak power, such pulses hard to transmit in the standard single-mode fiber, preventing the stretching of pulse conditioned by self-phase modulation and group-velocity dispersion [2]. Investigators applied hollow-core fiber [45] and large mode area fiber [46] for the solution of the issue. However, these fibers are not fit for conventional optical components and the standard single-mode fiber are more cost effective. In order to reduce the deformation caused by nonlinearity in conventional single-mode fiber, it was offered the pre-chirping and post chirping of pulse [47]. Yet, this system increases the difficulty and it is good to use the system in the case of short fiber length. In addition, the pulses with small energy is even difficult to deliver some meters of conventional single-mode fiber, the reason of that is the strong chromatic dispersion of silica for lengths of wave less than one micrometer[35].

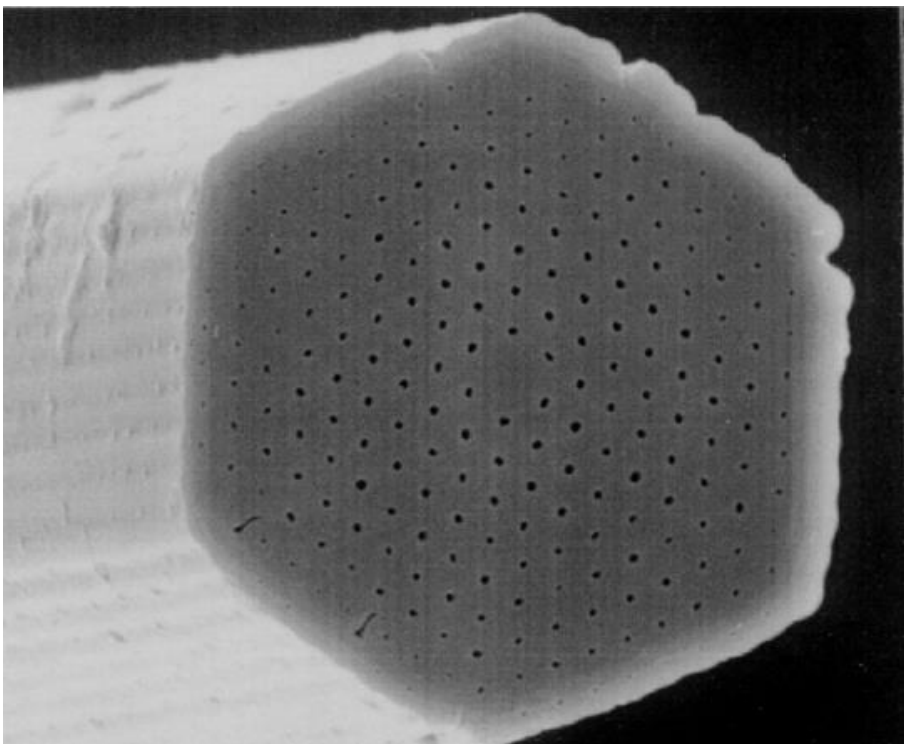

Fig. 1.1.2. *Scanning electron microscope image of the end of a photonic crystal fiber, showing the central core where a hole has been omitted.*

Since two decades ago, photonic crystal fiber has overturned basic investigation on and improvement of optical fibers [48]. The photonic crystal fiber considered adaptable and convenient for the transmission of pulses with high energies, are very dissimilar from conventional step-index fibers are now available for consumption [35]. There are several advantages of photonic crystal fibers, some of them are continues single mode operation, high nonlinear effects and etc. [49]. Due to advantages of the photonic crystal fibers is used in various fields [49]. The single- mode dual function through the central core and multimode transmit via inner cladding area with the high numerical aperture of photonic crystal fibers, which are from pure silica, cause the interest of investigators in bioimaging and biosensing to develop the effectiveness of system [35,50]. Though the photonic crystal fibers core size is greater than single-mode fiber, the photonic crystal fibers numerical aperture isn't generally large, because of that the laser coupling is not stable, and also the effectiveness of coupling is not high [35,51]. For the solving these problems, the multimode fibers can be alternative way for pulse transmission in imaging. The multimode fiber has greater numerical aperture, size of core, numerical aperture, the effectiveness of coupling than single-mode fiber and photonic crystal fiber.

It was shown that solid core fiber is able to implement the transmission only in the case of pulse with nanojoule energies. The notable characteristic is the small size of the restricted mode within the glass of fibre core. The radiation with high pea-k produces unfixable deformation caused by self-phase modulation or injures by dielectric-breakdown. The effort to increase the mode size has lead heavy multiple modes cross-coupling [35]. Therefore, it is seemed the optional fiber, like hollow core waveguide (HCW), is the most effective choice for transmission.

The HCW were applied for infrared laser transmission. In this case the size of mode is basically great, for example in the case of CO_2 laser with the ten micrometer length of wave, and multimode interference isn't destructive for the usage [35]. These circumstances aren't accurate in the case of infrared laser. It could be needed the scaling of the core low to a size that involve metal sediment on the internal side in order to propagate in a single-mode way. It is not easy to produce single mode metallic HCW via present approach in close to infrared. It is shown the capacity of the plastic 1D Bragg HCW in application of delivery of pulses with high power without deformation [35].

§1.2 Spectral compression

Thanks to fibers wide range features, they are used in many fields (in laser technology, in technology of handling of information and so on). One of the most remarkable and significant usages of nonlinearity of optical fiber is the spectrum compression.

In [52], it is investigated the process of SPM in SMF for pulses with initial chirp, and it was shown the possibility of the process of spectral compression based on the reversibility of fiber optic compression, spectral-temporal analogue and numerical investigations [52,53]. It was demonstrated spectrum compression up to 2.7nm spectrum for initial 10.6nm spectrum in the process of SPM for femtosecond pulses of Ti:sapphire laser, the pulses were previously chirped in the DDL [54].

The spectral compression of picosecond and femtosecond pulses were experimentally investigated in [55-60]. Recent times, in experimental and theoretical works it is shown the practical applications of spectral compression in ultrafast optics, mainly in the field of control and registration of laser radiation [55-63]. Particularly, it is shown that spectral compression can operate as effective nonlinear filter of radiation noise [62], optical processor time-spectrum Fourier conversion [63], the generator of temporal dark soliton [64] and etc. In [55,60] works, it is offered and tested modification of spectral compression based on cross-phase modulation and sum frequency generation. The scheme for classic spectrum compression is illustrated on Fig. 1.2.1 [65].

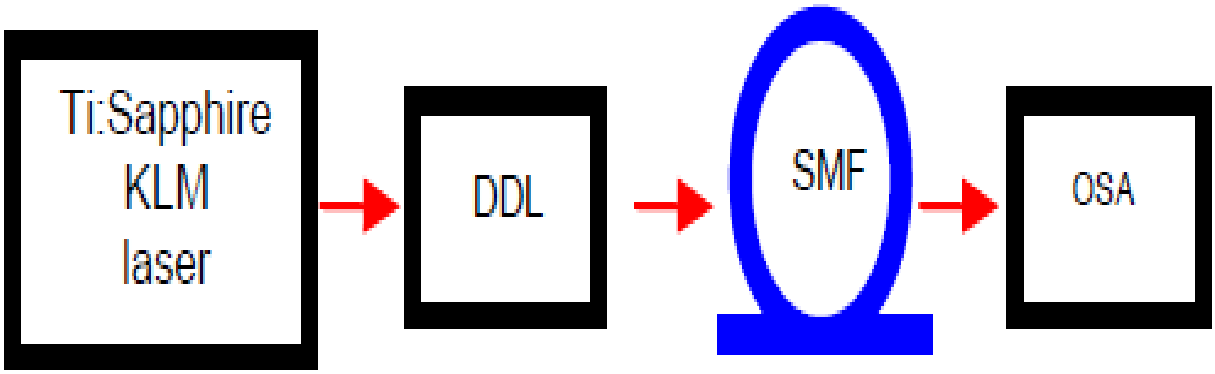

Fig. 1.2.1. *Scheme for classic spectrum compression (DDL- dispersive delay line, SMF- single-mode fiber, OSA-optical spectrum analyzer [65].*

In the SC schemes described above, it is used the standard silica fiber in such range of wavelengths where fibers have positive group-velocity dispersion (GVD). For fibers with negative dispersion the SC can be implemented directly in fiber without DDL: when the impact of dispersion is stronger than the influence of SPM the spectral self-compression (self-SC) takes place [66,4]. In this case, during initial propagation the pulse is stretched conditioned by GVD. Next, the obtained negative chirp is compensated by SPM during further propagation, in results we have spectrum compression [66,4].

§1.3 Pulse compression

Fibers have wide application in laser technology during construction different fiber optical sensors, in technology of handling of information and etc. due to their properties. One of the most interesting and important applications of nonlinear phenomena in optical fiber is the pulse compression. The bases of development of optical compression technology are introduced in works of Treacy [4, 67,68] and were based on the idea of turning of frequency modulation of pulse to the amplitude modulation. In the process of compression, which, in fact, represents the optical radiation focus in time, the pulses having frequency modulation with strong linear component are compressed in DDL. For the pulse generation with required frequency modulation in femtosecond range, it is the most convenient the using of SMF as modulator, where the SPM is conditioned practically by instantaneous electronic nonlinearity. Despite the small value of the Kerr index of silica $\tilde{n}_2 = 3.2x10^{-16} sm^2/W$, due to the large length of self-interaction in the fiber, the nonlinear additive $\delta n = \tilde{n}_2 I$ can become significant and play decisive role in the self-interaction [4]. In [69,70] works, it is studied self-interaction by the experimentally and numerically methods in silica fiber for powerful picosecond optical pulses ($P = 10kW$, $\Delta t = 5.5ps$, $\lambda = 0.59\mu m$). The GVD and nonlinear SFM lead to the stretching of pulse up to 20ps. Additionally the temporal profile of intensity obtains rectangular form, and the carrier frequency obtains the linear dependence on time. Directing the output radiation into the cell with vapor of sodium, which served as DDL with anomalous dispersion near the resonance, the authors observed pulse compression up to 1.5ps. The development of studies of pulse self-interaction and compression of radiation in fiber was mainly directed to the solution of problems in femtoseconds time range [4,71-74]. In [71], the pulses of

laser on dye with 1 kW power and 5.4 duration were compressed twelve times in system consisting from fiber and grid compressor. The authors of [72] are demonstrated the possibilities of similar system in femtosecond

time scale: pulses of ring laser on dye with 90fs duration were compressed up to 30fs duration after self-interaction in fiber with fifteen centimeters length. In works [4,73,74], directed to the creating of powerful sources of sub-picosecond pulses, it was used the laser on dye with 10ps pulses duration and power 10kW. At the output of such source, the pulse with 7 mW power and 0.7 ps duration has high spectral quality: $\Delta t \Delta \nu \sim 0.5$ [4].

As features of the process of femtosecond pulse compression, it can be mentioned the significant dispersive character even in the case of small length of fiber (~1cm). It is also typical the presence of asymmetry in spectral and temporal profiles of intensity. Small duration of pulse allows to replace the grid compressor to the DDL on prism [75] and interferometers [76]. We can mention also, although the fiber optical method of compression allows to solve the problem of the pulse formation with extremely short duration for optics duration, however the nonlinear character of the compression process leads to the unwanted sensitivity of compressed pulse parameters from stability of initial pulse parameters. The researches of self-interaction in field of anomalous dispersion are primarily related with fiber connection and the soliton problems [77-87]. The theoretical [77,78] and experimental [79,80] research of the pulse propagation in SMF is revealed the soliton regime of self-interaction[4].

For the research of parameters of controlling ultrashort pulses, it is typical the application of SPM and cross-modulation. Initial achievements in this field is related with the obtaining a large value of spectrum stretching in the process of self-modulation of radiation in liquid and solid nonlinear material [88-91]. The research by SPM and cross-modulation in SMF were mainly directed to the solution problem of coding for optical communication [4,92,93]. [94-96] works is typically are done for this direction. In [94], it is shown the theoretical and experimental results of research of SPM process of radiation in SMF. The research is implemented for picosecond pulses (for 532nm and 1064nm wave length). At the output spectrum of radiation, the characteristic substructure and stretching of spectrum depending of pulse intensity appears in the result of SPM. For the controlling of ultrashort pulses parameters, it is offered method based on the process of

cross-phase modulation in fiber [95]. The source was picosecond YAG:Nd laser. The radiation on main frequency served as reference wave, and the radiation of second harmonic as signal wave. In the measurements of the spectra of pump wave and examined wave it was observed phase modulation substructure which

typical for these process[4]. It is shown the possibility of frequency tuning of examined wave in the process of cross-modulation. In [96], it is implemented analogue research for pulse of femtoseconds range.

§1.4 Pulse compression of nonlinear-dispersive similaritons

Recent time, the theoretical and experimental studies of formation and propagation of similaritons (similariton are the pulse which save only its functional form as opposed to the soliton, which save its all characteristics) in fiber cause significant interest. The interest to the similariton method is mainly motivated by perspectives of their applications in analysis-synthesis problems in ultrafast optics [97]. The initial researches of optical similariton were in work [98], where it was explored conditions, which prevents the collapse of optical wave during propagation of pulses in optical fiber [2]. It was shown that in the case of high intensity the nonlinear Schrödinger equation, describing the propagation of optical pulses in fiber, has the asymptotic solution as pulses with parabolic temporal form of intensity and the linear chirp (parabolic phase)[4]. During the propagation along the fiber, the duration such pulses is changed, but the forms and phase save the parabolic shape. However, the quick increasing of duration and correspondingly the decreasing of intensity prevents the practical realization of parabolic pulses. Thus, further it was investigated the possibility of parabolic similariton realization in the fiber with amplifier. In [99], it was numerically shown that the any pulse is turned into the pulse with parabolic form and phase in the material with normal dispersion and amplification. It was attempt the experimental realization of parabolic pulses in erbium-doped fiber amplifier and their subsequent compression in DDL, however the methods of diagnostics of ultrashort pulses which were available for authors in this time does not allow reliably to confirm the generation of parabolic pulses[4].

Lately, a new kind of similariton was produced in a passive fiber with the joint effects of Kerr nonlinearity and dispersion [13].

These nonlinear-dispersive similaritons have numerous features [13]:

- spectrotemporal similarity /self-spectrotemporal imaging, with the accuracy determined by both the spectral and pulse stretching [13];
- linear chirp, which has not the dependence on the amplitude, chirp and power of the initial pulse and is defined only by the fiber dispersion [13];
- the bandwidth of similariton is only defined by the input pulse power [13].

The nonlinear-dispersive similaritons has numerous significant applications; one of them is pulse compression, where the positive phase caused by SPM in fiber compensated by the negative chirp obtained in DDL [1,2]. In fiber the spectral bandwidth is stretched and the compensation of phase obtained in DDL leads to the formation of shorter pulses. The standard scheme of pulse compression is introduced in Fig. 1.4.1.

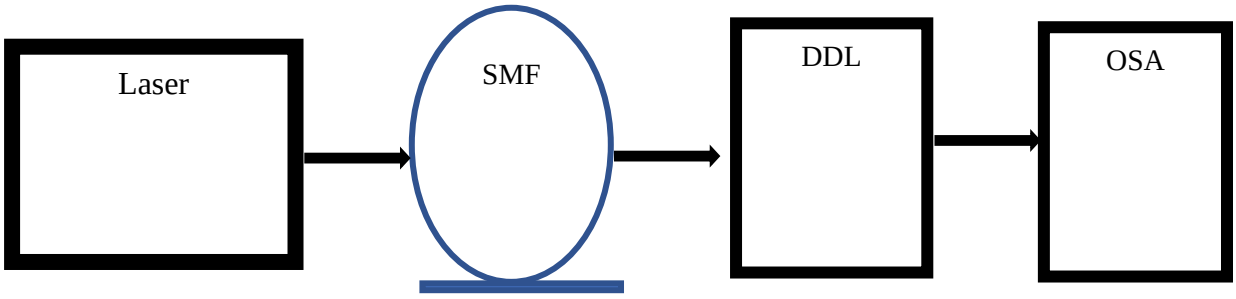

Fig. 1.4.1*. Scheme for classic pulse compression (SMF- single-mode fiber, DDL- dispersive delay line, OSA- optical spectrum analyzer)*

On the femtosecond time scale the high-order nonlinearity and dispersion are significantly restricting the pulse compression ratio, and the influence of residual third-order dispersion at the system output is the most significant among all high-order effects [100]. In [13], the uncompensated phase is compensated by taking into account the circumstance that the signs of third-order dispersion in fiber and dispersive delay line are not the same. Nevertheless, this approach restricts the parameters of fiber and dispersive delay line, and consequently, the compression size.

The cancellation of third-order dispersion impact can be realized via nonlinear effects [101,102]. It was introduced the mutual compensation of third-order dispersion and nonlinear phase shift in short-pulse amplified fibers [101]: the accumulation of nonlinear phase shift in the amplifier is canceled via the combined third-order dispersion in a fiber stretcher and grating compressor [101,102].

In [100] work, it is shown the possibility of compensation of third-order dispersion through pulse asymmetry manipulation at the fiber input.

1.5. Ultrashort pulse shaping technique

The development of the ultrafast laser source into a stable, easy-to-use source coupled with the development of computer control of spatial light modulators (SLMs) are the beginning of ultrashort pulse shaping, i.e., the synthesis of pulses with specific pulse shapes from a given input pulse. Pulse shaping technique is a widely used for applications such as pulse compression and dispersion control [103-105], coherent control of quantum systems [106,107], laser control of matter [108-110], telecommunications [111], optical metrology [112], bio-imaging [113,114], microscopy [115] and multidimensional spectroscopy [116-118]. There exist of three kind of pulse shaper: shaping of spectral phase [119], spectral phase and amplitude [120] or polarization [121].

Pulse shaping has been a known technique used for several decades. By spreading the frequency components in space using gratings in a zero dispersion stretcher, the manipulation of frequency bands, $\Delta\omega$, is possible. The first shaping was achieved with fixed pattern masks, which were created by varying the thickness of a substrate and many good results were obtained. Other approaches were the deformable mirrors [122], space-to-time conversion [123,124], volume holography [125] and some new mechanisms of pulse shaping [126-130]. The disadvantages of these methods are each substrate generated a fixed pattern, which cannot be rapidly changed and the masks were purely binary. Recently, computer programmable spatial light modulators have been developed, which allow for mask changes on the millisecond time scale, and also allow for a grey level variation.

Two of the most common in this new class are the acousto-optic modulators and the liquid crystal (LC) modulators. Acousto-optic modulators have a radio frequency voltage signal, which is transformed into a traveling acousto-optic wave along the modulator by a piezo electric transductor. The traveling wave creates a refractive index grating through the photo-elastic effect, creating the frequency mask. This thesis will focus on liquid crystal modulators, further information and references about acousto-optic modulators can be found in [131,132].

Liquid crystal modulators use one or two arrays of liquid crystal pixels to adjust the relative spectral phase and amplitude for small frequency bandwidths across the total frequency bandwidth of the pulse. The liquid crystals in the pixels rotate based on an applied voltage, which lengthens the optical path length and hence alters the phase. In the pioneer work [133] it was used 32 pixel array, but as technology improved the number of pixels have increased, and today modulators are being constructed with 2 arrays of much more pixels. The advantage of two arrays is that one can control the phase or amplitude independently.

By changing the spectral phase in frequency space, a change in the temporal shape of the pulse is created when recombined. The transforms can generally be considered using Fourier transformation. The temporal patterns that are created are almost limited by imagination; however there are a few physical properties which limit the complexity. These are the total bandwidth and the bandwidth per pixel.

The combination of ultrafast laser sources with temporal tailoring has created much interest recently in the spectroscopic community. Pulses can easily be manipulated to provide coherent control of the excitation paths of molecules, driving specific transitions. This tool can be further enhanced when used in a feedback controlled optimization algorithm, which corrects for the experimental apparatus as well as works around the approximations made in theory.

In the pulse shaping, the desired shaping is induced by functioning on the input pulse in the spectrum. To do this, the spectral components of the input pulse are divided and operated separately by adjusting the component's spectral phase and/or amplitude. Next, the spectral components form the shaped output pulse with the desired temporal profile.

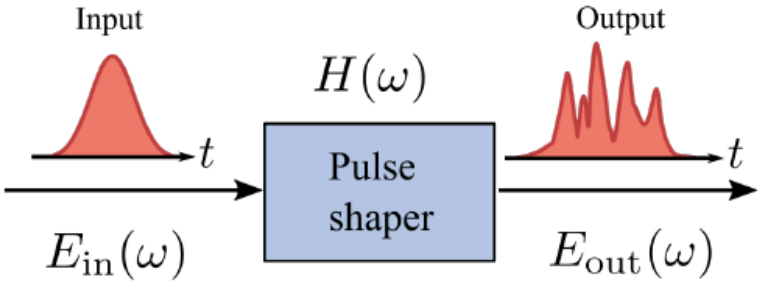

Fig. 1.5.1 *Block diagram representation of Fourier transforms pulse shaping. Figure adapted from* [134]

In other words, Fourier transform pulse shaping is based on linear, time-invariant filtering in the frequency domain [125], as schematically illustrated in fig. 1.5.1. The action of the pulse shaper on

the input field is given by the complex-valued transfer function [135]. The output field in the time domain can be obtained by simply taking the inverse Fourier transform of input field.

Experimentally, this realized by separating the spectral components of the input pulse spatially and using a spatial mask for management of spectral phase and amplitude. Consequently, the spatially divided components are recollected and form a shaped output pulse with a temporal profile. A schematic drawing of the setup most commonly used for Fourier transform pulse shaping, the so-called 4f-line [136], is shown in Fig. 1.5.2. The spectral components of the incident laser pulse are angularly dispersed by a grating (G) located in the focal plane of a lens (L). The lens collimates the dispersed input beam and focuses each spectral component on a mask (M), or spatial light modulator, situated in the rear focal plane of the lens [127,135]. Here, phase and/or amplitude of the spectral components are manipulated. After traversing the mask, a second lens (L) focuses the light onto another grating (G) where the spectral components recombine. Remarkably, the symmetry of the 4f-line allows for a furled operation of the setup where a furling mirror is placed in the central focal plane of the system. This suggests the profit of reduced size and a smaller number of optical components, which simplifies alignment of the setup. In the furled configuration, the SLM is placed directly in front of the furling mirror [127,135]. The laser pulse thus traverses the SLM twice, in that way increasing the modulation ranges of the pulse shaper. However, to maintain a good spectral resolution, the mask must be placed within one Rayleigh length from the furling mirror to ensure that the focal spot size at the mask is sufficiently small. This imposes additional constraints on the setup.

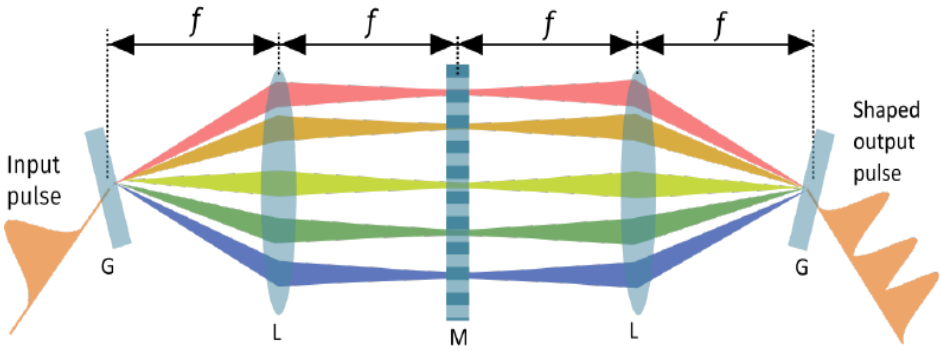

Fig. 1.5.2. *A 4f-line for Fourier transform pulse shaping consisting of two gratings (G), two lenses (L) and a spatial mask (M). The spectral components of the ingoing pulse are spatially separated by the first grating before being collimated and focused onto the mask by the first lens. After the mask, the spectral components are recombined. f is the focal length of the lenses. Figure took from [127].*

1.6. Pulse shaping using liquid crystal spatial light modulators

As we have mentioned above, the most practical types of spatial masks are acoustooptical modulators and liquid crystal spatial light modulators (LC-SLM) [128,136]. Both methods have been reviewed extensively [124,125,128,136]. In this thesis, the focus will be on pulse shaping using liquid crystal modulators, a technique which has been pioneered by Weiner and co-workers in the early 1990s [118-133].

Pulse shapers based on LC-SLMs use the birefringence of nematic liquid crystals (NLC), i.e., the fact that the optical properties of the medium depends on the light wave propagation in the respect of the molecules orientation. NLC are typically fluids of relatively rigid rod molecules that tends to orient parallel to each other and compose long range orientational order. The NLC materials in their LC state possess very interesting functionalities such as self-assembly, controllable fluidity with a long-range order, molecular and supramolecular cooperative motion, large birefringence and anisotropy in various physical properties, alignment change induced by external fields at surface and interfaces, and macroscopic deformation in response to stimuli such as electric, magnetic, photo, thermal, and mechanical forces. In LC the unite vector in the preferred direction of molecules orientation is called the director **n**. Thus, by ruling the orientation of the LC director with respect to incident light propagation, it is possible to manage the effective refractive index. This, consequently, allow control the spectral phase which is collected by the light wave upon travelling through the LC. This is the basis of phase and amplitude shaping using LC modulators [128,136].

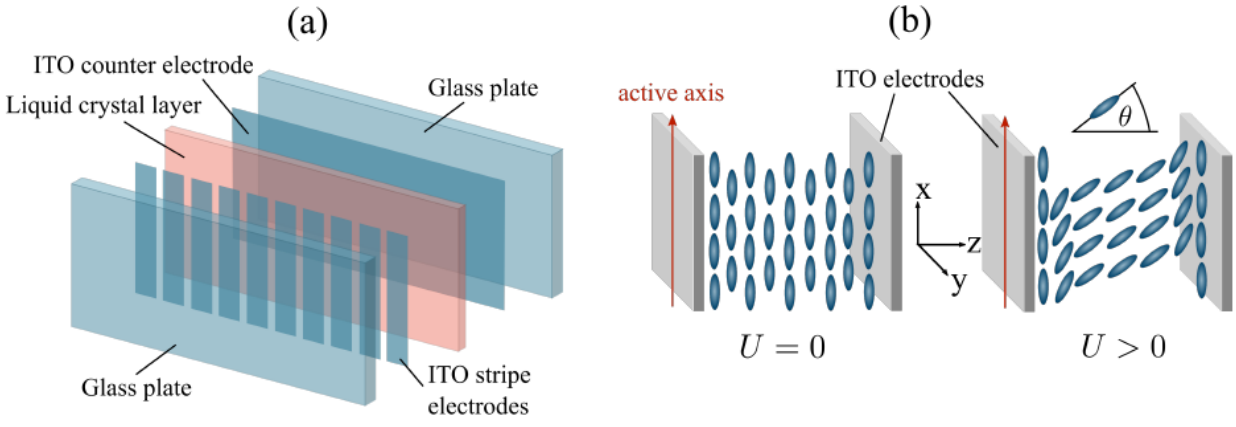

Fig. 1.6.1. *(a) Exploded view drawing of a single LC mask. The thin LC layer is embedded between two glass slides. A driving voltage applied via transparent ITO electrodes controls the orientation of the LC molecules. The LC mask is subdivided into several pixels which are defined by gaps between the ITO*

electrodes. (b) Schematic diagram of a single pixel within the LC display. In the case of no voltage, the LC molecules are aligned along the pixel's active axis which is defined by the surface structure of the ITO layer. A non-zero driving voltage results in a tilt of the LC molecules toward the z-axis. θ denotes the angle between the longitudinal axis of the LC molecules and the z-axis. Figure took from [127].

The schematic drawing of the structure of a LC-SLM for phase shaping most commonly used for Fourier transform pulse shaping, is shown in Fig. 1.6.1. The SLM consists of a NLC layer which is inserted between two glass slides. The LC mask is split into a linear array of pixels which can be controlled individually using a driving voltage. It is applied via two transparent indium tin oxide (ITO) electrodes which are deposited on the inner surface of the glass slides [127]. The pixels are defined by patterning of one ITO layer into stripe-shaped electrodes, with neighboring pixels being separated by thin gaps (typically a few μm) in the ITO layer. Fig. 1.6.1 also shows a sketch of a single LC pixel. When no voltage is applied, the LC director aligns along a direction which is forced by surface patterning of the ITO layer. According to [137], this zero voltage direction will from now on be referred to as the active axis of the LC mask. In the case of a non-zero driving voltage, the director reorient along the light wave propagation direction due to its tendency to align with the electric field. This effectively changes the extraordinary refractive index for the light. Now it is obvious that the spectral phase of a light wave after travelling through the pixel can be ruled via the motivating electrical field by the reorientation of the NLC director. This means that it is possible to create desired phase pattern on the spectrum of input laser pulse by applying the appropriate electrical field distribution to the SLM.

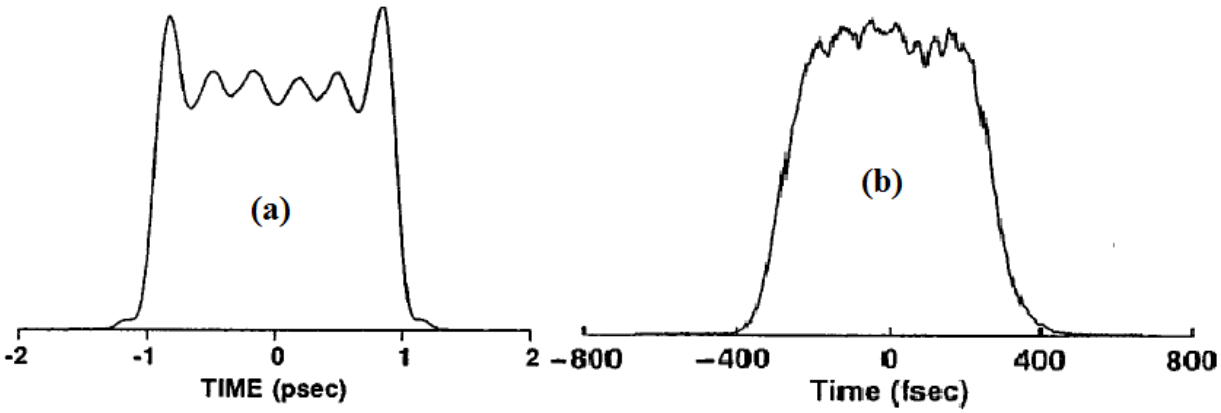

Fig. 1.6.2. (a) *Optical square pulses: (a) measurement of a 2 ps optical square pulse, (b) measurement of a square pulse with reduced ripple [132].*

Thus in the enough early work [138] it was reported on the generation of ultrafast square pulses using fixed masks. They have done intensity cross correlation measurement of a 2 ps square pulse produced by using masks truncated after five side lobes on either side of the main spectral peak (see Fig. 1.6.2a). The rise and fall times of the square pulse were found to be on the order of 100 fs. The ripple present on the square pulse arises because of the truncation of the spectrum and was in good qualitative agreement with the theoretical intensity profile. Square pulses with reduced ripple have also been obtained (see Fig. 1.6.2b), by avoiding truncation of the spectrum and instead using a gentler spectral anodization. Other interesting result is encoding of femtosecond pulses by utilizing pseudorandom phase patterns to scramble (encode) the spectral phases [131,139]. The clear aperture of the mask was divided into 44 equal pixels, each of which corresponds to a phase shift of either zero or π. Spectral encoding spreads the incident femtosecond pulses into a complicated pseudo noise burst within an ~8 ps temporal envelope. The peak intensity is reduced to ~8% compared to that of an uncoded pulse of the same optical bandwidth. The agreement between theory and experiment was excellent. Similar coding and decoding has been demonstrated with longer phase codes (up to 127 pixels) [131] and also using programmable SLMs [140].

Next interested result is the use of periodic phase-only spectral filters to produce high quality pulse trains [141,142]. The envelope of the pulse train depends on the structure of the phase response within a single period of the phase filter. The measured pulse train with 4.0 THz repetition rate, induced by 75 fs input pulses and binary phase mask is shown in Fig. 1.6.3a [134]. As it is well seen the pulse train is clean, and the pulses are well separated.

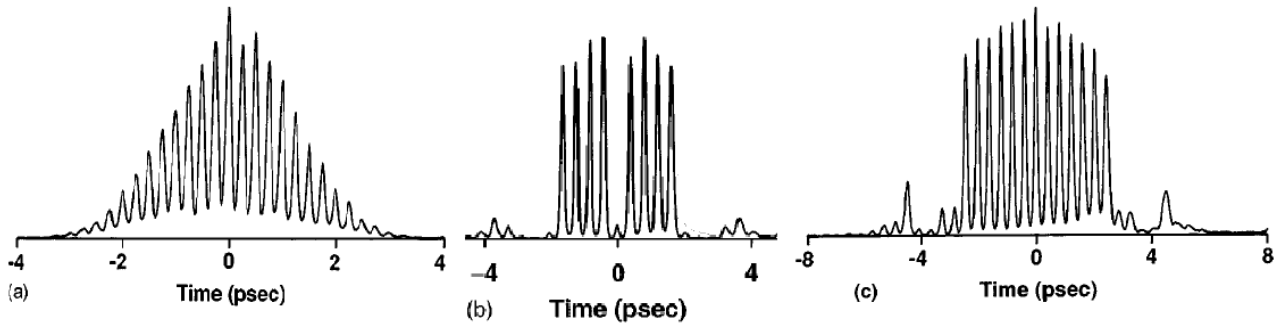

Fig. 1.6.3. *(a) Pulse trains generated by phase-only filtering. (a) Pulse train under a smooth envelope. (b) and (c) Pulse trains under a square envelope [132].*

Time domain experimental result, obtained by placing a binary phase mask fabricated according to a specific grating design into a femtosecond pulse shaper, is shown in Fig.1.6.3b. Used specific gratings are computer generated holograms that have previously been used to split an individual laser beam into an equally spaced, equal intensity array of beams in space. The structure for this grating consists of a periodic binary phase function, where the period of the phase modulation is selected to yield the desired beam separation in the spatial output array and the phase structure within a single modulation period is designed using numerical global optimization techniques to provide the desired number of beams, with as little energy as possible outside the target array area [125,132]. The picture in Fig.1.6.3b consists of a relatively uniform sequence of eight pulses, with one central pulse missing. Waveforms with the missing central pulse restored have been obtained by adjusting the phase difference on the mask to be less than π [141] (see Fig. 1.6.3c). In [118,119] was experimentally studied programmable shaping of femtosecond pulses by using a 128-element LC-SLM to control the phases of spectral components which were spatially dispersed within a grating-and-lens pulse shaping apparatus. This setup allows gray-level switch of the spectral phases and make possible adjustment of the pulse shape on a millisecond time scale under electric field regulation. Fine-tuning in the scheme of the pixelated modulator result in pulse shaping truly equivalent to micro-lithographically created masks. Numerous models of pulse shaping operation, among them pulse position modulation, programmable pulse compression, and adjustable cubic phase distortion, were described [118,119]. In [143] it was demonstrated really whole dispersion compensation for 400-fs pulses over a 10-km fiber connection using dispersion compensating fiber and a programmable femtosecond pulse shaper functioning as a spectral phase equalizer. The pulse shaper excites variable quadratic and cubic phases onto the spectrum and removes all the residual dispersion and dispersion slope in the dispersion compensated fiber connection. This work shows that the pulse shaper technique provides a powerful and convenient tool for programmable fiber dispersion compensation over broad optical bandwidth. This allows distortion-free femtosecond pulse transmission over a fiber link in excess of 10 km without requiring the exact trimming of the dispersion-compensating fiber [133]. LC SLMs have also been used for phase-only filtering and shaping of pulses with temporal resolution approaching 10 fs. The results of [144] shown in Fig. 1.6.4. 13 fs pulses from a mode locked Ti:sapphire laser with a center wavelength of 800 nm are

shaped using an all-reflective-optics pulse shaper. The LCM imparts a cubic spectral phase variation, leading to an asymmetric distortion and in good agreement with the calculated pulse shape [137].

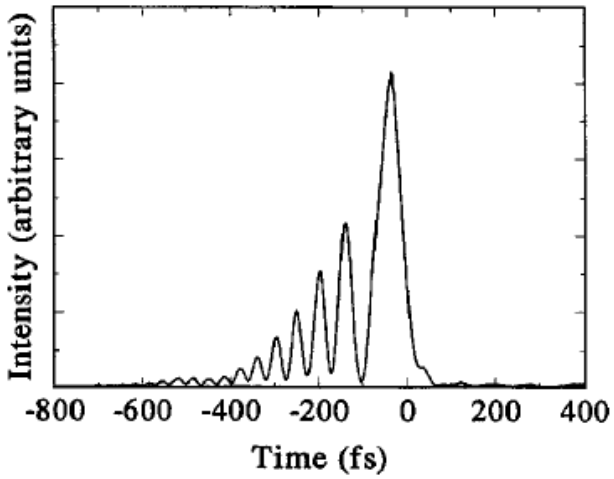

Fig. 1.6.4. *Shaping of 13 fs pulses using a phase-only LC phase modulator array. In this example, the LCM produces a cubic spectral phase variation, leading to the asymmetric distortion seen in the intensity cross-correlation plot [132].*

For the more rich pulse shaping, it is necessary independent government of spectral phase and amplitude. For this purpose the use of two LC arrays is required. Originally this was accomplished by modifying the setup two telescopic lens pairs (four lenses) between the gratings, with separate LC SLMs between the first and second and third and fourth lenses, respectively [145]. Very simple and enhanced setup, which has broad use today for independent phase and amplitude variation, was achieved by joining two LC arrays into a single scheme [146]. This type of setup with dual LC SLM array gave the results with four examples of pulse shaping [147,132] showing in the Fig. 1.6.5. The input pulses duration were 70 fs with central wavelength approximately 800 nm and all the pictures are intensity cross-correlation measurements using unshaped reference pulses directly from the laser. In the mentioned work there were generated and registered a 800 fs square pulse, a five pulse sequence of equal amplitude pulses in which both the pulse timings and phases are specified, a three pulse sequence with different chirp rates per pulse, and a sequence of ten 70 fs pulses with pulse timings, phases, and amplitudes all specified. In Fig. 1.6.5c and d the desired intensity profiles are also shown with dashed lines. It was obvious that waveforms with more high degree of complexity could be generated as well and even random pulses. Let us note that dual LC SLMs may be useful for controlling the time-dependent polarization profile of ultrashort pulses.

These possibilities, as well as a simple experimental demonstration, are discussed in [139,146]. Unfortunately, the diffraction efficiency of the gratings usually have a strong polarization sensitivity, and this fact make polarization pulse shaping much more difficult.

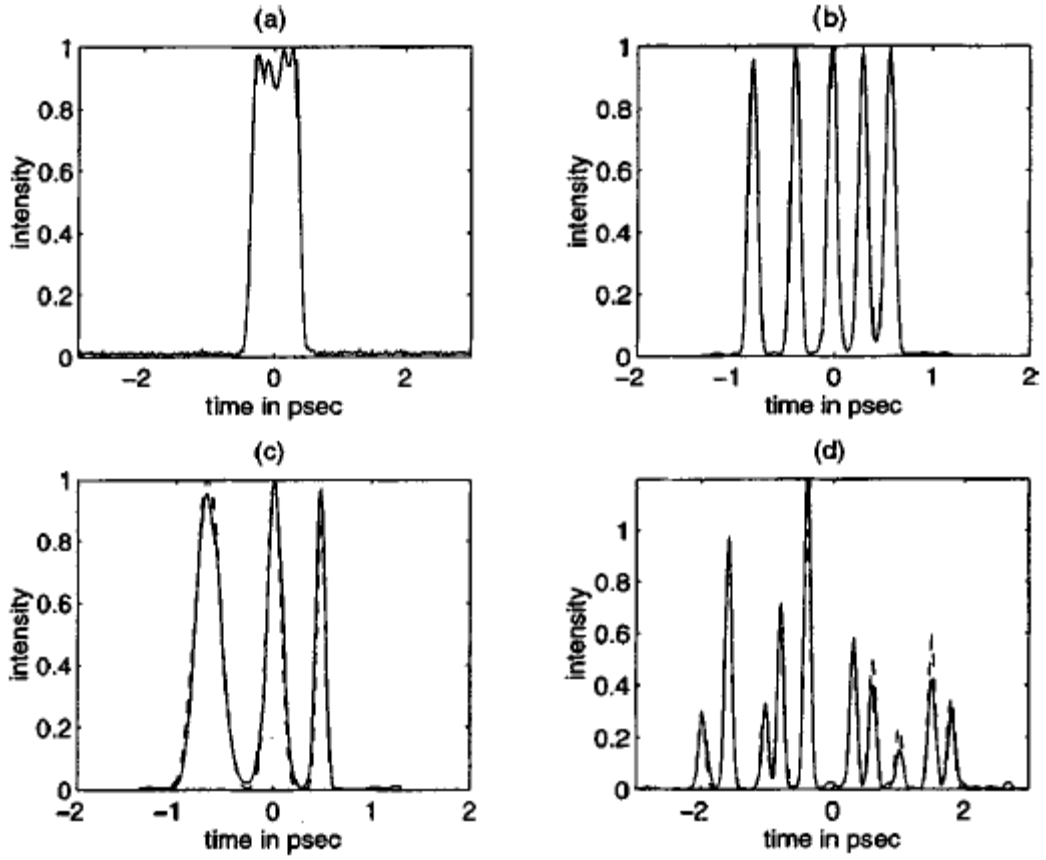

Fig. 1.6.5. *Intensity cross-correlation pictures of shaped pulses using the dual LCM array. (a) 800 fs square pulse. (b) Sequence of five, equal-amplitude pulses. (c) Three pulse sequence with different chirp rates per pulse. (d) Ten pulse sequence with pulse timing, amplitude, and phase control.*

Instead of electrical control it was possible to perform pulse shaping using an optically switched LC SLM [148]. This type of SLM is also known as a liquid crystal light valve. The motivation for this work is to avoid pixilation of the pulse shaping SLM. The light valve is made up with two continuous transparent electrodes and continuous layers of a twisted NLC and of photoconductive material (BSO). Light wave change the conductivity of BSO layer. When an dc electric field is applied between the two electrodes, a local change in the BSO conductivity results in a change in the voltage drop across the LC layer [141]. This leads to rotation of the LC director and a phase change for light passing through the layer. In their experimental work [149] the LC light valve was

allow to run a phase shift more than 12 rad. As we know, instead of this, the pixelated LC modulators allow to rum maximum 2π phase difference between neighboring pixels. That is why, the optically controlled SLM is better suited for correction of small residual phase in chirped pulse amplifier systems than it is for generation of strongly modulated spectral phase profiles. On the other hand, liquid crystal light valves with significantly improved spatial frequency response have been reported [150], which could potentially be applied to improve spectral resolution for pulse shaping applications. In [151] was reported the automated generation of spatiotemporally shaped femtosecond pulses by use of an optically controlled, two-dimensional LC-SLM. A single input pulse was divided into many independent regions, and each region was shaped temporally. By changing the imaging geometry they accomplished either real-space or wave-vector shaping. In [152] they presented an improved design and adjustment concept for femtosecond pulse shaping. The concept results in a compact and robust pulse shaping setup. A systematic adjustment procedure, high reproducibility and stability, as well as easy adaptability to different femtosecond laser sources were the key features of the presented design. The constructed prototype pulse shaper was tested in an open loop and feedback-controlled adaptive pulse shaping on two different femtosecond laser sources. A femtosecond pulse shaper in phase and amplitude using two LC devices with 640 pixels, leading to a wide temporal window around 25 ps at 800 nm was presented in [153]. It was shown that this device has very high resolution. The use of a folded zero dispersion line is also successfully demonstrated. It was demonstrated new technique for correcting arbitrary spectral-phase aberrations in a single iteration with no reference pulse [154]. By utilizing spectral-phase interferometry for direct electric field reconstruction and a programmable LC-SLM [155], it was achieved compression of complex pulse shapes from nearly picosecond extent down to 70 fs. In [156] was reported on a beam shaping technique for femtosecond laser pulses based on a LC display. The system was capable of modifying femtosecond Gaussian beams to a flattop beam. A pattern projected onto LC display modifies the incoming Gaussian beam intensity so that flattop intensity profile is obtained. The process was monitored online using a charge-coupled device camera so that the intensity distribution of each pulse was known. An experimental example of the depth profile of a Cr layer on a Si substrate obtained using such a modified beam was presented. The detailed analysis of commonly encountered waveform distortions in femtosecond pulse shaping

with pixelated devices on LC-SLM, including the effects of discrete sampling, pixel gaps, smooth pixel boundaries, and nonlinear dispersion of the laser spectrum was presented in [157]. Experimental and simulated measurements were used to illustrate the effects. The results suggested strategies for reduction of some classes of distortions. The study [158] demonstrated spectral phase pulse shaping with a functionality that is independent of input polarization through the use of a single-layer LC-SLM array and a quarter waveplate in a double-pass pulse-shaping geometry. Ultrashort pulse shaping through arbitrary phase modulation with a reflective, 1 x 4096 element, LC-SLM was demonstrated in [159]. The exclusive creation of this device offers a very 85% efficiency when it is used for phase modulation only in a prism based pulse shaper. They presented a single shot characterization of the pulse shaper in the spatial and the spectral domains. These methods make available a complete picture of how the LC-SLM adjusts the spectral phase of an ultrashort pulse. The programmable, high-rate scanning femtosecond pulse shaper based on a two-dimensional LC on silicon SLM was introduced in [160]. Whereas horizontal resolution of 1920 controllable pixels make available excellent preciseness in order to make complex wave shapes, scanning across the vertical dimension 1080 pixels has been used to simplify at least 3 orders of magnitude speed increase as compared with typical LC-SLM-based pulse shapers. They demonstrate a new scanning femtosecond pulse shaping technique that enables modulation of pulse shapes at hundreds of kilohertz rates. This technique is particularly useful for lock-in on the pulse shape measurements [161]. An ultrafast pulse shaper, capable of both phase and amplitude shaping, was constructed as well in [162] using a single high-resolution LC phase mask. The shaper was calibrated with an inline spectral interferometry technique. Amplitude shaping was accomplished by writing to the mask a phase grating, whose period was smaller than the spectral focus, diffracting away selected frequencies in a controllable manner. In the review article [163] was given an overview of the most widespread techniques of both ultrashort pulse shaping and pulse characterization [164].

In [165] has been demonstrated the annular flattop beam shaping technique with dual phase only LC-SLM based on the refractive laser beam shaping systems. First LC-SLM reorganizes the intensity distribution, and the second restores the initial basic wave front. Contrary from the conventional annular beam shaping technique, the wave front of the output beam could be maintained. The influences of deviations of beam waist and beam shape on the output beam profile

were discussed in detail. Detailed description of the alignment of a pulse shaper optimized for mode locked semiconductor lasers was presented in [166]. Several methods to calibrate the phase-retardance-LC-voltage relationship were reviewed and a calibration method was presented which is robust to non-idealities of the components of the setup. A new calibration method for dual-mask LC-SLM was presented [167], which can be applied while the SLM is in the setup of a pulse shaper optimized for semiconductor laser sources. An evolutionary algorithm was used to retrieve the phase retardances from the transmitted spectral intensity. In [168] it was demonstrated through a combination of adaptable diffractive and reflective optical elements a LC-SLM and a deformable mirror - decoupled spatial control over the pulse front (temporal group delay) and phase front of an ultra-short pulse was enabled. Pulse front modulation was confirmed through autocorrelation measurements. This new adaptive optics technique, for the first time enabling in principle arbitrary shaping of the pulse front, promises to offer a further level of control for ultrafast lasers.

CHAPTER 2. SPECTRAL DOMAIN SOLITON-EFFECT SELF-COMPRESSION

§2.1. Introduction

The results of this chapter are based on the publications [20-25].

The nonlinear process of spectral compression (SC) in a DDL followed by a nonlinear fiber demonstrates promising applications to the signal analysis-synthesis problems in ultrafast optics [169]. In the SC system, the negative phase of pulse obtained in a DDL is compensating by the positive phase acquired by nonlinear SPM in a fiber with normal dispersion [170,171]. The impact of group-velocity dispersion (GVD) on SC for sub-picosecond pulses in the range of normal dispersion, i.e. at wavelengths <1.3μm for standard silica fibers, is analyzed in [172] in view of shaping flattop pulses. In the range of anomalous dispersion, i.e. at wavelengths >1.3μm for silica fibers, the combined impact of GVD and SPM leads to the formation of solitons [78,173], when the contributions of GVD and SPM balance each other. The pulse self-compression phenomenon arises when the impact of SPM exceeds the GVD, and high-order solitons are shaped [174]. Recently, generation of sub-two-cycle pulses by soliton self-compression of 100-fs pulses from a Ti:sapphire laser at 85 MHz using a 4.85-mm long nonlinear photonic crystal fiber are demonstrated numerically [175] and experimentally [176]. The efficient soliton self-compression down to 5.07 fs is demonstrated also in As_2Se_3 and As_2S_3 chalcogenide photonic nanowires [177].

When the contribution of GVD exceeds the SPM impact in the single-mode fiber (SMF) with anomalous dispersion, the soliton spectral self-compression (self-SC), a spectral analogue of soliton self-compression, is anticipated. Recently, the self-SC realization in a standard silica fiber with negative dispersion at the wavelength $\geq 1.3\mu m$ was predicted numerically [66] and observed experimentally [65].

In this chapter we study soliton self-SC, which takes place when fiber has anomalous dispersion and the dispersive length in the fiber is shorter than the nonlinearity length. Therefore, at first the GVD stretches the pulse and obtains a chirp. Afterwards, the accumulated impact of nonlinear SPM leads to the chirp compensation, and as a result, the spectrum is compressed. We study the soliton self-SC process revealing its nature, peculiarities and general regulations on the basis of physical pattern of the process.

§ 2.2. Mathematical modeling of propagation process and the self-interaction of ultrashort pulses in single-mode fiber

The mathematical modeling of nonlinear self-interaction of powerful laser radiation in optical fiber based on Maxwell's equations and firstly it was developed for spatial effects, which takes place on the influence of diffraction, nonlinear self-interaction, when radiation is propagated in fiber. Next, the spatial equations, written for plane waves were generalized to spatial-temporal taking into consideration dispersion and mode structure of the fiber [178].

While spatial effects appear on the longitudinal scale on distance ~ 10^{-1}-10^{-2} cm in fibers, as the dispersion phenomenon appears on distances ~ 10^{1}-10^{2} cm in the case of sub-picosecond pulses, and for picosecond pulses on distances ~ 10^{2}-10^{3} m. This circumstance allows to divide spatial and temporal effects and to examine the changing temporal characteristics of the pulse during propagation in the SMF, regardless of the spatial properties of the radiation. The impact of SPM on the spatial profile of the beam is important in the case of the self-interaction of radiation in multimode fibers. In the SMF the cross-section effects of the self-interaction appear in the case of high intensity of radiation $I \sim 10^{12} W/sm^2$, usual for pulses with $\tau \sim 10\, fs$ duration. [4]

For the description of the pulse propagation in the SMF, it is used slowly varying amplitudes method, which allows us to express the self-interaction of the pulse with the generalized nonlinear Schrödinger equation [1,2]:

$$i\frac{\partial \psi}{\partial \zeta} = \frac{1}{2}\frac{\partial^2 \psi}{\partial \eta^2} + R|\psi|^2\psi + \mu_{TOD}\frac{i}{6}\frac{\partial^3 \psi}{\partial \eta^3} - i\mu_{SH}R\frac{\partial |\psi|^2 \psi}{\partial \eta} - \mu_R R_\psi \frac{\partial |\psi|^2}{\partial \eta} \qquad (2.2.1)$$

In the equation the slowly varying amplitude of the field $\psi(\zeta,\eta) = A(\zeta,\eta)/A(0,0)$ is normalized to its peak value at the system input, $\zeta = z/L_D$ is the dimensionless propagation distance and $\eta = (t - z/u)/\tau_0$ is the running time, which are normalized to the dispersive length $L_D = \tau_o^2/|k_2|$ (k_2 is the coefficient of second - order dispersion), and the initial pulse duration τ_0 (τ_0 is the initial pulse duration at the level of e^{-1} measured from maximum value of intensity), respectively. $k_j = |d^j k/d\omega^j|$ is the absolute value of *j*-th derivative of k wave number with respect to ω frequency (*t* is the time, *z* is the longitudinal spatial coordinate, *u* is the group velocity). The nonlinearity parameter R is given by the expression $R = L_D/L_{NL}$, where $L_{NL} = (k_0 n_2 I_0)^{-1}$ is the nonlinearity length, n_2 is the Kerr

index of silica, I_0 is the peak intensity at the input of system. The first and second terms of the right side of Eq. (2.2.1) describe the dispersive and nonlinear effects, respectively [4].

The coefficient $\mu_{TOD} = k_3/(k_2\tau_0)$ describes the impact of the third dispersion, $\mu_{SH} = T/(\pi\tau_0)$ is the contribution of the nonstationary wave, and $\mu_R = \tau_R/\tau_0$ is the nonstationary nonlinear response (where τ_R is the time of nonlinear response). The values of coefficients μ decrease within increasing of pulse duration and the describing of sub-picosecond pulses propagation is implemented by nonlinear Schrödinger equation, that is by (2.2.1) equation with $\mu_{TOD} = 0$, $\mu_{SH} = 0$, $\mu_R = 0$ [4].

$$i\frac{\partial\psi}{\partial\zeta} = \frac{1}{2}\frac{\partial^2\psi}{\partial\eta^2} + R|\psi|^2\psi \qquad (2.2.2)$$

The case of *R=0* corresponds to the dispersive propagation of the pulse, and the linear dispersive material (DDL) is described by equation (2.2.1), when R=0. When it is studied the formation and propagation of parabolic pulses in amplified fibers, there is such $ig\psi$ term in the right side of (2.2.1) and (2.2.2) equations, which describes the amplification with the g coefficient. However, our investigations are done with passive fibers and the energy of the pulse is conserved.

Last three terms of (2.2.1) equation describes the high-order nonlinear and dispersive effects. The third-order dispersion (term with μ_{TOD}) essentially takes place on the distance of $L_D^{(3)} \equiv 2\tau_o^2/|k_3|$, when the dispersive parameter is $k_2 \approx 0$. The third-order dispersion can appear, when duration of pulse is $\tau \le 50\,fs$ [2,4] for the visible range for standard fiber ($k_2 = 0$ when $\lambda = 1.3\mu m$), and also in the case of substantial broadening of spectrum in the process of SPM. In equation (2.2.1), the only nonlinear effect which can cause the distortion of the pulse envelope shape is nonstationary wave (μ_{SH}). The consideration this term leads to the dependence of GVD on the intensity of pulse. Also in the material with $n_2 > 0$, it is occurred the wraparound tail of the pulse. Accumulated changes of pulse envelope can be substantial for pulses with $\tau_0 \le 30-40\,fs$ duration [1,2,4]. As the impact of this term is not significant on the large distance, so it can be ignored. The last term of equation (2.2.1) describes the impact of nonlinear relaxation response of material, which becomes substantial for such durations of pulse which comparable with nonlinear

response of material $\mu_R = \tau_R / \tau_0 \sim 1$. For standard silica fiber it corresponds to the duration of few femtoseconds [1,4,179].

Although, in this work such ultrashort pulses does not studied, it can be mentioned that in the case of such duration of pulse, the (2.2.1) equation does not describe the process adequately, as the equation was obtained by assumption that $\mu_R << 1$. The first phenomenon which is competed with SPM is the Raman scattering above all nonlinear processes occurring by propagation of pulse in the fiber. Silica fibers has wide Raman line $\Delta\nu = 250 sm^{-1}$ (the time of relaxation is $\sim 100\, fs$), so Raman scattering can appear for pulses with $\tau \geq 100\, fs$ durations. Additionally Raman scattering process has substantially nonstationary character. The intensity of radiation I^0 which is needed for generation stokes component is given by length of fiber ℓ: $I^0 = C_S (gl)^{-1}$ [4,180]. The value of C_S constant is changed in the range of $C_S = 16 - 25$ related with material of fiber core, and the g coefficient of amplification of Stokes wave has $g = 10^{-11} sm/W$ in the range of $\lambda = 1.06 \mu m$. The impact of Raman scattering on SPM is experimentally studied in [4,181]. For $I > I^0$ the stokes component increases with $\Delta\nu_s \sim 440 sm^{-1}$ spectral sift, taking energy pump pulse which has the impact of SPM. Also, at the central energy-carrying part of pulse of the main wave (which has linear part of frequency modulation) forms a trough. It can be mentioned that the feature of Raman scattering nonstationary is the limitation of the length of nonlinear interaction due to the group delay. Because of this, while for picosecond pulses with $10^{-11} - 10^{-10} s$ durations, Raman scattering is the one of the main nonlinear processes, but in the case of sub-picosecond and femtosecond pulses for the observation of the Raman scattering it is needed high powers with such order that superior powers contemporary standard femtosecond laser system. So, the process of propagation of laser pulses in SMF is adequately described by Schrödinger equation (2.2.2) in the range of durations of sub-picosecond and picosecond for powers up to $P \sim 10^9$ W. In the femtosecond time scale, it is used generalized equation (2.2.1). The describing linear dispersive material is implemented by (2.2.2) with R=0 [4].

§ 2.3 Method of numerical solution of Schrödinger equation

The (2.2.1) and (2.2.2) equations does not have analytical solution except in the case of some particular situations when it is applied the method of inverse scattering problem [182]. Therefore, it is common the practice of approximate analysis and numerical solution. As Schrödinger equation describes a wide range of physical phenomena it is motivated to develop various method of numerical solutions of equation, comparative analysis is implemented in [183]. All this methods are separated into two classes: differential and pseudo-spectral methods. In this work, it is used pseudo-spectral method for the problem solution of propagation pulse in the nonlinear medium with dispersion: the split-step Fourier method on physical factors [184,185]. The base of numerical solution of equation according to the scheme of dividing of physical factor is the following: the material is considered as different, consecutive layers possessing different physical features, but one layer has one physical feature. The using of fast Fourier transform algorithm [186] on the dispersive step makes the method fast and economical [4].

It should be mentioned that the algorithm of dividing of physical factors along with other benefits, has the advantage of physical clarity of the mathematical procedures, which makes it convenient for the solving problems of the self-interaction of ultrashort pulses.

§2.4. Spectral domain soliton-effect self-compression

In our numerical experiments, we study the pulse and spectrum evolution during the propagation through a fiber with Kerr-nonlinearity and anomalous dispersion.

In the SMF, the pulse propagation is described by nonlinear Schrödinger equation for normalized complex amplitude of field, considering only the influence of GVD and Kerr nonlinearity [61].

$$i\frac{\partial\psi}{\partial\zeta}=\frac{1}{2}\frac{\partial^2\psi}{\partial\eta^2}+R|\psi|^2\psi \qquad (2.4.1)$$

where $\zeta = z/L_D$ is the dimensionless propagation distance, $\eta=(t-z/u)/\tau_0$ is the running time, which are normalized to the dispersive length $L_D=\tau_o^2/|k_2|$ (k_2 is the coefficient of second - order dispersion), and initial pulse duration τ_0, respectively. The nonlinearity parameter R is given by

the expression $R = L_D / L_{NL}$, where $L_{NL} = (k_0 n_2 I_0)^{-1}$ is the nonlinearity length, n_2 is the Kerr index of silica, I_0 is the peak intensity. The first and second terms of the right side of Eq. (2.4.1) describe the impact of GVD and nonlinearity, respectively. We use the split-step Fourier method during the numerical solution of the equation, with the fast Fourier transform algorithm on the dispersive step [184,185].

The combined impact of GVD and SPM leads to the formation of solitons [78,80], when the contributions of GVD and SPM balance each other. If the broadening of spectrum conditioned by SPM is occurred in shorter length of fiber than dispersive effects then $L_D > L_{NL}$ or R>1. In this case, firstly the spectrum is stretched and pulse obtains a positive chirp, which is partially compensated by negative chirp. As a result pulse is compensated [187].

We study the soliton self - SC, which occurs when the dispersive length in the fiber is shorter than the nonlinearity length ($L_D < L_{NL}$, i.e. $R < 1$). Therefore, at first the GVD stretches the pulse by acquiring a chirp. Afterwards, the accumulated impact of nonlinear SPM leads to the chirp compensation, and as a result, the spectrum becomes compressed. [4]

The subject of our research is the process of the soliton self - SC revealing its nature, peculiarities and general regulations on the basis of physical pattern of the process(Fig. 2.4.1). Simulations were carried out for initial Gaussian, secant-hyperbolic and super-Gaussian pulses.

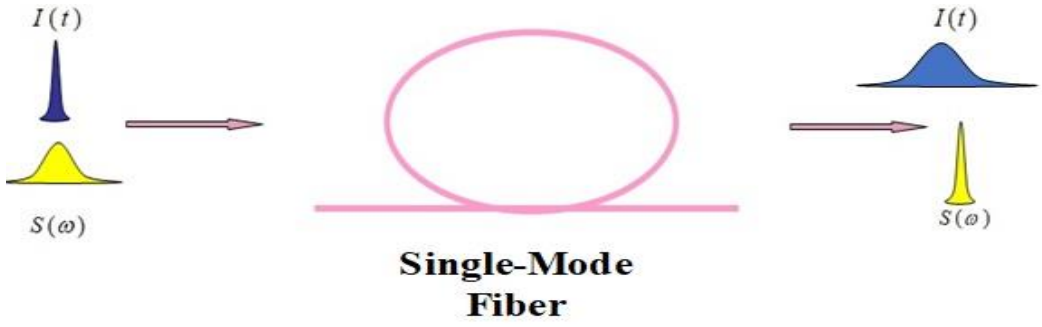

Fig. 2.4.1. *Scheme for spectral self-compression*

We have shown the soliton self - SC in the fiber "directly", without DDL, in the fiber with anomalous dispersion for different initial pulses. It is shown that there is an analogue between the processes of soliton self-compression and soliton self - SC for different initial pulses. The studies show that the periodicity of the process decreases when the nonlinearity parameter reduces. Our detailed study has shown that the frequency of compression has polynomial and exponential

approximations. We study behavior of the pulse in a fiber with negative dispersion for different values of the nonlinearity parameter and fiber length. We also investigate the features of spectral self-compression of pulses with different initial positive and negative chirp.

§2.5. Numerical results introducing the physical pattern of soliton spectral self-compression

Fig. 2.5.1 illustrates the process of propagation of Gaussian (a, b, R = 0.6) and secant-hyperbolic (c, d, R = 0.4) pulses and their spectra, where $\Omega \equiv (\omega - \omega_0)/\Delta\omega_0$ (ω is the current frequency, ω_0 is the central frequency, $\Delta\omega_0$ is the half of width of spectra on the level 1/e from peak intensity). In this case, we study the process for short fiber lengths where the efficiency of the process is high for the nonlinearity parameter values of R=0.6 (Gaussian pulse) and R= 0.4 (secant-hyperbolic pulse). It can be observed that the pulse is stretched and the spectrum is compressed in the initial propagation step. Afterwards, the width of central peak of the spectrum decreases and the main part of the pulse energy goes to the spectral satellites. At the certain fiber length, the reverse process starts the pulse self-compression.

The process can be explained in the following way: in the initial propagation step the spectrum is compressed, which leads to the decreasing of dispersion impact. As a result, the dispersive length increases, therefore, the nonlinearity parameter also increases. When the condition $R > 1$ is satisfied ($L_D > L_{NL}$), the pulse is compressed. Then, the spectrum is stretched, which leads to the increasing of dispersion impact (the decreasing of L_D and R). When the condition $R < 1$ ($L_D < L_{NL}$) is satisfied, the spectrum is compressed.

The process, which is described above has periodic character, but in the case of every next cycle, the quality of the SC is worse than in the case of the previous SC as spectral satellites increase within propagation. It can be obviously seen in Fig. 2.5.2 for the initial Gaussian and secant-hyperbolic pulses.

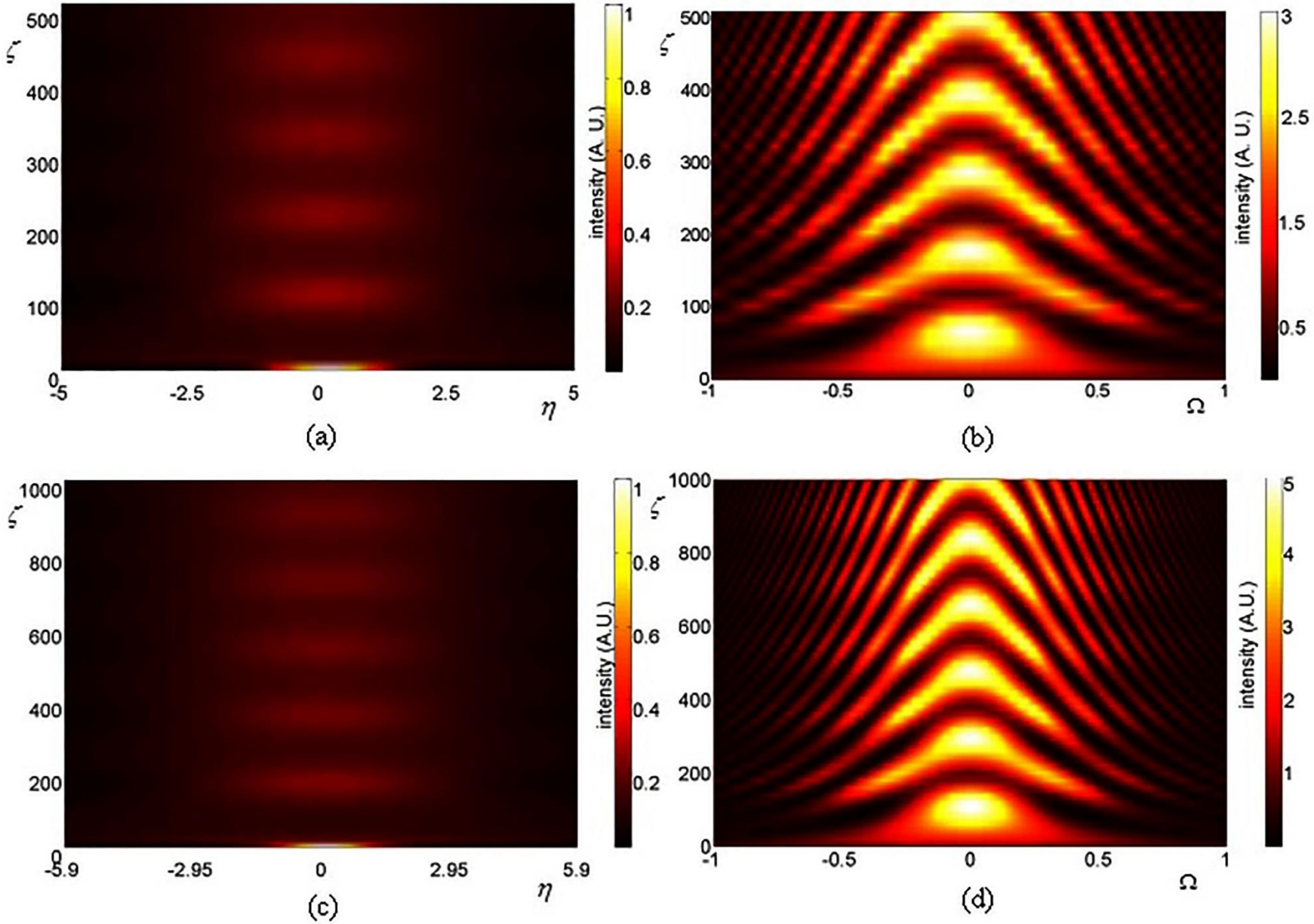

Fig. 2.5.1. *The 3D map of the propagation of Gaussian (a, b) and secant-hyperbolic (c, d) pulses and their spectra.* $\Omega = (\omega - \omega_0) / \Delta\omega_0$

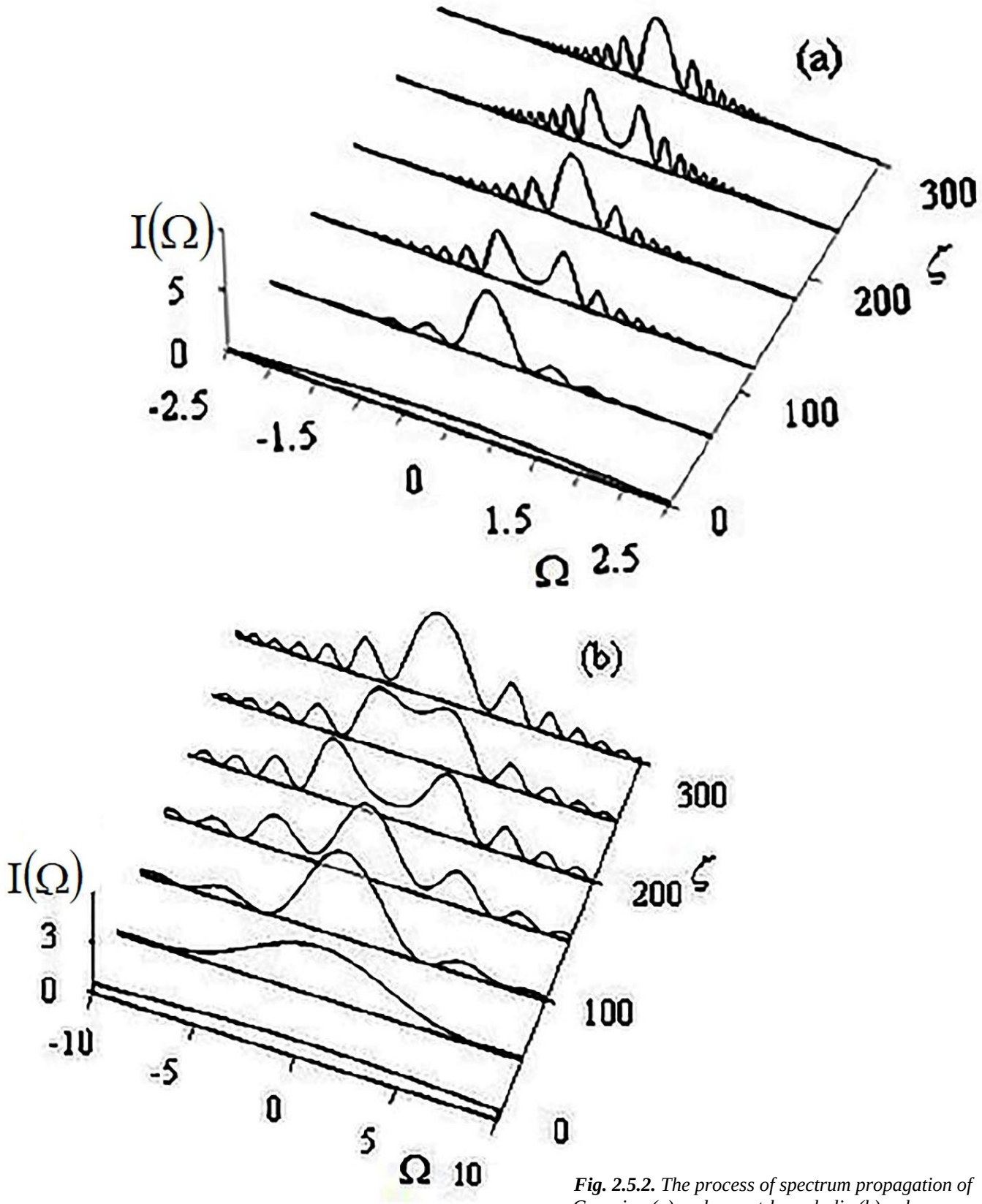

Fig. 2.5.2. *The process of spectrum propagation of Gaussian (a) and secant-hyperbolic (b) pulses.*
$\Omega = (\omega - \omega_0) / \Delta\omega_0$

Fig. 2.5.3 shows the peak value of spectra (1) and pulses (2) for initial Gaussian (a) and secant-hyperbolic (b) pulses, which shows that the process has a periodic character not only for Gaussian pulses but also for secant-hyperbolic pulses. The difference between Gaussian and secant- hyperbolic pulses is the speed of the process: as we see in Fig. 2.5.3 every next spectrum compression occurs in the short distance in the case of Gaussian pulses as compared with the case of secant-hyperbolic pulses. On Fig. 2.5.4 it is illustrated the peak value of spectra (1) and pulses (2) for initial Gaussian (a) and secant-hyperbolic (b) pulses, for fiber length up to 5000.

As we see on Fig. 2.5.3 and Fig. 2.5.4, the peak values decrease within the distance which is conditioned by the fact that the energy of spectral satellites increases.

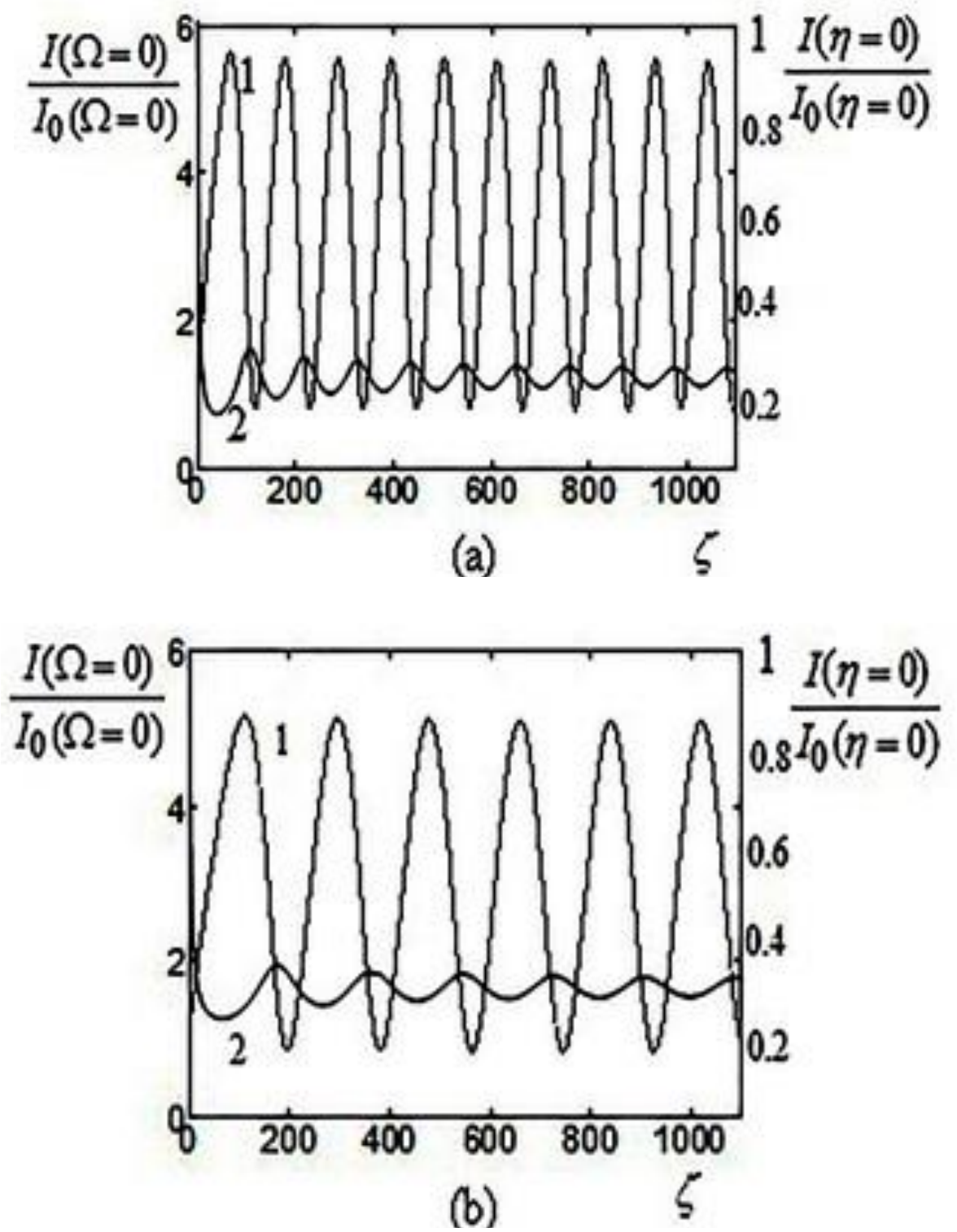

Fig. 2.5.3. *The peak values of spectra (1) and pulses (2) vs fiber length for initial Gaussian (a) and secant-hyperbolic (b) pulses (for fiber length up to 1000).*

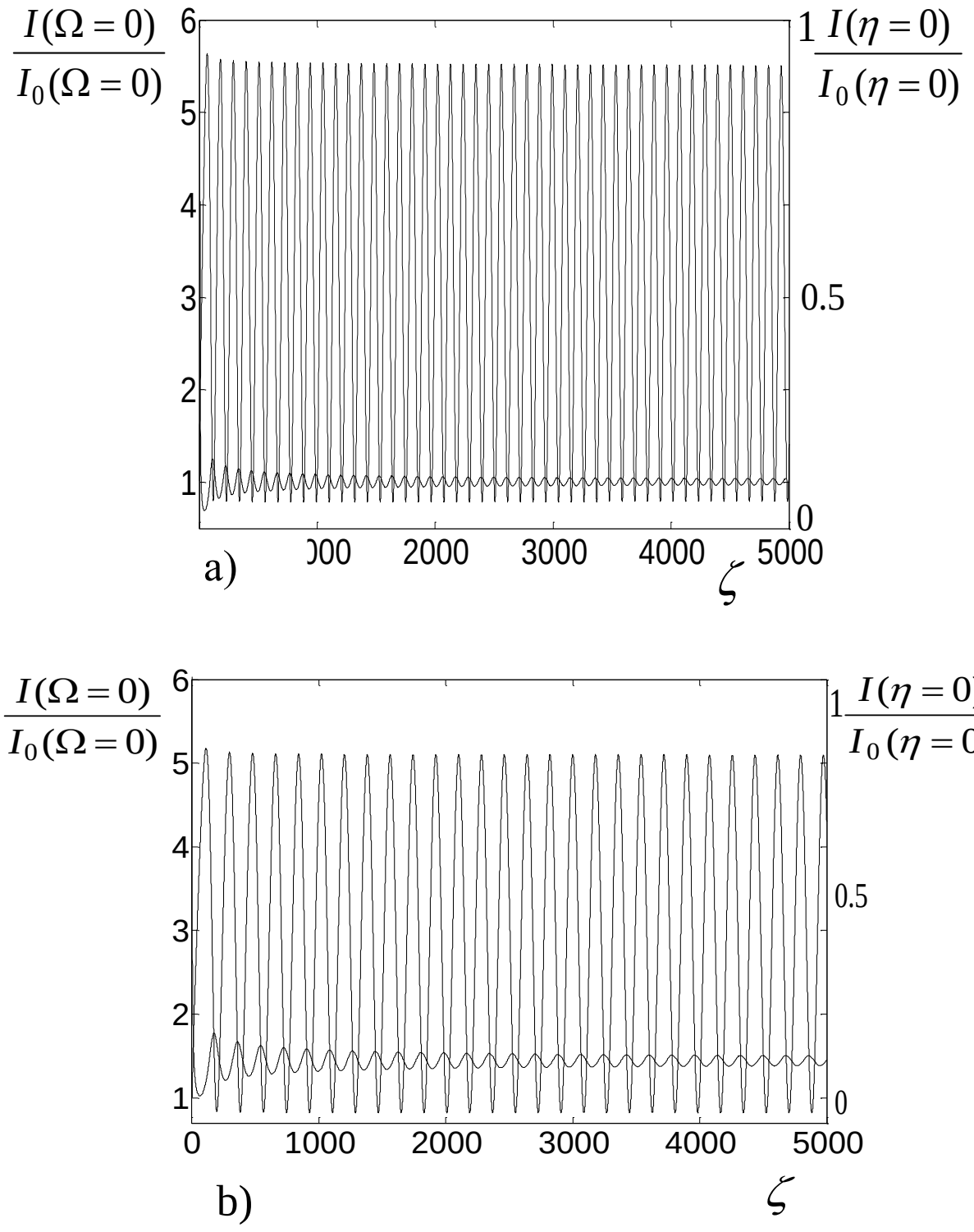

Fig. 2.5.4. *The peak values of spectra (1) and pulses (2) vs fiber length for initial Gaussian (a) and secant-hyperbolic (b) pulses (for fiber length up to 5000).*

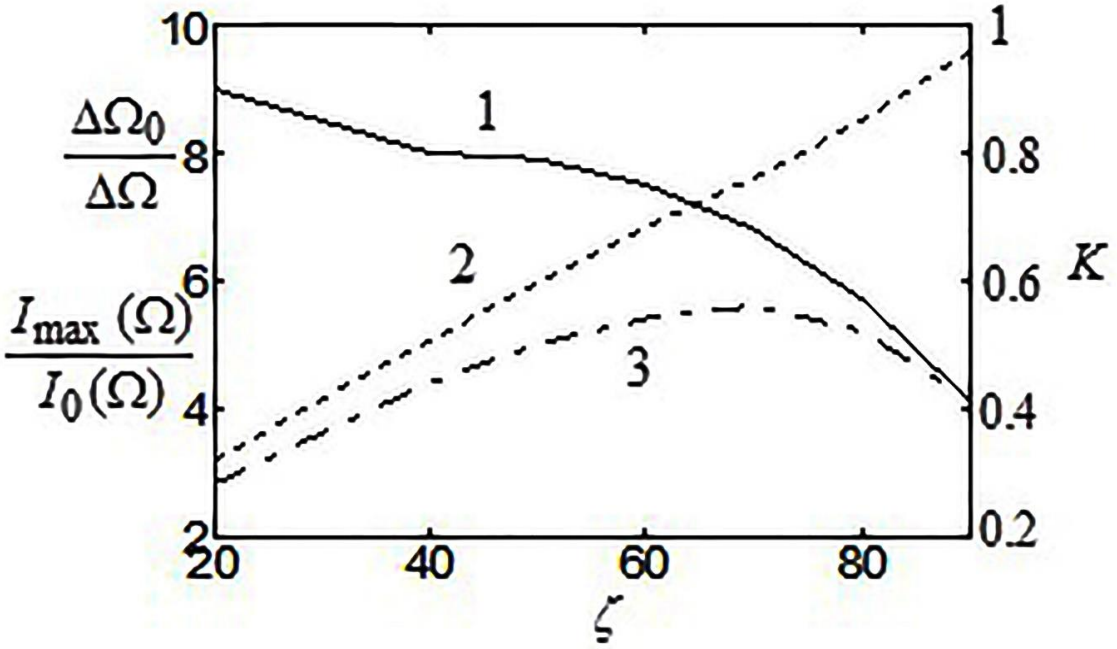

Fig. 2.5.5. *The K (1) and self - SC ($\Delta\Omega_0 / \Delta\Omega$) (2), $I_{max}(\Omega) / I_0(\Omega)$ (3) vs fiber length for initial Gaussian pulse.*

This fact is proved by the coefficient of SC quality, K, (the ratio of the energy in the central part of pulse to the whole energy) (Fig. 2.5.5). As we see in Fig. 2.5.5, the coefficient of SC quality decreases within the fiber length.

In the process of propagation, the behavior of the spectrum is similar to the pulse behavior in the case of the soliton compression. As it is known, the propagation of the high - order solitons have periodic character with a $(\pi/2)L_D$ periodicity. On the distance equal to the periodicity, at first pulse is compressed, then it is stretched taking initial shape. In our case, the spectrum has similar behavior. However, due to the incomplete cancellation of the chirp, the changing of the spectrum does not have the strict periodic character.

The process is different from soliton compression due to the fact, that spectrum changes depend on a nonlinear phase, which depends on the shape of the pulse. In the case of soliton propagation, the changes of the pulse depend on a dispersive phase, which depends on neither spectral nor temporal shape of the pulse.

The study shows that the periodicity of the SC and stretching decreases with the reduction of nonlinearity parameter (Fig. 2.5.6). It is shown that there are polynomial (Eq. (2.5.1), (2.5.2)) and

exponential (Eq. (2.5.3), (2.5.4)) approximations of the curve introducing nonlinearity parameter dependent frequency (Fig. 2.5.6), which is the frequency of the SC and stretching.

$$1/T = 1/(1.6 \cdot 10^{7} \cdot 10^{-30 \cdot R} + 7821 \cdot 10^{-4.79 \cdot R}) \quad (2.5.1)$$

$$1/T = 1/(5.09 \cdot 10^{6} \cdot 10^{-19.8 \cdot R} + 731.3 \cdot 10^{-3.83} \cdot R) \quad (2.5.2)$$

$$1/T = 1/(0.004 \cdot e^{3.08 \cdot R}) \quad (2.5.3)$$

$$1/T = 1/(0.001 \cdot e^{3.73 \cdot R}) \quad (2.5.4)$$

There is another situation for small values of nonlinearity parameter. So, in the case of R=0.25, it is formed such pulses which changes its sizes but save the shape during propagation in fiber. The investigations are done for fibers length of $\zeta \approx 17000$, in this case the ratio of soliton self-SC is 4. However, the efficiency of compression decreases within distance, and for example after $\zeta \approx 11000$ the changes of spectra equal approximately $\approx 1\%$ (Fig. 2.5.7). The reason of this is the following: the pulse large stretching (~6000 times) decrease the peak intensity of pulse which results in practical absence of the nonlinear self-interaction.

On Fig. 2.5.8 it is shown the results of numerical investigations of soliton self-SC for Gaussian ($A(t) = \exp(0.5 \cdot t/\tau_0)^2)$), secant-hyperbolic ($A(t) = \sec h(t/\tau_0)$) and super-Gaussian ($A(t) = \exp(0.5 \cdot t/\tau_0)^4$) pulses. The results correspond to the maximal value of soliton self-SC for fiber lengths up to 100. The compression ratio of Gaussian pulses is $\Delta\Omega_0 / \Delta\Omega \approx 5.9$ ($\Delta\Omega_0$ is the width of initial spectrum on half high from maximum value of intensity and $\Delta\Omega$ is the width of output spectrum), where the pulse is stretched 5.26 times for $\zeta = 50$, $R = 0.6$ (Fig. 2.5.8 a, d) [4].

The evaluation of soliton self-SC is implemented by the coefficient of SC quality, K, (the ratio of the energy in the central part of pulse to the whole energy). In the regime of the maximal soliton self-SC K equals to ≈ 0.8 for Gaussian. For secant-hyperbolic pulse the soliton self-SC ratio is ≈ 5 (Fig. 2.5.8 b, e), when $\zeta \approx 81, R = 0.4$, and for the super-Gaussian pulse the soliton self-SC ratio is (Fig. 2.5.8 c, f, $\zeta \approx 80$, $R = 0.7$)[4]. The value of K equals to 0.8 and 0.6 for the secant-hyperbolic and super-Gaussian pulses, correspondingly.

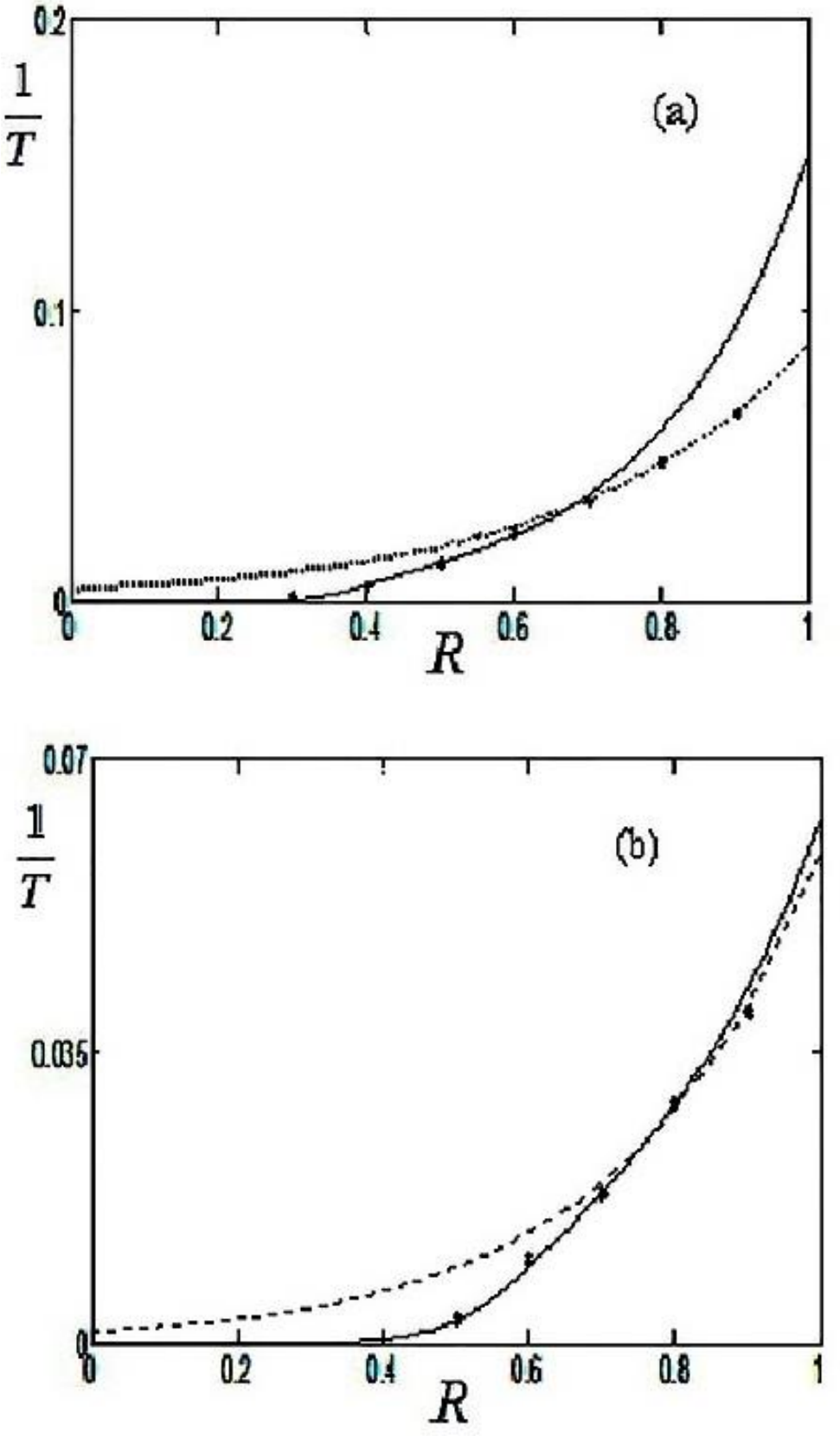

Fig. 2.5.6. *The frequency vs nonlinearity parameter for initial secant-hyperbolic (a) and Gaussian (b) pulses. The points correspond to the numerical investigations, solid lines introduce the approximation of results (Eq. (2), Eq. (3)) by all points, while the dotted lines correspond to the approximation by last 3 points (Eq. (4), Eq. (5)).*

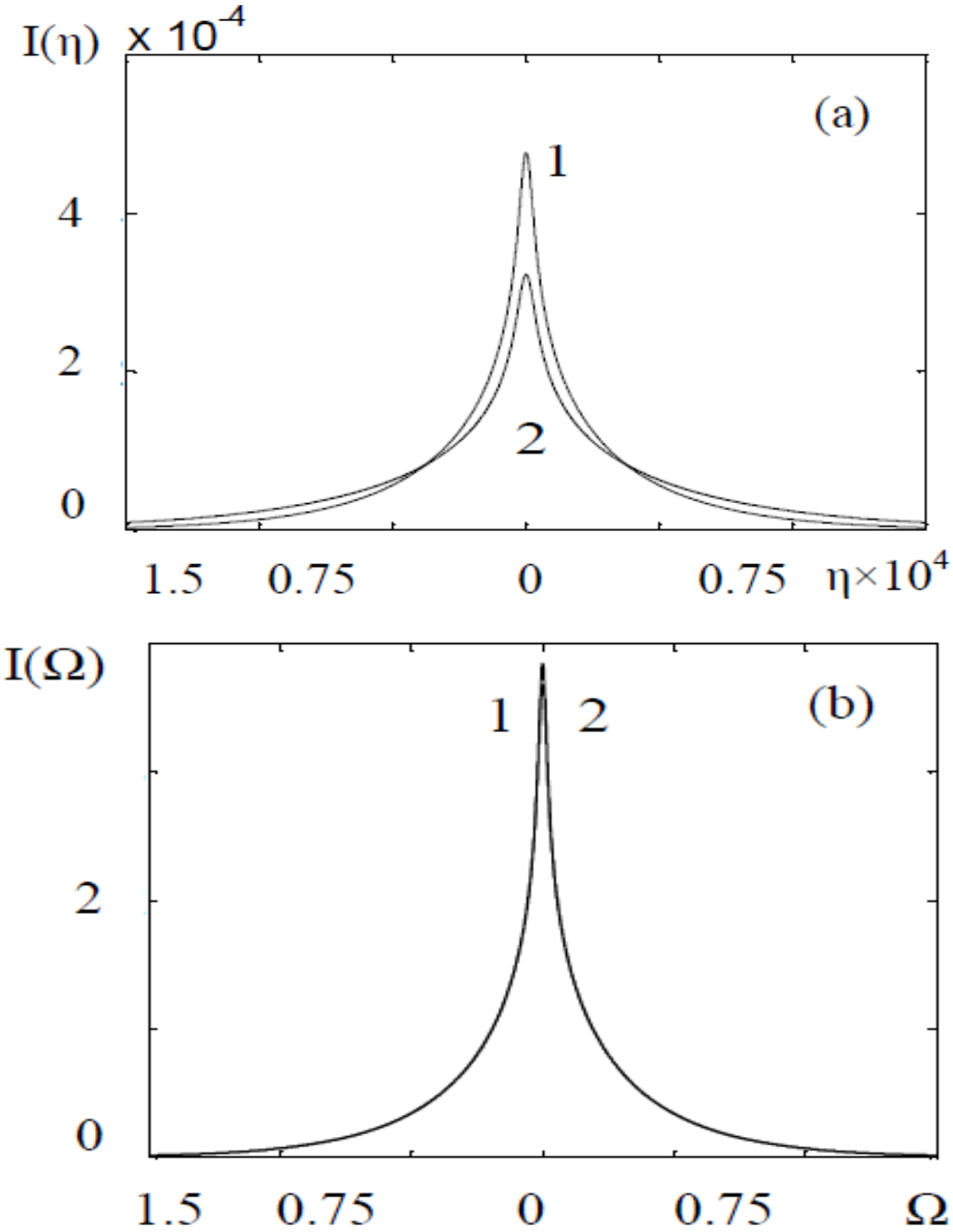

Fig. 2.5.7. *Pulses (a) and compressed spectra (b)* $\zeta \approx 11000$ *(1),* $\zeta \approx 17000$ *(2).*

We have studied also the soliton self-SC for slightly chirped pulses. The studies are carried out for the Gaussian pulses depressively stretched (1.2 times, 1.4 times, 2.2 times) and chirped (with the chirp coefficients C = 0.83; 0.7 and 0.45) in the +/- dispersive medium. The results of studies for C = -0.7 are shown in Fig. 2.5.9. In this case the SC factor is ~ 24, for R = 0.5, $\zeta \approx 700$, and $K \approx 0.3$. The same SC factor we have for the C = +0.7 and also for transform limited pulses with the parameters for R = 0.46 (adequate to the 1.4 times stretched pulse with R = 0.5), and $\zeta \approx 600$. This compassion shows that only the pulse peak intensity and spectral bandwidth are important for the process, and initial phase of pulses (with the chirp coefficients C= -0.83 to +0.83) does not impact on the process.

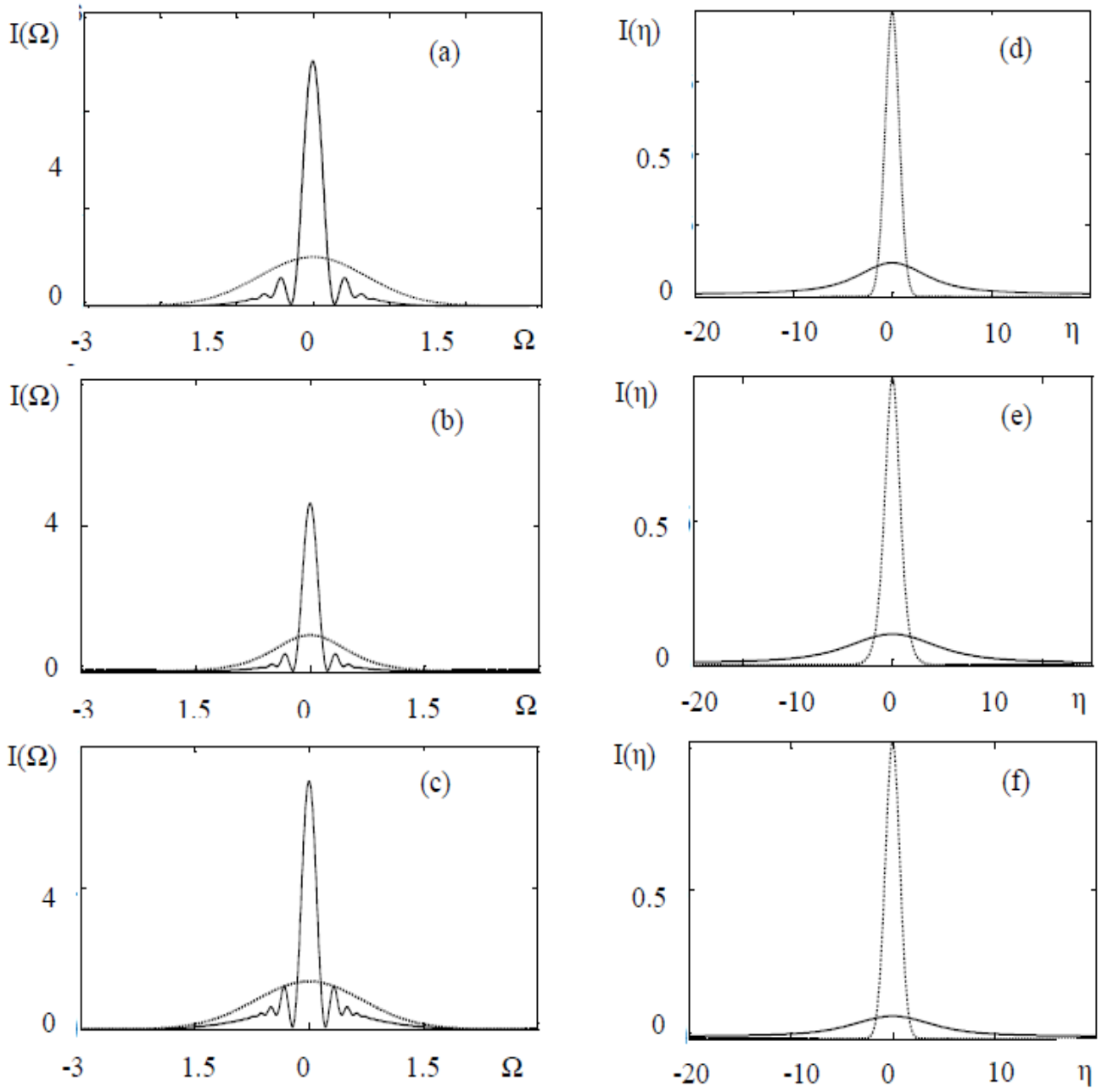

Fig. 2.5.8. *Initial (dashed line) and compressed (solid line) spectra for the initial transform-limited Gaussian (a), secant-hyperbolic (b) and super-Gaussian (c) pulses, which correspond to the case of maximal soliton self-SC, and pulses (d), (e), (f)), correspondingly[4].*

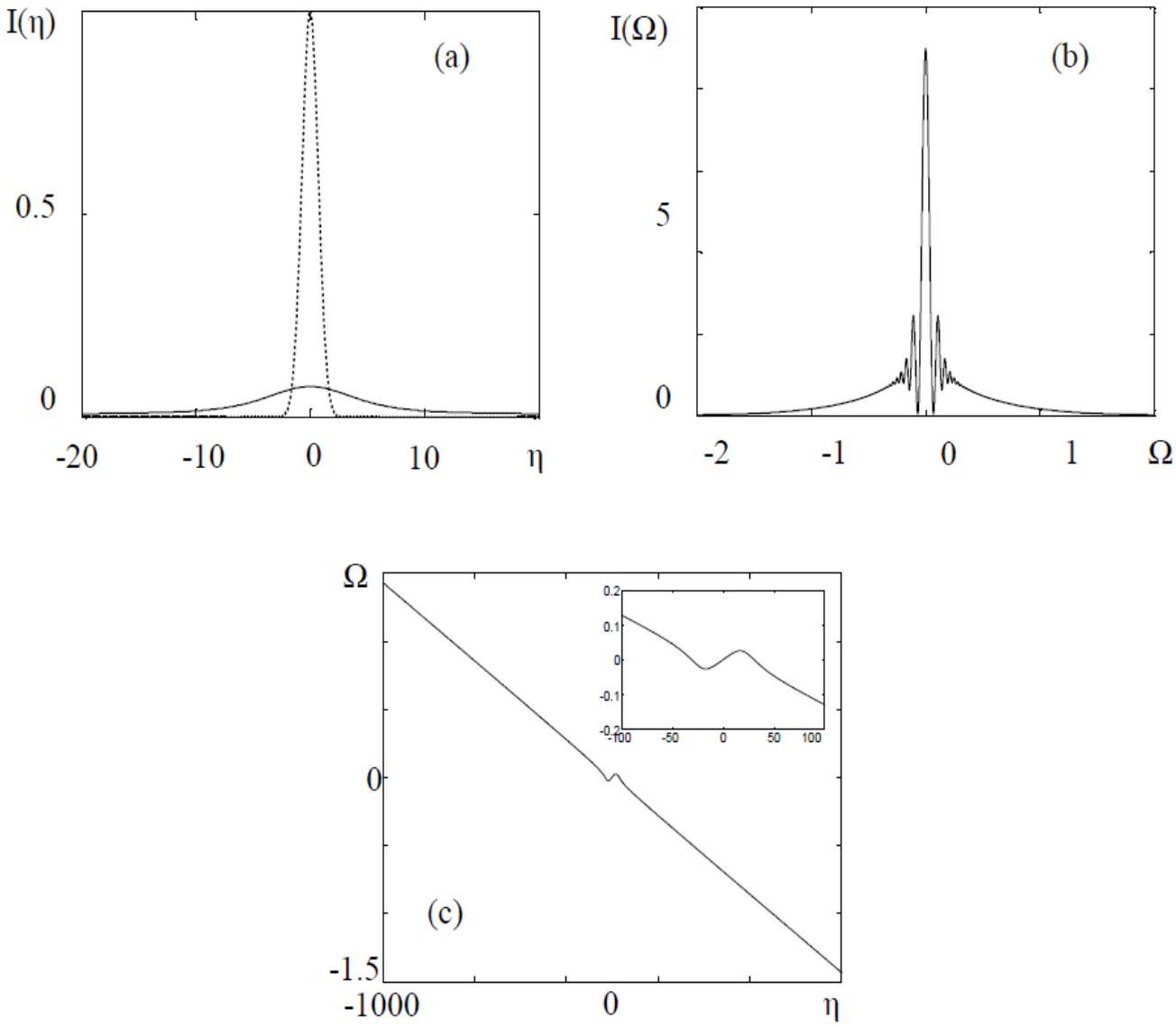

Fig. 2.5.9. *The pulse (a), spectrum(b), and chirp(c) for initially slightly chirped Gaussian pulses (stretching factor of the initial pulse is* ~ 1.4 *)*

§ 2.6. Conclusion to the chapter 2

- Our detailed study has shown the soliton spectral self-compression in the fiber "directly" with anomalous dispersion, without dispersive delay line, which occurs when the dispersive length in the fiber is shorter than the nonlinearity length ($L_D < L_{NL}$, i.e. $R < 1$). At first the group-velocity dispersion stretches the pulse by acquiring a chirp. Afterwards, the accumulated impact of the nonlinear self-phase modulation leads to the chirp compensation. As a result, the spectrum becomes compressed.

- We have demonstrated that there is an analogue between the soliton self-compression and soliton spectral self-compression processes: soliton spectral self-compression has periodic character. However, due to the incomplete cancellation of the chirp, the changing of the spectrum does not have the strict periodic character, that is the process is not completely similar to the soliton compression. It is conditioned by the fact that spectrum changes depend on a nonlinear phase which depends on the shape of the pulse. In the case of soliton propagation, the changes of the pulse depend on a dispersive phase which depends on neither spectral nor temporal shape of the pulse.

- We show that the periodicity of the process decreases when the nonlinearity parameter is reduced. We have shown that the frequency dependence on the nonlinearity parameter has polynomial and exponential approximations.

- Our studies carried out for the Gaussian, secant-hyperbolic, and super-Gaussian pulses, in the range of parameters R=0.25 to 1 and $\zeta \approx 1$ to 20000, show up to 30 times spectral self-compression ratio.

- For small values of nonlinearity parameter, such pulses are formed which change their sizes but save the shape during propagation in fiber with great length ($\zeta \approx 17000$). The research also shows that the changes of spectrum slow dawn for fibers with large lengths (approximately $\zeta \approx 11000$). The reason for this is the following: due to the large stretching of the pulse (~6000 times), the peak intensity of pulse decreases resulting in the practical absence of the nonlinear self-interaction.

- The coefficient of the soliton spectral self-compression quality decreases when the fiber length increases. This is conditioned by the fact that the energy of spectral satellites increases during propagation in the fiber.
- The studies for the initially slowly +/- chirped pulses (with the chirp coefficients C = -0.83 to +0.83) show that only the pulse peak intensity and spectral bandwidth are important for the process, and initial phase of pulses does not impact to the process.

CHAPTER 3

THE IMPACT OF ASYMMETRY AND COHERENCY ON THE PROCESS OF PULSE AND SPECTRAL COMPRESSIONS

§3.1. Introduction

The results of this chapter are based on the publications [26-31].

The interest in the nonlinear-dispersive similariton is conditioned by the wide range applications related to the problems of signal analysis and synthesis in ultrafast optics and photonics, such as temporal and spectral compression, fine frequency tuning and different methods characterizing ultrashort pulses. One of the interesting and practical important application is the temporal compression of optical pulses, in this case the positive phase obtained in the fiber due to the SPM is compensated via DDL with the negative GVD [1,2]. In the fiber the spectral width of pulse is stretched and the compensation of phase obtained in DDL leads to the formation of shorter pulse.

Usually the compression is implemented in such circumstances, when the impact of dispersion in fiber is small [1,2] which is conditioned by the fact that dispersion leads to the stretching of pulse and intensity decreasing which prevent the required stretching of spectrum. However, in such regime the phase of pulse can have quite complex shape after fiber and it cannot be completely compensated in DDL.

From this point of view it is preferable such regime of compression when it is formed the similariton in fiber, as the linear chirp of similariton (the parabolic phase) gives the opportunity to compensate the chirp in DDL and reach the effective temporal compression.

The compression of pulse up to few tens or the units of femtosecond has practical interest due to their applications in science, engineering, medicine and etc. For the obtaining such short pulses it is needed to generate similariton with spectral width up to several tens THz in fiber.

For similaritons with such wide spectrum, the role of third-order dispersion (TOD) is substantial, which can lead to the limitation of compression efficiency [4]. In the following paragraph it is studied the opportunities of temporal compression of nonlinear-dispersive similariton and the impact of TOD on pulse compression [26,4].

§3.2 Optimization of Femtosecond Pulse Compression by Pulse Asymmetry Management

The technique of pulse compression, which provided transition to the femtosecond time scale in the 80s, is of interest till now, despite the achievements of contemporary ultrafast laser technology. In the systems of pulse compression, the positive parabolic phase obtained in a normally dispersive single-mode fiber (SMF) is compensated by the negative phase obtained in a dispersive delay line (DDL) [170, 2]. However, on the femtosecond time scale the high-order nonlinear and dispersive effects are substantially limiting the pulse compression ratio, and the impact of residual TOD at the system output is the most substantial among all high-order effects. In [13], the residual phase compensation is carried out using the fact that the signs of TOD in fiber and prism DDL are opposite. However, such phase compensation limits the parameters of fiber and DDL, and thus, the compression ratio.

The TOD compensation is possible to implement with the help of nonlinearity [101,102]. In [101], it was shown that nonlinear phase shift and TOD can compensate each other in short-pulse fiber amplifiers. The nonlinear phase shift accumulated in the amplifier can be compensated by the TOD of the combination of a fiber stretcher and grating compressor.

In this paper, we show that it is possible to compensate the TOD via shaping of asymmetric pulses at the system input. Due to the fiber nonlinearity, the pulse obtains a phase depending on its initial intensity $I_0(t)$. This allows to control its phase at the end of the fiber by the initial pulse intensity. This approach of the use of asymmetric pulses has improved the efficiency of pulse compression, as compared to the compression of regular pulses.

Numerical Studies and Results

The pulse compressor consists of SMF and DDL [170, 2]. In SMF, the pulse obtains a positive phase and its spectrum expands due to self-phase modulation. This phase should be compensated by the negative parabolic phase obtained in the DDL; as a result, the pulse is compressed. Maximum pulse compression is achieved when transform-limited pulses are obtained. However, for short pulses, the high-order nonlinear and dispersive effects limit the pulse compression ratio substantially. The influence of the TOD is the most substantial among all high-order effects.

In the SMF, the pulse propagation is described by nonlinear Schrödinger equation 170]:

$$i\frac{\partial\psi}{\partial\zeta} = -\frac{1}{2}\frac{\partial^2\psi}{\partial\eta^2} + R|\psi|^2\psi + i\frac{\mu_{TOD}}{6}\frac{\partial^3\psi}{\partial\eta^3} \qquad (3.2.1)$$

where $\zeta = z/L_D$ is the dimensionless propagation distance, $\eta = (t - z/u)/\tau_0$ is the running time, which are normalized to the dispersive length $L_D = \tau_o^2/|k_2|$, and initial pulse duration τ_0, respectively (k_2 is the coefficient of second - order dispersion). The nonlinearity parameter R is given by the expression $R = L_D / L_{NL}$, where $L_{NL} = (k_0 n_2 I_0)^{-1}$ is the nonlinearity length, n_2 is the Kerr index of silica, I_0 is the peak intensity. The first and second terms of the right side of Eq. (3.2.1) describe the impact of GVD and nonlinearity, respectively. The third term describes the impact of TOD. Pulse propagation in DDL is described by Eq. (3.2.1) when *R* = 0.

We have used the split-step Fourier method during the numerical investigation of Eq. (3.2.1), which describes the pulse propagation in a fiber-DDL system, with the fast Fourier transform algorithm on the dispersive step.

As it was mentioned above, in case of symmetric pulses, TOD limits the pulse compression ratio substantially. Fig. 3.2.1 illustrates the results of numerical studies on the compression of a Gaussian pulse. It shows the initial (dotted line) and compressed (solid line) pulses (a), corresponding spectra (b) and the derivative of the spectral phase ($\phi'(\Omega)$, c) of the compressed pulse. As one can see, the compression is not effective: the compressed pulse has many satellites and the compression ratio is less than the spectral broadening coefficient ~3 times. The figures correspond to the case of maximum pulse compression, which was obtained when the parameter of nonlinearity was *R* = 50, the fiber and the DDL lengths were both $\sim 5L_D$. The maximum value of pulse compression was ~3, when the spectrum was broadened ~10 times [4].

Low compression efficiency is conditioned by the incomplete cancellation of phases, which are obtained in fiber and DDL. The incomplete cancellation of phases is a result of the TOD contribution in DDL and fiber. Due to the opposite signs of the TOD of the prism DDL and the fiber [188], it is possible the implementation of such regime, when phases cancel each other [13].

In fiber, due to combined impact of dispersion and self-phase modulation, the pulse obtains the spectral phase $\phi_f(\omega, z) = \phi_f^{(2)}(\omega, z) + \phi_f^{(3)}(\omega, z)$ where $\phi_f^{(2)}(\omega, z) = -k_2^f z\omega^2/2$ [189]

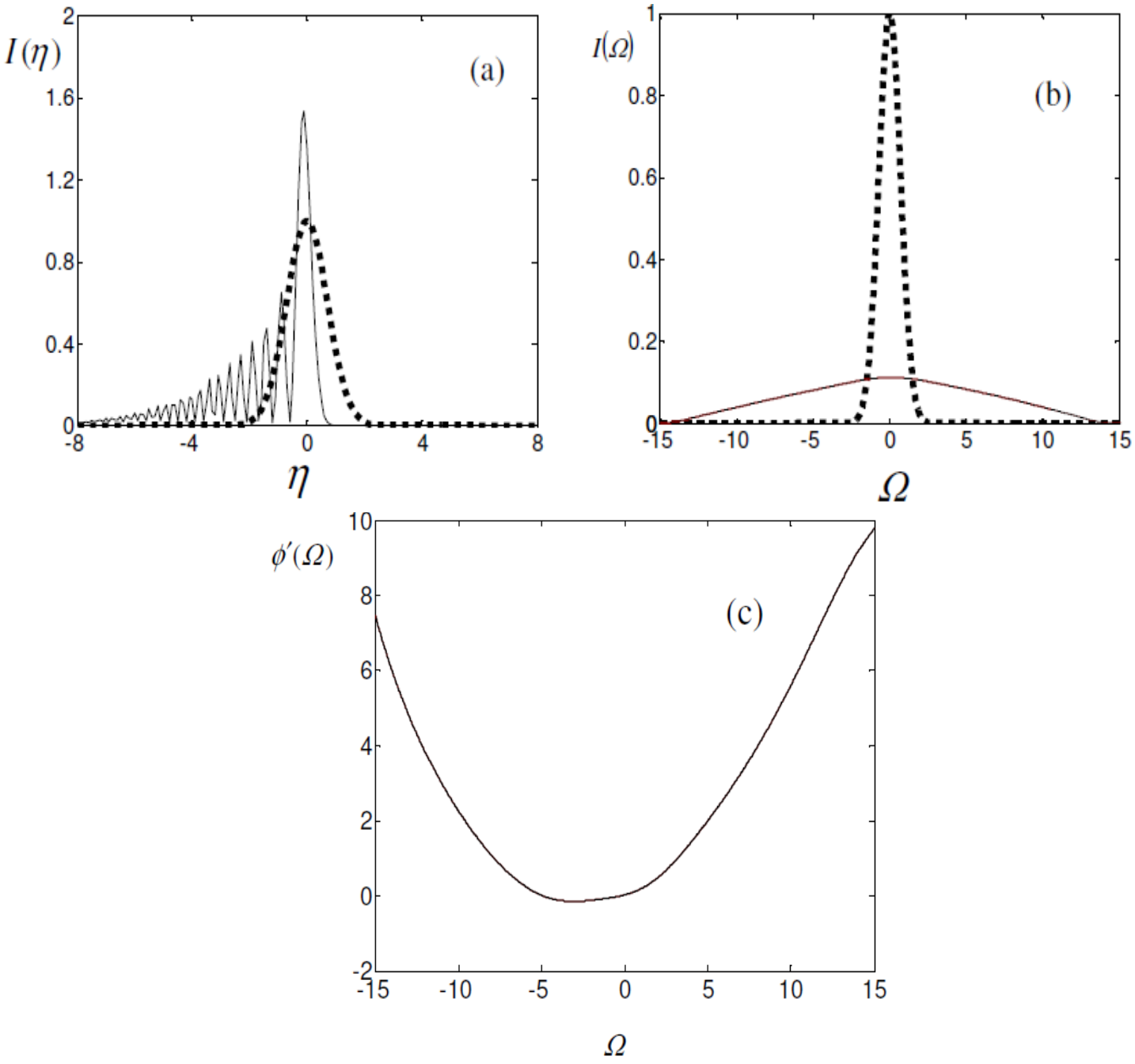

Fig. 3.2.1. *(a) Initial (dotted line) and compressed (solid line) pulses, (b) corresponding spectra, and (c)* $\phi'(\Omega)$ *for Gaussian pulse. The spectral broadening ratio ~10 and the pulse compression ratio ~3.*

$$\Omega = (\omega - \omega_0)/\Delta\omega_0$$

$\phi_f^{(3)}(\omega, z) = -\phi'''(\omega)|_{\omega=\omega_0}\ \omega^3/6$. Since self-phase modulation is conditioned by the pulse intensity, in case of asymmetric pulses the asymmetry in the phase is caused not only by TOD but also by the self-phase modulation. This allows to control the phase of the pulse at the fiber output by the initial pulse intensity, and to achieve effective pulse compression. The numerical studies were implemented for pulses with different asymmetries.

Fig. 3.2.2 shows the initial (dotted line) and compressed (solid line) pulses (a), corresponding spectra (b), and $\phi'(\Omega)$ (c) in case of the initial asymmetric pulse. The figures correspond to the maximum pulse compression, which was achieved when the parameter of nonlinearity was R = 20, the fiber length was $5L_D$, and the DDL length was $5.4L_D$. The maximal value of the pulse compression was ~20 in case when the spectrum was broadened ~26 times [4, 26].

As one can see from Fig. 3.2.2, the quality of the pulse compression is better than that of Fig. 3.2.1 (the compressed pulse has less satellites): the compression efficiency is also higher.

In Fig. 3.2.3, initial (dotted line) and compressed (solid line) pulses (a), corresponding spectra (b), and $\phi'(\Omega)$ (c) for another asymmetric pulse are depicted. In this case, the maximal value of pulse compression was ~10, when spectrum was broadened 10 times [4, 26].

The chirp is practically constant at the central energy-carrying part of the compressed pulse, which means that the pulse is approximately transform-limited. Fig. 3.2.3 corresponds to the case of maximum pulse compression, which was obtained when the parameter of nonlinearity was R = 7, the fiber length was $5L_D$, and the DDL length was $\approx 5.6L_D$ [4].

We show that via initial asymmetric pulses it is possible to compensate the impact of TOD in fiber and in DDL which allows reaching the effective pulse compression with the ratio of compression equals to the ratio of spectral compression.

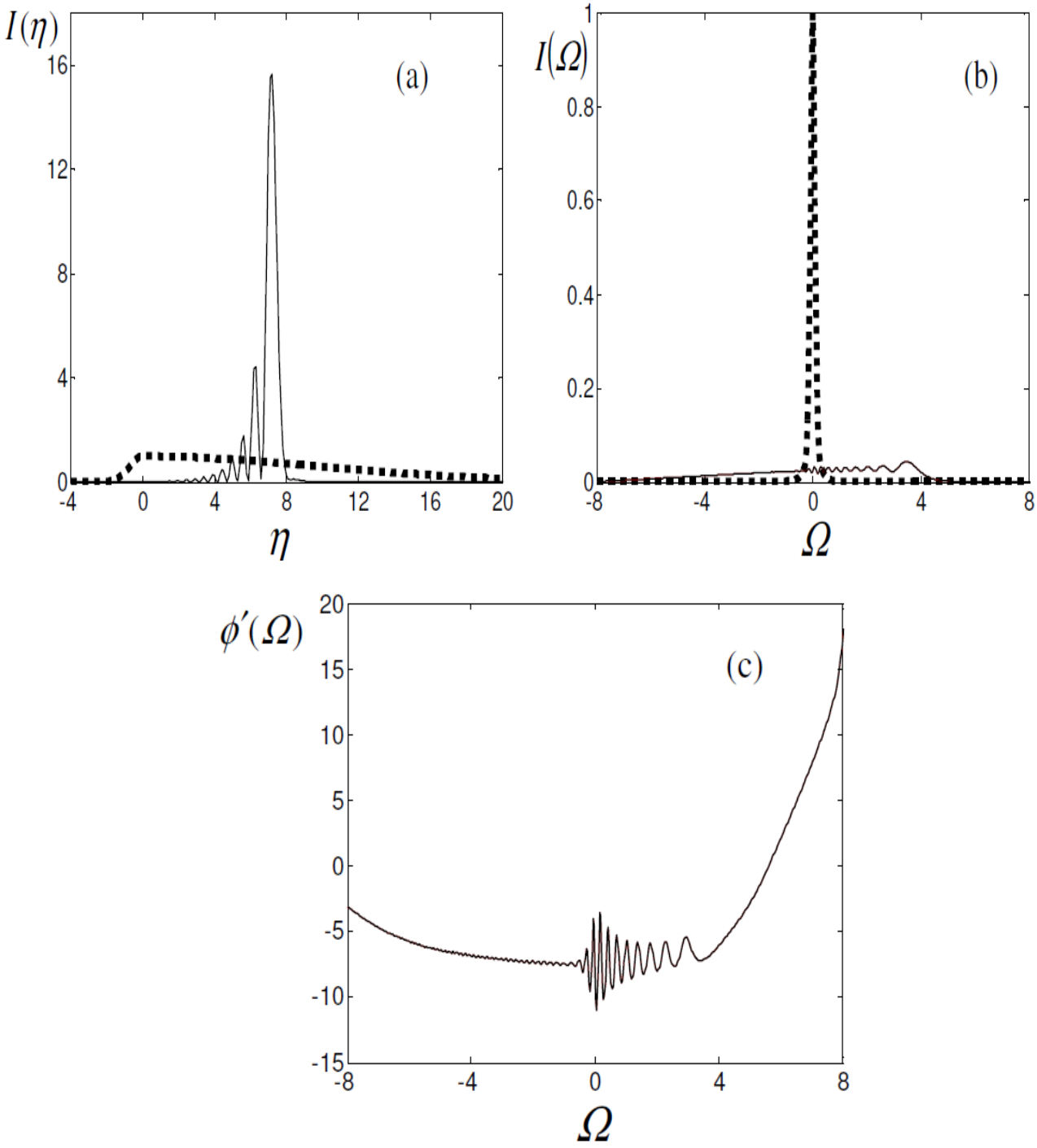

Fig. 3.2.2. *(a) Initial (dotted line) and compressed (solid line) pulses, (b) corresponding spectra, and (c)* $\phi'(\Omega)$ *for asymmetric pulse. Spectral broadening ratio ~ 26 and pulse compression ratio ~20.* $\Omega = (\omega - \omega_0)/\Delta\omega_0$.

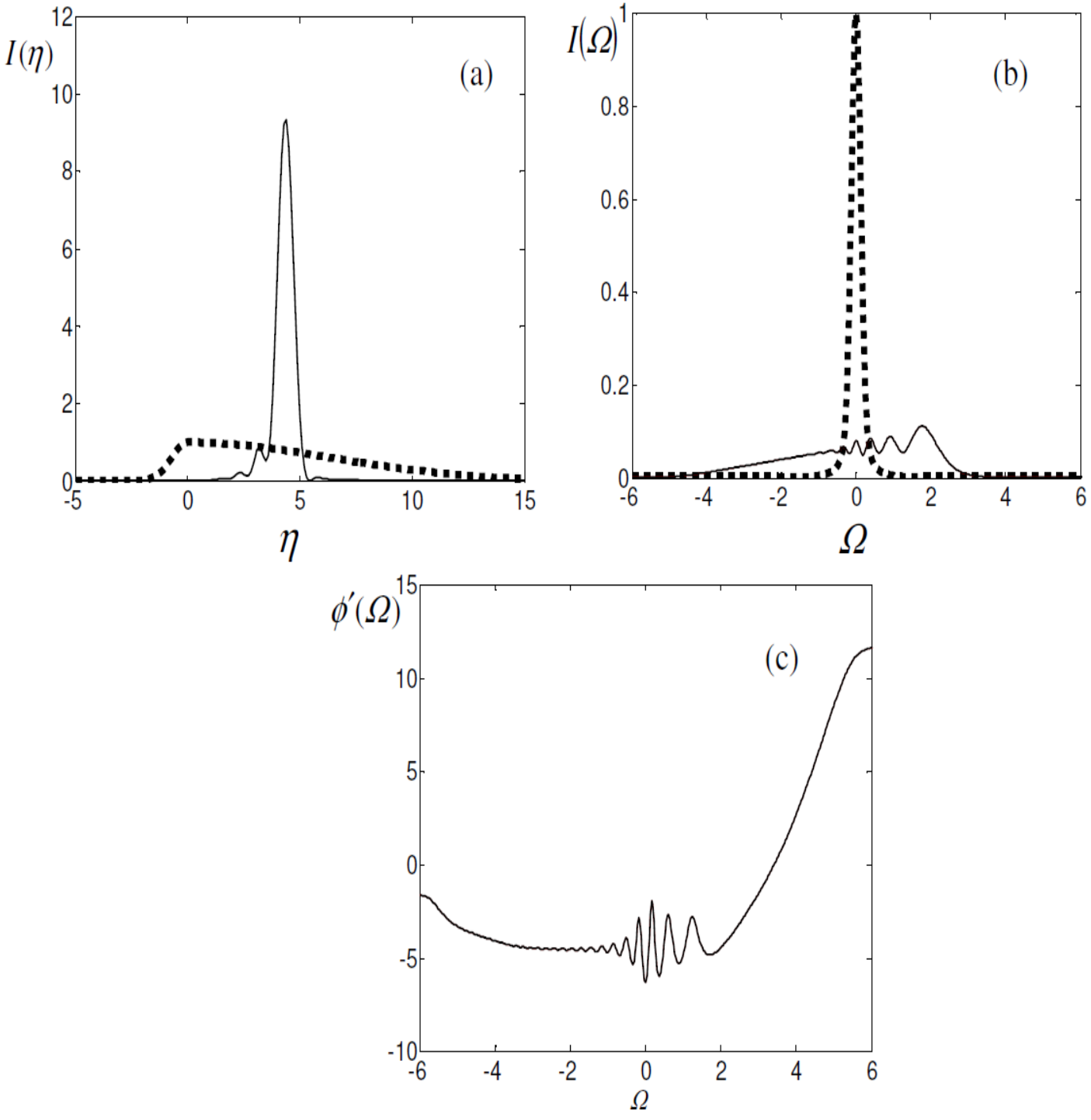

Fig. 3.2.3. *(a) Initial (dotted line) and compressed (solid line) pulses, (b) corresponding spectra, and (c)* $\phi'(\Omega)$ *for asymmetric pulse. Spectral broadening ratio ~10 and pulse compression ratio ~10.* $\Omega = (\omega - \omega_0)/\Delta\omega_0$.

§3.3 Impact of Coherency on the Process of Spectral Compression of Randomly Modulated Pulses

Advance in ultrafast optics, photonics, laser physics and, especially, in optical communication transfers the noise suppression and filtering problem from radio-physics to optics, stimulating the studies of self-interaction of randomly modulated optical signals. The nonlinear process of spectral compression (SC), based on self-interaction of optical pulses, initially stretched and chirped in a dispersive medium [190], is of special interest on this view [191]. The spectral compressor consists of prism compressor, as a dispersive delay line (DDL), where the pulse is stretched and negatively chirped, and single-mode fiber (SMF), where nonlinear self-phase modulation leads to the chirp compensation and spectral narrowing [192,193]: the phase induced by nonlinear self-phase modulation in SMF compensates the negative phase of the pulse obtained in a DDL. The SC process has numerous interesting applications in ultrafast optics and laser technology [194-200]. The spectral temporal imaging of ultrashort pulses through Fourier transformation in the SC systems, and fine frequency tuning along with SC are demonstrated [194]. Applying of SC is proposed in a fiber laser instead of strong spectral filtering to benefit the laser's power efficiency and obtain transform-limited pulses [199]. The urgent applications demand the development of new effective SC systems, and the process efficiency improvements by means of amplitude modulation of signal at the system entry are demonstrated [201].

In this work the SC process for randomly modulated pulses in view of the noise nonlinear suppression and filtering is studied. Particularly, the impact of signal coherency on the SC process based on numerical solution of nonlinear Schrödinger equation for signals with different coherence time is numerically studied.

The mathematical modeling of the process

In the SMF, the pulse propagation is described by nonlinear Schrödinger equation for normalized complex amplitude of field, considering only the influence of GVD and Kerr nonlinearity [61].

$$i \cdot \frac{\partial \psi}{\partial \zeta} = -\frac{1}{2} \cdot \frac{\partial^2 \psi}{\partial \eta^2} + R|\psi|^2 \psi \qquad (3.3.1)$$

where $\zeta = z/L_D$ is the dimensionless propagation distance, $\eta = (t - z/u)/\tau_0$ is the running time, which are normalized to the dispersive length $L_D = \tau_o^2/|k_2|$ (k_2 is the coefficient of second - order dispersion), and initial pulse duration τ_0, respectively. The nonlinearity parameter R is given by the expression $R = L_D / L_{NL}$, where $L_{NL} = (k_0 n_2 I_0)^{-1}$ is the nonlinearity length, n_2 is the Kerr index of silica, I_0 is the peak intensity. The first and second terms of the right side of Eq. (3.3.1) describe the impact of GVD and nonlinearity, respectively. The split-step Fourier method during the numerical solution of equation with the fast Fourier transform algorithm on the dispersive step is used. Pulse propagation in DDL is described by Eq. (3.3.1) when *R* = 0.

The initial pulses with random amplitude modulation are formed by the model of additive noise [202], and for Eq. (3.3.1) the initial conditions are given as follows:

$$\psi(0,\eta) = \psi_0(\eta) + \sigma\xi(\eta) \tag{3.3.2}$$

Here ψ_0 is the regular component of normalized amplitude, $\xi(\eta)$ is the stationary noise with a Gaussian correlation function, and σ is its amplitude.

§3.4 Numerical Studies and Results for the Spectral Compression of Randomly Modulated Pulses

The statistic parameters of radiation are determined by sampling of a large number realizations (*N* =100), which are solutions of Eq. (3.3.1). The studies are carried out for signals with the same value of the noise component amplitude ($\sigma = 0.6$) and different coherence time (τ_c). On Fig. 3.4.1 two examples of the randomly modulated initial pulses are shown with correlation times $\tau_c = 0.75$ (a) and $\tau_c = 0.17$ (b). A randomly modulated optical signal with higher coherency (a) has a smoother shape than signal with a lower coherency (b). The period of oscillation is given by the coherence time, and their amplitude is given by the amplitude of noise component.

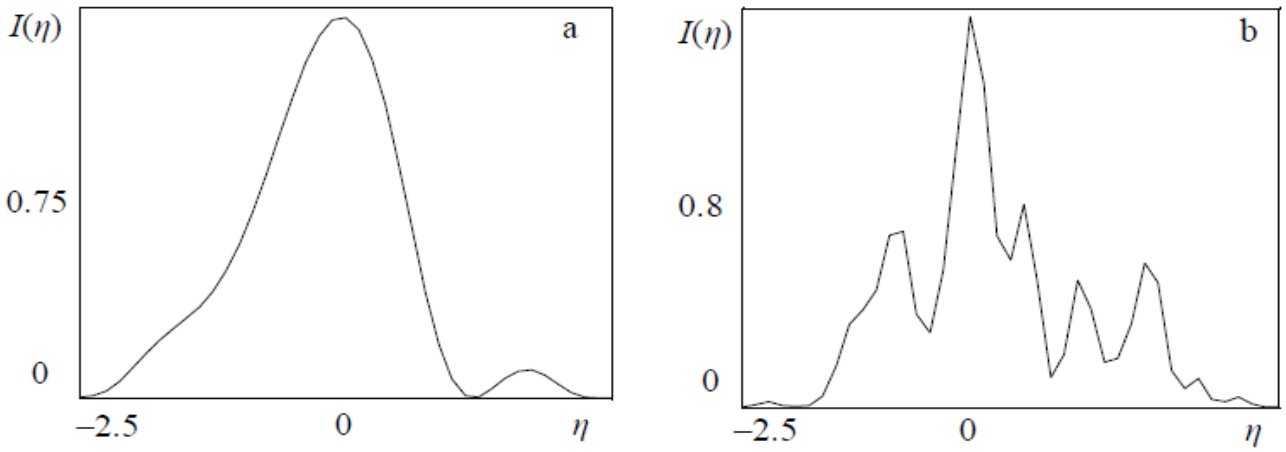

Fig. 3.4.1. *Two realizations of randomly modulated pulses with the coherence time 0.75 (a) and 0.17 (b).*

In Fig. 3.4.2 compressed spectra and corresponding pulses for the SMF length f =7 and DDL length d =14 are shown. The lines 1–5 correspond to the τ_c = 0.75, 0.5, 0.33, 0.25 and 0.17 values of coherence time, respectively.

As in Fig. 3.4.3 is shown, the SC ratio increases with decreasing of the initial signal coherency. This can be explained in the following way: a signal with the shorter coherence time, i.e. the wider spectrum, is stretching more rapidly in DDL, and the amplitude of random oscillations during the signal is decreasing and such a signal is spectrally compressed more efficiently in the fiber. The maximal value of the SC was 4.27 (Fig. 3.4.3). For comparison, SC for the regular Gaussian pulse in the system with the same parameters is implemented (f = 7, d = 14, Fig. 3.4.4). The maximal SC ratio is 5.9 for such a regular Gaussian pulse.

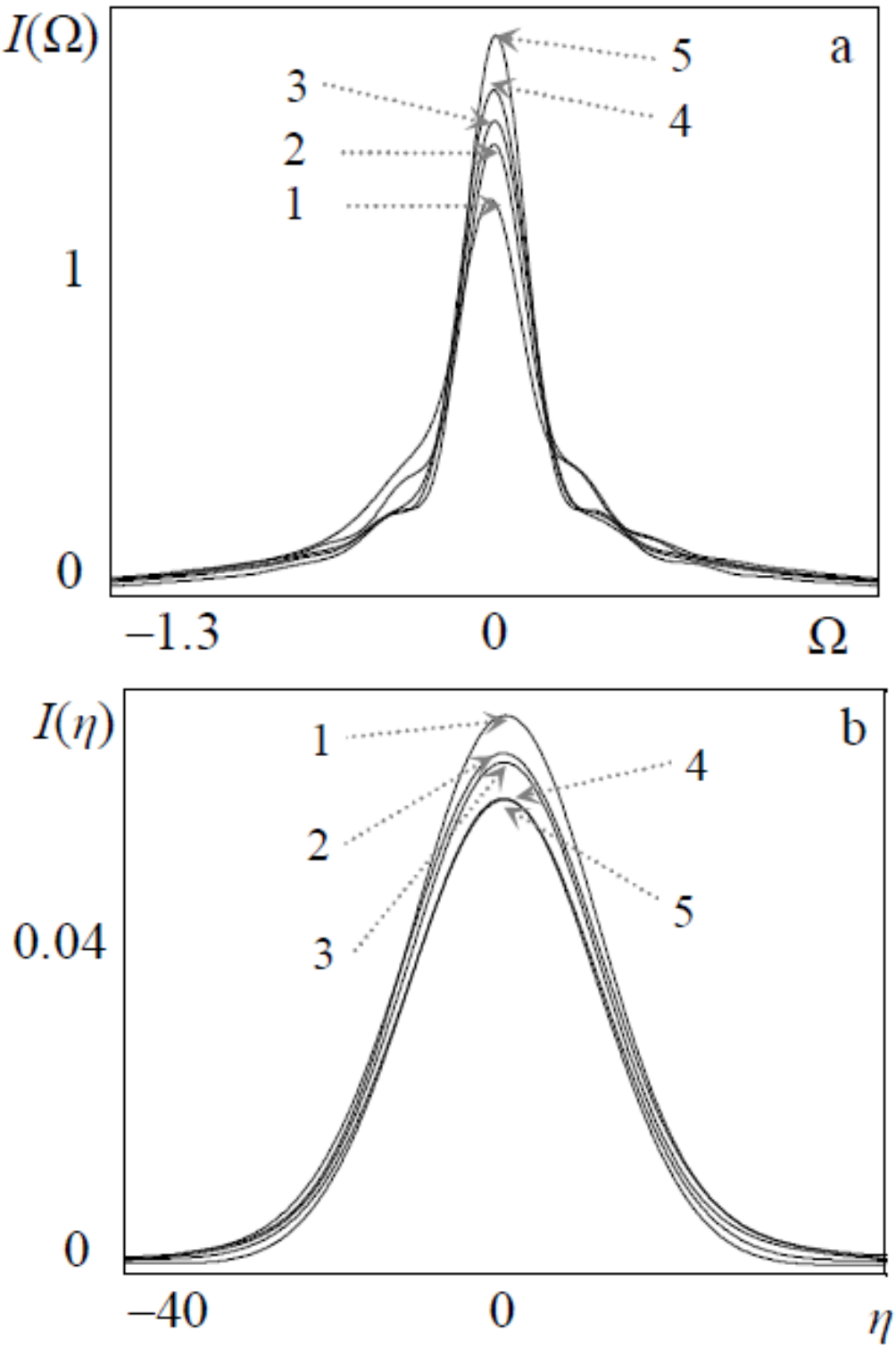

Fig. 3.4.2. *Average spectra (a) and pulses (b) of spectrally compressed randomly modulated signals with different coherence time N = 100, f = 7, d = 14.*

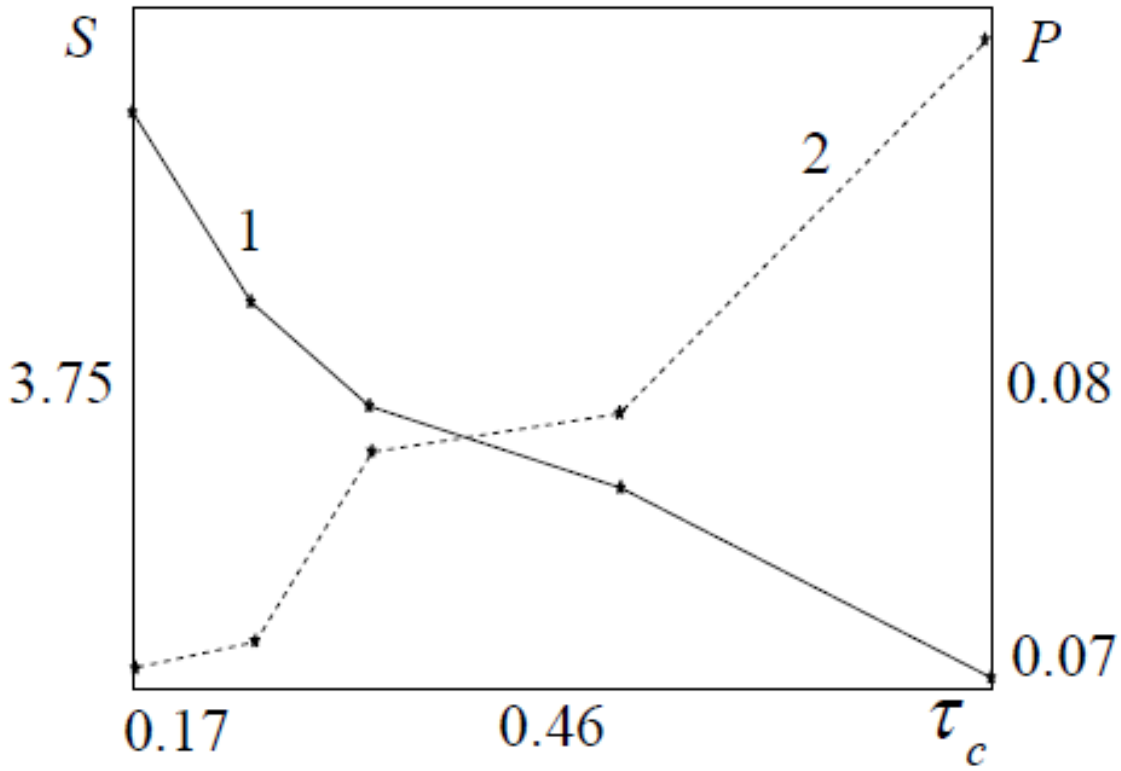

Fig. 3.4.3. *The SC factor* $S = I_{in}(\Omega = 0)/I_{out}(\Omega = 0)$ *(1) and pulse stretching factor* $P = I_{out}(\eta = 0)/I_{in}(\eta = 0)$ *(2) ratios vs coherence time for randomly modulated optical signal. Parameters of SC system and radiation: fiber length f = 7, DDL length d = 14, N = 100,* $\sigma = 0.6$.

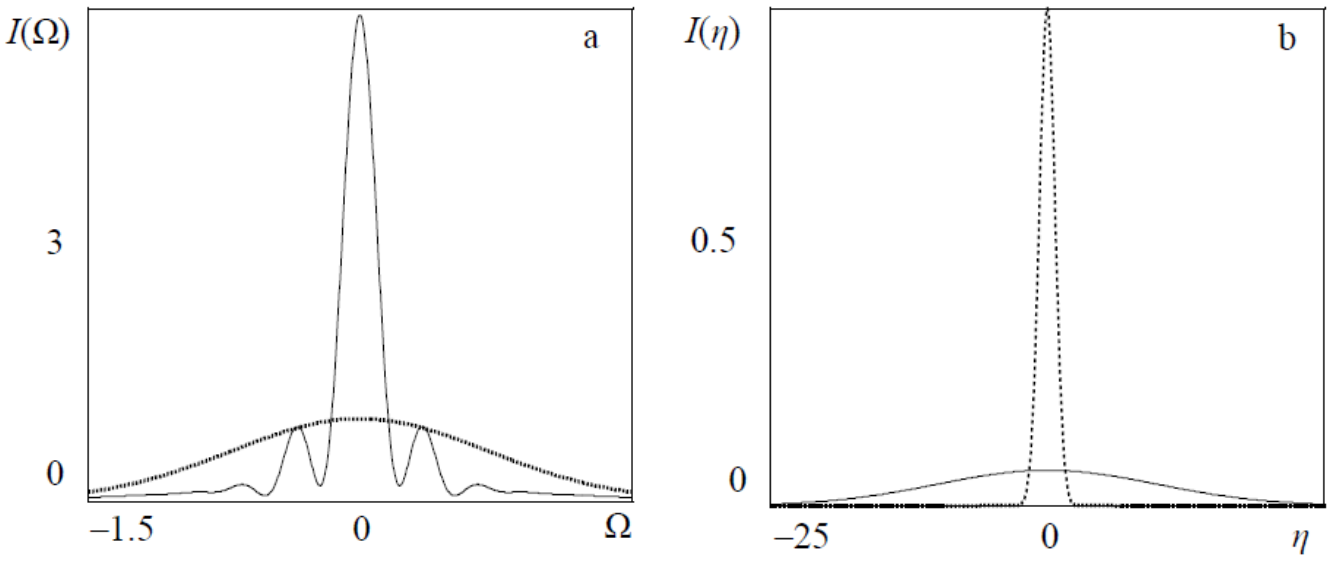

Fig. 3.4.4. *Initial (dashed line) and compressed (solid line) spectra (a), and corresponding pulses (b) for regular Gaussian signal. The maximum value of SC was = 5.9 (f = 7, d = 14).*

§3.5 Spectral Self-Compression of Randomly Modulated Pulses

The nonlinear process of spectral compression (SC) in a dispersive delay line (DDL) followed by a nonlinear fiber demonstrates promising applications to the signal analysis-synthesis problems in ultrafast optics [61]. In the SC system, the pulse expands and obtains a negative phase in a DDL. This phase should be compensated by the positive phase acquired by nonlinear self-phase modulation (SPM) in a fiber with normal dispersion; as a result, the spectrum is compressed [2]. The impact of group velocity dispersion (GVD) on SC for sub-picosecond pulses in the range of normal dispersion, i.e. at wavelengths <1.3μm for standard silica fibers, is analyzed in [64] in view of shaping flattop pulses. In range of anomalous dispersion, i.e. at wavelengths ≥1.3μm for silica fibers, the combined impact of GVD and SPM leads to the formation of solitons [78,80], when the contributions of GVD and SPM balance each other. The pulse self-compression phenomenon arises when the impact of SPM exceeds the GVD, and high-order solitons are shaped [174].

Under the opposite condition, i.e. when the impact of dispersion exceeds the nonlinearity, we can expect spectral self-compression (self - SC) by the analogue of the pulse self - compression. Recently, the self - SC implementation directly in a fiber with negative group-velocity dispersion (at the wavelength range ≥1.3μm for standard silica fibers) was proposed [18] and studied [20].

In this work, we carried out detailed numerical studies on the process of self - SC for randomly modulated pulses. The self - SC is shown in the fiber with anomalous dispersion, without dispersive delay line, when the impact of GVD in the fiber stronger than the influence of SPM.

Numerical Studies and Results

The pulse propagation in a single-mode fiber (SMF) is described by nonlinear Schrödinger equation for normalized complex amplitude of field, considering only the influence of GVD and Kerr nonlinearity [2]:

$$i\frac{\partial\psi}{\partial\zeta}=\frac{1}{2}\frac{\partial^2\psi}{\partial\eta^2}+R|\psi|^2\psi \qquad (3.5.1)$$

where $\xi = z/L_D$ is the dimensionless propagation distance, $\eta=(t-z/u)/\tau_0$ is the running time, which are normalized to the dispersive length $L_D=\tau_o^2/|k_2|$ (k_2 is the coefficient of second - order dispersion), and initial pulse duration τ_0, respectively. The nonlinearity parameter R is given by

the expression $R = L_D / L_{NL}$, where $L_{NL} = (k_0 n_2 I_0)^{-1}$ is the nonlinearity length, n_2 is the Kerr index of silica, and I_0 is the peak intensity. The first and second terms of the right side of Eq. (3.5.1) describe the impact of GVD and nonlinearity, respectively. We use the split-step Fourier method during the numerical solution of the equation, with the fast Fourier transform algorithm on the dispersive step [184,185].

The initial pulses with random amplitude modulation are formed by the model of additive noise [17], and for Eq. (3.5.1) the initial conditions are given as follows:

$$\psi(0,\eta) = \psi_0(\eta) + \sigma\xi(\eta) \tag{3.5.2}$$

In Eq. (3.5.2) ψ_0 is the regular component of normalized amplitude, $\xi(\eta)$ is the stationary noise with a Gaussian correlation function, and σ is its amplitude.

The purpose of our work is to study the self - SC for randomly modulated pulses, which takes place when the dispersive length in the fiber is shorter than the nonlinearity length ($L_D < L_{NL}$, i.e. $R < 1$). At first, the GVD stretches the pulse by acquiring a negative chirp. Afterwards, the accumulated impact of SPM leads to the compensation of the chirp. As a result, the spectrum is compressed. We study the pulse behavior in a fiber with negative GVD for different values of nonlinearity parameter and fiber length (the fiber length is less than 100).

The statistical parameters of radiation are determined by sampling of a large number realizations-*N* =150, which are solutions of Eq. (3.5.1). The studies are carried out for signals with the same value of the noise component amplitude $\sigma = 0.6$ and coherence time $\tau_c = 0.33$ ($\tau_c = \tau_0 / 3$).

A randomly modulated optical signal with higher coherency has a smoother shape than signal with a lower coherency. The period of oscillation is given by the coherence time, and their amplitude is given by the amplitude of noise component. Fig. 3.5.1 illustrates two realizations of randomly modulated initial pulses with coherence time $\tau_c = 0.33$ ($\sigma = 0.6$).

The maximal value of the self - SC for different values of the nonlinearity parameter and the fiber length (the fiber length is less than 100) is studied. As shown in Fig. 3.5.2, the maximum value

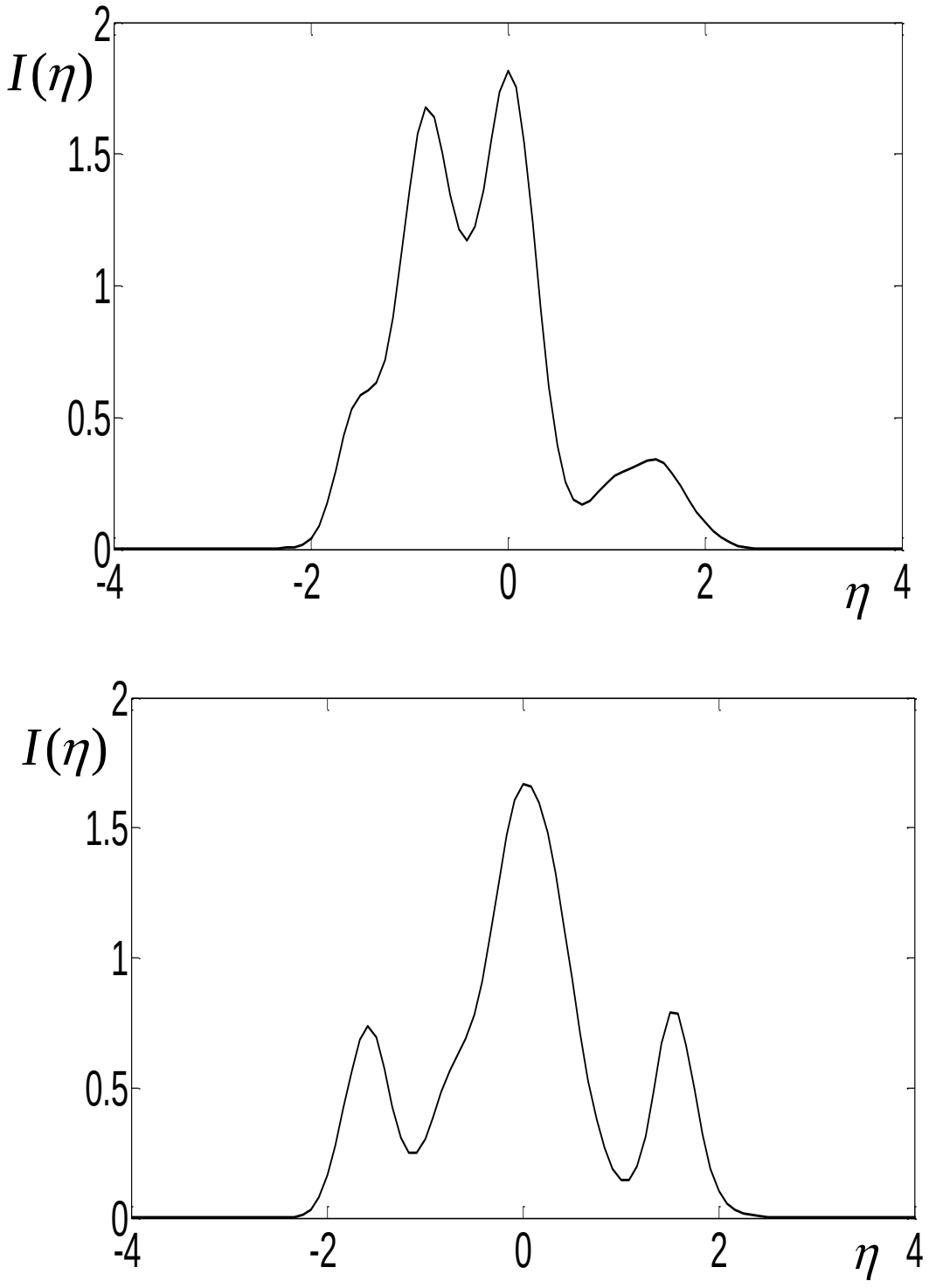

Fig. 3.5.1. *Two realizations of randomly modulated initial pulses.*

of the self - SC ($\Delta = \max(I(\Omega)/I_0(\Omega))$) is ≈ 3, where the nonlinearity parameter and the fiber length equal to 0.4 and 65, correspondingly (Fig. 3.5.2).

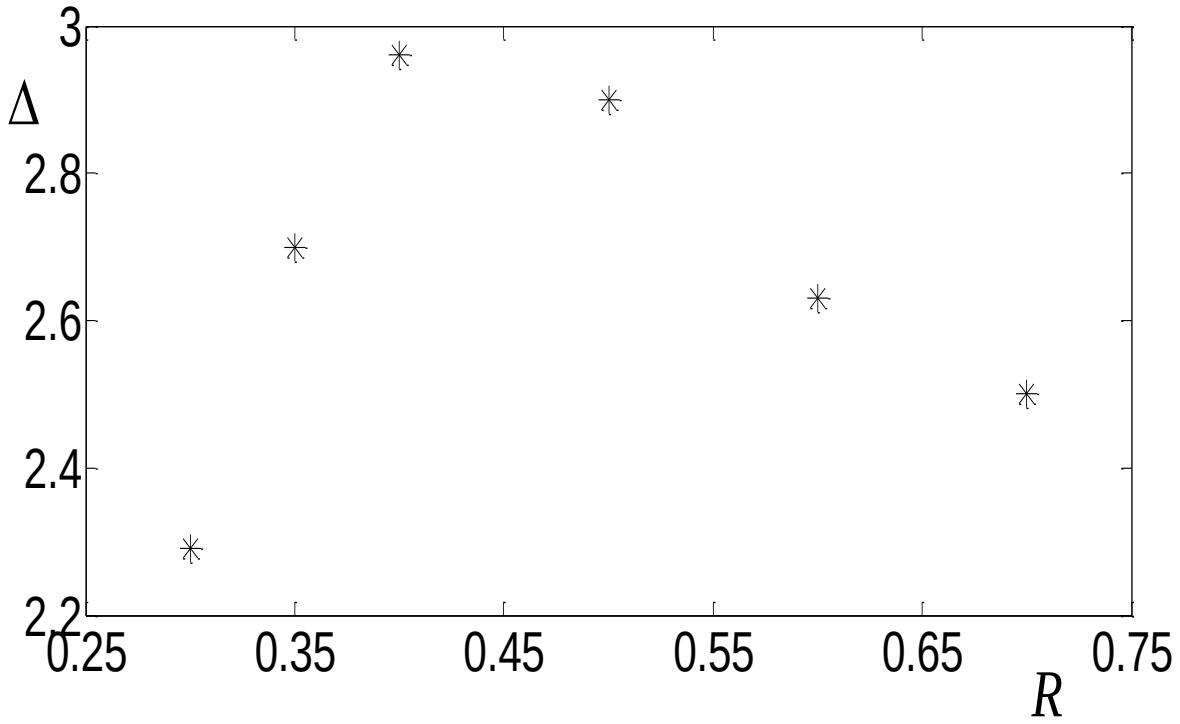

Fig.3.5.2. *The maximal values of the self - SC vs nonlinearity parameter (for fiber lengths less than 100).*

For comparison, self - SC for the regular Gaussian pulse and randomly modulated pulses in the system with the same parameters is implemented (the nonlinearity parameter and fiber length equal to 0.6 and 50, respectively). As we see on Fig. 3.5.3 (a, b), the self - SC is ≈ 5.9 for initial Gaussian pulses meanwhile the self - SC is ≈ 2.5 for initial randomly modulated pulses Fig. 3.5.3 (c, d).

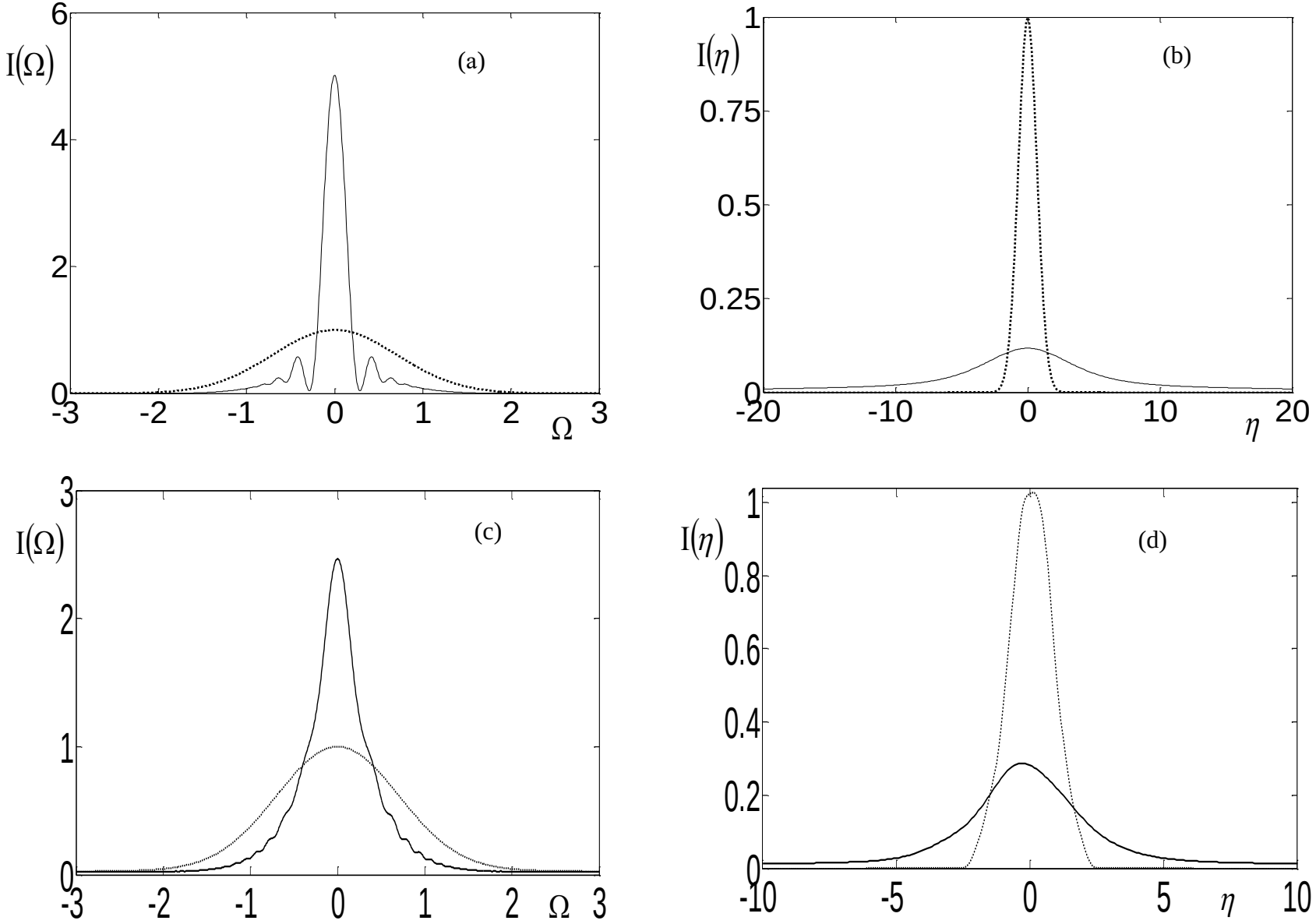

Fig 3.5.3*. Spectral self-compression of initial Gaussian (a, b) and randomly modulated (c, d) pulses (the nonlinearity parameter and the fiber length equal to 0.6 and 50, respectively).*

§ 3.6. Conclusion to the chapter 3

- We present results of numerical studies of the phase compensation in the pulse compression process via the shaping of asymmetric pulses at the system input. In this case, an effective pulse compression is achieved with a ratio corresponding to the pulse spectral broadening in fiber: as the phase obtained by self-phase modulation conditioned by pulse shape, the phase can be controlled by shaping of asymmetric initial pulses.

- In the result of our studies, for asymmetric pulses at the system input, we obtain pulse compression ratio of ~10 when the spectral broadening factor is of 10 and also compression ratio of ~20 for 26^X spectral broadening. Thus, the pulse compression efficiency can be improved by third-order dispersion compensation through pulse asymmetry manipulation at the fiber input.

- The study of spectral compression of randomly modulated optical signals is reported. The research of the spectral compression process is carried out for the additive noise model for initial pulses with different coherence times. The results show that the ratio of spectral compression increases with the reduction of the coherence time of the initial signal.

- Our numerical studies show the possibility of the spectral self-compression for randomly modulated pulses in the fiber "directly" with anomalous dispersion, without dispersive delay line.

- The study of the spectral self-compression for randomly modulated pulse is carried out for the additive noise model. The peculiarities of the process for different values of the fiber length and the nonlinearity parameter are studied.

- We have shown that the maximum value of spectral self-compression for randomly modulated pulse is ~3 for fiber lengths less than 100.

CHAPTER 4. FEMTOSECOND PULSE SHAPING WITH SPATIAL–LIGHT MODULATOR BASED ON CHIRAL LIQUID CRYSTAL CELL WITH HOMEOTROPIC BOUNDARY CONDITIONS

§4.1. Introduction

The results of this chapter are based on the publications [32-34].

As it was mentioned in the first chapter, in the last two decades, much attention has been paid to the development of a technique for the shaping and compression of femtosecond optical pulses using a grating–lens apparatus with a liquid crystal spatial light modulator [132-168]. Such LC-SLMs can independently control the amplitude and the phase of the transmitted light giving possibility to programmable generate pulses with practically arbitrary (within physical limits) shaping and are now commercially available. The commercial LC-SLMs most often have a twisted nematic structure [203], and the amplitude and the phase of the transmitted light are coupled in a specific manner. That is why in [204] they focused on pulse shaping with such LC-SLMs in the time domain, and investigated the potential of the technique. In [205,206] we have considered the distribution of the director of a cholesteric liquid crystal (CLC) in planar cells on whose walls the director orientation is maintained rigidly along the normal to the boundary. This kind of structure has also twist nematic with cholesteric mixture (TNCM) and with homeotropic boundaries. Near the critical cell thickness this system becomes sensitive to the external fields and at a very low electrical voltage a transition of the Fréedericksz type takes place from a stable twisted distribution to a stable homogeneous homeotropic distribution.

In this study, we have theoretically characterized the properties of a TNCM SLM with homeotropic boundary conditions. We developed the relevant mode extraction method for the calculation of mask patterns which can generate multiple pulse sequences with arbitrary relative amplitudes and phases. By the choosing relevant distribution of the electric field voltages (lower than 0.1V) across the mask with TNCM SLM we get very different pulse shaping. By varying the modulation depth (by altering the amplitude of the electric field voltages distribution), we generate different number of pulses and intensity ratio of them. This method could allow us to generate much

type of desired waveforms: square pulses, double pulses, triple pulses, multiple pulses, pulses train, symmetric and asymmetric pulses and random pulses.

§4.2. Femtosecond pulse characterization

Femtosecond pulse can be subjected to the spectral resolution

$$e(t) = \frac{1}{2\pi}\int_{-\infty}^{\infty} E(\omega)e^{-i\omega t}d\omega, \tag{4.2.1}$$

where the Fourier components are given in terms of the function $e(t)$ by the integrals

$$E(\omega) = \int_{-\infty}^{\infty} e(t)e^{i\omega t}dt. \tag{4.2.2}$$

Because $e(t)$ must be real,

$$E(-\omega) = E^{*}(\omega). \tag{4.2.3}$$

Let us express the total intensity of the wave, i.e. the integral of e^2 over all time, in terms of the intensity of the Fourier components. Using (4.2.1) and (4.2.2), we have:

$$\int_{-\infty}^{\infty} e^2 dt = \int_{-\infty}^{\infty}\left\{e\int_{-\infty}^{\infty} Ee^{-i\omega t}\frac{d\omega}{2\pi}\right\}dt = \int_{-\infty}^{\infty}\left\{E\int_{-\infty}^{\infty} ee^{-i\omega t}dt\right\}\frac{d\omega}{2\pi} = \int_{-\infty}^{\infty} E(\omega)E(-\omega)\frac{d\omega}{2\pi}$$

or, using(4.2.3)

$$\int_{-\infty}^{\infty} e^2 dt = \int_{-\infty}^{\infty}|E|^2\frac{d\omega}{2\pi} = 2\int_{0}^{\infty}|E|^2\frac{d\omega}{2\pi} \tag{4.2.4}$$

The time-dependent complex electric field $e(t)$ in the slow varying envelope approximation can be separated in

$$e(t) = e_0(t)e^{-i(\omega_0 t+\varphi(t))}, \tag{4.2.5}$$

where $e_0(t)$ is the temporal amplitude, $\omega_0 t + \varphi(t)$ is the temporal phase factor, ω_0 is the carrier frequency and $\varphi(t)$ is the additional phase. This approximation is true if pulses have at list few optical cycles, when $\Delta\omega << \omega_0$, where $\Delta\omega$ is the spectral full-width at half-maximum. The time derivative of the phase factor $\omega_0 t + \varphi(t)$ gives the instantaneous frequency as a function of time

$$\omega(t) = \omega_0 + \frac{d\varphi(t)}{dt} \tag{4.2.6}$$

Developing the phase $\varphi(t)$ around t_0 in Taylor series gives a closer look at the chirp in time domain:

$$\varphi(t) = \varphi(t_0) + \frac{d\varphi(t)}{dt}|_{t_0}(t - t_0) + \frac{1}{2}\frac{d^2\varphi(t)}{dt^2}|_{t_0}(t - t_0)^2 + \cdots \tag{4.2.7}$$

or

$$\varphi(t) = \varphi_0 + \varphi_1(t - t_0) + \frac{1}{2}\varphi_2|_{t_0}(t - t_0)^2 + \cdots \tag{4.2.8}$$

The quantity $\varphi_0 = \varphi(t_0)$ represents the constant phase of the electric field which determines the relative position of the fast oscillations of the electric field with respect to the pulse envelope. The linear variation of the phase $\varphi(t)$ in time is described by the term $\varphi_1 = d\varphi(t)/dt|_{t0}$ which gives the shift of the carrier frequency ω_0. For a transform-limited pulse the temporal phase depends linearly with time: $\varphi(t) = \varphi_0 + \varphi_1 (t - t_0)$. The quadratic term $\varphi_2 = d^2\varphi(t)/dt^2|_{t0}$ gives the linear chirp, i.e. the linear variation of the instantaneous frequency with time (see equation $\omega(t) = \omega_0 + \frac{d\varphi(t)}{dt}$ (4.2.6)). If $d^2\varphi(t)/dt^2|_{t0} > 0$ the instantaneous frequency increases with time; this is the case of a positive chirp or upchirp. The opposite situation, when $d^2\varphi(t)/dt^2|_{t0} < 0$, i.e. the instantaneous frequency decreases in time, is described as a negative chirp or downchirp. For $d^3\varphi(t)/dt^3|_{t0}$ and higher orders, the terms give the quadratic and higher order chirps. Nonlinear phase modulation of unchirped femtosecond pulse can be realized in many methods. One of them is self-phase modulation. The modulation phase term is described as

$$\varphi = \frac{2\pi}{\lambda_0} nL \tag{4.2.9}$$

where λ_0 is the central wavelength of the pulse, L is the thickness of the optical medium in the pulse propagation direction and n the time-dependent (temporal modulation) or position-dependent

(spatial modulation) or frequency-dependent (spectral modulation) refractive index. In the case of temporal modulation this phenomenon leads to a change in the spectrum without affecting the time duration of the pulse.

Since the laser's inception in 1961, considerable research has been performed to make the output stronger, more stable, and in the cases of pulsed lasers, there has been a drive to make the pulse durations shorter because a vast range of fundamental processes occur on the pico- and femtosecond time scale [132]. To understand time dynamics of a process, usually a shorter time scaled reference must be used. From the Heisenberg relationship,

$$\Delta\omega\Delta\tau \geq s + 2\pi \tag{4.2.10}$$

where s is a constant dependent on the assumed pulse shape (i.e. for a Gaussian pulse $s = 0.441$), the greater the frequency bandwidth the shorter the pulse duration. The dependency arises from the Fourier transform relationship between the pulse duration and the bandwidth. Another stipulation for a short pulse is the large bandwidth must have a fixed phase relationship. The equality holds when there is no chirp across the frequencies (i.e. the phases of all the frequency components are the same). When the pulse conforms to this equality, it is a Fourier transforms limited pulse, or also known as a bandwidth limited pulse.

The laser pulse duration propagation in different media has undergoes dispersion which lengthens the pulse by changing the phase relationship between different frequency components. In the frequency domain complex electric field $E(\omega)$ can be separated in

$$E(\omega) = E_0(\omega)e^{-i(\omega_0 t + \psi(\omega))}, \tag{4.2.11}$$

where $E_0(\omega)$ is the spectral amplitude, $\omega_0 t + \psi(\omega)$ is the spectral phase factor, ω_0 is the carrier frequency and $\psi(\omega)$ is the additional phase, that can be expended in a Taylor series if $\Delta\omega << \omega_0$,

$$\psi(\omega) = \psi'\Delta\omega + \frac{1}{2!}\psi''(\Delta\omega)^2 + \frac{1}{3!}\psi'''(\Delta\omega)^3 + \cdots \tag{4.2.12}$$

where ψ' is the group dispersion delay, ψ'' is the group velocity dispersion, and ψ''' is the third order dispersion coefficient. The pulse duration is defined as the complete derivative with respect to frequency.

$$\tau = \frac{d\psi}{d\omega} \tag{4.2.13}$$

§4.3. Grating and lens apparatus action

As it was mentioned in the section 1.5, to filter spectral components, using the LC-SLM, one needs to image the focused spectrum into the LC-SLM. For a single LC-SLM this is most easily accomplished by a pair of gratings and lenses configured in a 4-F (shown setup in Fig. 4.3.1). This arrangement has been developed first in [207,208] as a way to create positive group-velocity dispersion. The first grating angularly disperses the spectral components of the ultrashort incident pulse. The grating is located in the back focal plane of a first lens, so that the lens collimates the spatially separated spectral components and focuses the discrete spectral components onto the spatially varying LC-SLM positioned in the front focal plane of the lens [118]. The LC-SLM is in the back focal plane of a second lens (so that the lens pair forms a telescope around the LC-SLM), which collimates the discrete spectral components and curves them toward a second antiparallel grating that is in the front focal plane of the second lens. The second lens and the second grating thus recombine the spectrally filtered pulse, yielding a shaped pulse in the time domain [118].

For LC-SLM made up of a linear collection of regularly spread out pixels it is important that each pixel sample a spectral range of the same size so that linear sampling is kept.

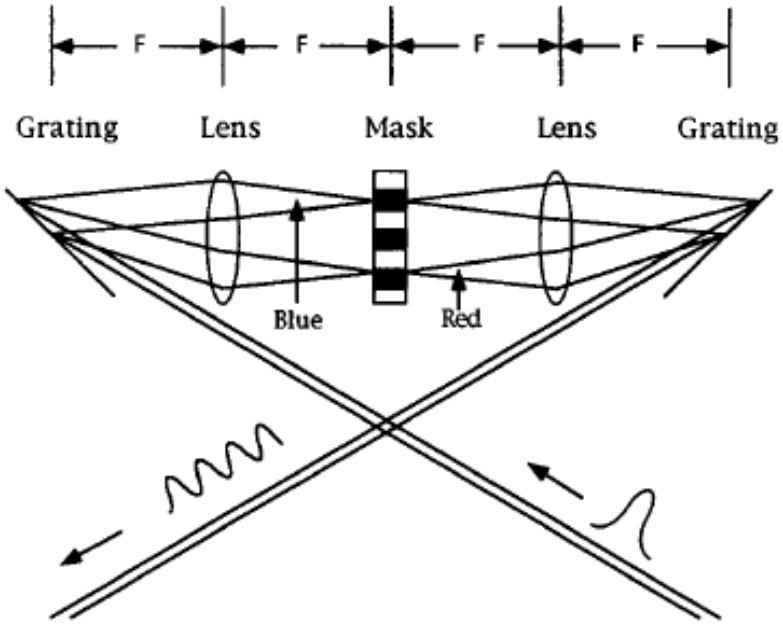

Fig. 4.3.1. *4-F pulse-shaping apparatus.*

First order diffraction off a grating is given by

$$\lambda = d(\sin\theta_{in} + \sin\theta_d), \tag{4.3.1}$$

where λ is the wavelength, d is the spacing between grating lines, and θ_{in} and θ_d are angles of incidence and diffraction, respectively, for the specific wavelength. The first lens, with the focal length f, brings the diffracted rays from the first grating parallel. Let us denote the position of spectral component λ_0 on LC-SLM trough x_0. Then from (4.3.1) we get the position for component λ as

$$x = f \tan[\theta_d(\lambda) - \theta_d(\lambda_0)]. \tag{4.3.2}$$

Expending x as a power series in angular frequency ω gives

$$x = f\left[\frac{\partial\theta_d}{\partial\omega}\Big|_{\omega=\omega_0}(\omega-\omega_0) + \frac{\partial^2\theta_d}{\partial\omega^2}\Big|_{\omega=\omega_0}(\omega-\omega_0)^2 + \cdots\right], \tag{4.3.3}$$

where

$$\frac{\partial\theta_d}{\partial\omega}\Big|_{\omega=\omega_0} = \frac{-2\pi c}{\omega_0^2 d\cos\theta_d(\omega_0)}, \tag{4.3.4}$$

c is the light speed, and ω_0 is the central carrier frequency of the input pulse. This expansion could be terminated after the linear term, if input pulse duration $\geq$ 20fs. In this paper we assume that this limitation takes place and

$$x(\omega) = \alpha(\omega - \omega_0), \tag{4.3.5}$$

where the spatial dispersion term, α, is given as

$$\alpha = \frac{\lambda_0^2 f}{2\pi c d\cos\theta_d(\lambda_0)} \tag{4.3.6}$$

with units $cm(rad/s)^{-1}$.

§4.4. Liquid crystal modulator

The SLM consists of a TNCM or CLC layer which is embedded between two glass slides. The TNCM mask is subdivided into a linear array of pixels which can be controlled individually using a driving voltage. It is applied via two transparent indium tin oxide (ITO) electrodes which are deposited on the inner surface of the glass slides. The pixels are defined by patterning of one ITO layer into stripe–shaped electrodes, with neighboring pixels being separated by thin gaps (typically a few μm) in the ITO layer.

Generally for a birefringent material, the optical phase difference between extraordinary and ordinary waves with refractive indexes n_e and n_o, respectively, or retardance, is given as

$$\Delta\psi = \frac{2\pi L}{\lambda}(n_e - n_o), \tag{4.4.1}$$

where L is the thickness of the material and λ is the wavelength. The axes of liquid crystal modulator (LCM) pixels are defined as follows. The x–axis is directed along the spatial frequency spread, the y–axis is orthogonal to x and the direction of light propagation, z–axis. The unite vector **n** describing preferred orientation of LC molecules is called director. Initial orientation of director **n** in the every pixel cell has twisted structure [209]. At a cell thickness $L_{cr} = K_3P/2K_2$,, where P is the pitch parameter of the free CLC or TNCM and K_i are Frank's elastic constants, a transition of the Fréedericksz type takes place from a stable homogeneous homeotropic distribution (for $L < L_{cr}$) to a stable twisted distribution (for $L > L_{cr}$) rotation angle $\varphi(z)=2\pi z/P$. For twist nematic with cholesteric mixture $\varphi(L) = \pi/2$. In general director distribution has the form

$$\boldsymbol{n} = \left(\boldsymbol{e}_x \cos\varphi + \boldsymbol{e}_y \sin\varphi\right)\sin\theta + \boldsymbol{e}_z \cos\theta, \tag{4.4.2}$$

where $\mathbf{e}_i$ are orts of coordinate system, and θ is the polar angle dependent only on z. Homeotropic boundary conditions mean that $\theta(z = 0, L) = 0$. Above and very close to the critical thickness distribution of polar angle could be approximated as

$$\theta(z) = \theta_m \sin\frac{\pi z}{L}, \qquad \sin\theta_m = (2K_2L/K_3P - 1)^{1/2}. \tag{4.4.3}$$

And this director distribution could be controlled by electric or magnetic fields with very low threshold values near the critical thickness:

$$\frac{\varepsilon_a}{4\pi K_3}E_{cr} = \left(\frac{2\pi K_2}{K_3}\right)^2 - \left(\frac{\pi}{L}\right)^2 \quad \text{and} \quad \frac{\chi_a}{K_3}H_{cr} = \left(\frac{2\pi K_2}{K_3}\right)^2 - \left(\frac{\pi}{L}\right)^2, \tag{4.4.4}$$

where E and H are electric and magnetic field strengths, ε_a and χ_a are electric and magnetic susceptibility anisotropies. We will work very close and above to the electric field threshold. The orientation of the LC molecules lies, mainly, in the plane parallel to the wall surfaces (expects, very thin layers close to the walls where they are normal to them) when no voltage is applied, and is twisted from one surface to the other by an angle (twist angle) of around ϕ. Very weak electrical field (less than 0.1V) reorients LC director to the z–axis direction, which results in a variable refraction index for light polarized along the $\mathbf{n}_0$–axis. However, for light polarized perpendicularly to the $\mathbf{n}_0$–axis the refraction index remains constant. So retardance (4.4.7) depends on electric field voltage V.

$$\Delta\psi(V) = \frac{2\pi L}{\lambda}\Delta n(V), \tag{4.4.5}$$

where $\Delta n = n_e(V) - n_o$. To describe the modulation of light electric field mathematically as it passes through the LC arrays, it is best to use Jones matrix formalism. Fourier transform of general light electric field is represented as

$$E(\omega) = \begin{pmatrix} E_x(\omega) \\ E_y(\omega) \end{pmatrix} e^{i\omega t} \tag{4.4.6}$$

The output electric field, $E_{out}(\Omega)$, with $\Omega = \omega - \omega_0$, after passing through the modulator apparatus can be generally written as

$$E_{out}(\Omega) = A(\Omega)E_{in}(\Omega) \tag{4.4.7}$$

where A is a transform matrix resulting from the optical components. To receive this transform matrix we have to write the matrixes of all optical components. First light passes through polarizer P_x:

$$P_x = \begin{pmatrix} 1 & 0 \\ 0 & 0 \end{pmatrix} \tag{4.4.8}$$

Then linear polarized light passes through LC retardation plate rotated at the angle $\theta_1 = -45^o$. Jones matrix for this anisotropic plate could be received from the matrix for retardation plate in the laboratory (x, y, z) system

$$W_0 = e^{i\Phi/2} \begin{pmatrix} e^{-i\psi/2} & 0 \\ 0 & e^{i\psi/2} \end{pmatrix} \tag{4.4.9}$$

by the rotation to the coordinate system connected with rotated plate

$$W(\theta) = R(-\theta)W_0R(\theta) \tag{4.4.10}$$

where $R(\theta)$ is the coordinate rotation matrix. So for the rotated retardation plate we get

$$\mathrm{W}(\theta) = \exp(i\Phi/2) \begin{bmatrix} cos(\psi/2) - isin(\psi/2)cos2\theta & -isin(\psi/2)\sin 2\theta \\ -isin(\psi/2)\sin 2\theta & cos(\psi/2) + isin(\psi/2)cos2\theta \end{bmatrix} \tag{4.4.11}$$

where $\Phi = 2\pi L(n_e + n_o)/\lambda$ is the absolute phase delay. In our case we have two plates with $\theta_1 = -45^o$ and $\theta_2 = 45^o$. Then we get

$$\mathrm{W}_{1,2}(\theta) = \exp(i\Phi_{1,2}/2) \begin{bmatrix} cos(\psi_{1,2}/2) & \pm isin(\psi_{1,2}/2) \\ \pm isin(\psi_{1,2}/2) & cos(\psi_{1,2}/2) \end{bmatrix} \tag{4.4.12}$$

After these two plates light passes through the second polarizer oriented at x direction. So for the transform matrix A we get

$$A = P_xW_2W_1P_x = e^{i\frac{\Phi_1+\Phi_2}{2}} \begin{bmatrix} cos\left(\frac{\psi_2-\psi_1}{2}\right) & 0 \\ 0 & 0 \end{bmatrix} \tag{4.4.13}$$

In the calculations we omitted constant phases from polarizers because they are same for all LC pixels, and thus the transformation is written as

$$\begin{pmatrix} E_{xout}(\Omega) \\ E_{yout}(\Omega) \end{pmatrix} = e^{i\frac{\Phi_1+\Phi_2}{2}} \begin{bmatrix} cos\left(\frac{\psi_2-\psi_1}{2}\right) & 0 \\ 0 & 0 \end{bmatrix} \begin{pmatrix} E_{xin}(\Omega) \\ E_{yin}(\Omega) \end{pmatrix} \tag{4.4.14}$$

The phase modulation term is

$$\Phi_s = \frac{\pi}{\lambda}[n_e^1(V_1)L_1 + n_e^2(V_2)L_2 + n_o^1 L_1 + n_o^2 L_2] \tag{4.4.15}$$

and the transmission is

$$T = \cos^2\left\{\frac{\pi}{\lambda}[n_e^1(V_1)L_1 - n_e^2(V_2)L_2 - n_o^1 L_1 + n_o^2 L_2]\right\} \tag{4.4.16}$$

The filter or masking function, can be simplified to

$$A(\Omega) = B_n(\Omega) \propto exp\left\{i\frac{1}{2}\left[\Phi_n^{(1)} + \Phi_n^{(2)}\right]\right\} \cos\left\{\frac{1}{2}\left[\psi_n^{(1)} - \psi_n^{(2)}\right]\right\} \tag{4.4.17}$$

where the subscripts (1) and (2) denote the first and second arrays, respectively and *n* denotes the pixel number.

The polarization properties of light transmitted through a twist nematic is presented in [210]. The amplitude and the phase of the transmitted light trough TNCM with homeotropic boundary conditions in the present polarization combination can be derived in a similar manner. The resulted complex transmission coefficient is

$$T(V) = \frac{\sin^2(\phi\sqrt{1+u^2})}{1+u^2} \exp(-i\frac{\pi u}{2}), \tag{4.4.18}$$

where $u(V) = \Delta\psi(V)/\pi$ is the Mauguin parameter and the twist angle could be equal to $\pi/2$. Let us consider crossed polarizers before and after the LC-SLM. So, *u* can be changed from 0 (complete transmission) at the moderate voltage to $\sqrt{3}$ (no transmission) without electrical field by changing the voltage applied to the LC.

§4.5. Mask Pattern Design and Results

As it was mentioned above, the modulator consists of array of LC pixels. Due to the electrically variable birefringence of LC the transmission (4.4.18) for each pixel $T_n = T(V_n)$ is also controllable. In order to impose each spectral component of ultrashort pulse to carry out own retardance one needs to image the focused spectrum onto the LC-SLM. We consider the single LC-SLM. In this case the easiest realization is to use a pair of gratings and lenses configured in a 4–F

arrangement [118], when two gratings and LC-SLM are placed exactly in the focuses of two lenses. The first lens collimates the spatially separated by first grating spectral components of ultrashort pulse and focuses the each spectral component onto the spatially varying LC-SLM placed in the front focal plane of the lens. The LC-SLM is in the back focal plane of a second lens (so that the lens pair forms a telescope around the LC-SLM), which collimates the each spectral component and curves them to the second grating that is in the front focal plane of the second lens. The second lens and the second grating thus recombine the spectrally filtered pulse, yielding a shaped pulse in the time domain.

The modulator operates by applying voltages to liquid crystals causing rotation of a certain angle, thus changing the optical path length (which affects the phase) or retardance. Each of the pixels is driven with a voltage. From these voltages, there is a conversion into drive levels which handled by the driver and computer programs. By varying the voltage and measuring the transmission signal, one can make a calibration curve of the response of the modulator.

Now we can write a masking filter $M(x)$ including both the pixels and the gap responses [118]

$$M(x) = \delta(x - x_0) \otimes \sum_{n=-N/2}^{N/2-1} \{[T_n \delta(x - na)] \otimes squ\left(\frac{x}{ra}\right) + \left[T_g \delta(x - (n + 1/2)a)\right] \otimes squ(x/(1 - r)a)\}, \quad (4.5.1)$$

where N is the total number of pixels per array, x_0 is the displacement of the center of the middle pixel (n = 0) of the LC-SLM from the $\omega = \omega_0$ central spectral component, T_n is the response for each pixel n, T_g is the response for the gaps, a is the center to center pixel distance (including gaps), $\delta(x)$ is the Dirac delta function, r is the pixel width divided by the pixel width plus the gap width, $squ(x)$ is a function defined as

$$squ(x) = \begin{cases} 1 & |x| \le 1/2 \\ 0 & |x| > 1/2 \end{cases}. \quad (4.5.2)$$

Note that T_i are necessarily less than or equal to 1. Sign $\otimes$ means the convolution of two functions $f(x)$ and $g(x)$ to give $h(x)$ is defined as

$$h(x) = f(x) \otimes g(x) = \int_{-\infty}^{\infty} dx' f(x - x')\, g(x'). \quad (4.5.3)$$

We take the effect of the gaps as 0 because our spot size at the modulator is much larger than the width of the gap (we take the ratio of 3:100), thus the convolution will “hide” these smaller term.

Furthermore, given the dimensions of the liquid crystal modulator, r is equal to 97/100, which is approximately one. With these approximations, equation (4.5.1) can be written as

$$M(x) = \delta(x - x_0) \otimes \sum_{n=-\frac{N}{2}}^{\frac{N}{2}-1} \left\{ [B_n \delta(x - na)] \otimes squ\left(\frac{x}{a}\right) \right\}. \tag{4.5.4}$$

Furthermore, the delta function convoluted with the sum, results in only a shift to x_0. Theoretically considering this equation, the shift is irrelevant because the center frequency can be set to the center pixel. Experimentally, it is also possible to set this condition. The further simplified equation becomes [118],

$$M(x) = \sum_{n=-N/2}^{N/2-1} \{ [B_n \delta(x - na)] \otimes squ(x/a) \}. \tag{4.5.5}$$

When the spot size, w_0, is smaller than the individual pixel width, the frequency filter becomes equivalent in form to the physical LC-SLM

$$M_{eff}(\omega) \sim M(x/\alpha). \tag{4.5.6}$$

Now let us calculate the Fourier transformation of (4.5.1) $M(k)$. For simplicity we assume that the pattern defined by the N pixels of the SLM repeats infinitely for $x \to \pm\infty$. With this assumption, $M(k)$ will be expressed by Fourier transformation of masking function when it is repeated infinitely. The result is

$$M(k) = \exp(ik\,x_0) \frac{\sin(rka)}{\pi k} \left[\sum_{n=-\infty}^{\infty} (-1)^n \delta\left(k - n\frac{2\pi}{a}\right) \right] \left\{ \sum_{n=-\infty}^{\infty} T_{rem(n,N)}\, \delta\left(k - n\frac{2\pi}{na}\right) + B_g \frac{\sin[(1-r)ka]}{\pi k} \right\}, \tag{4.5.7}$$

where $rem(n,N)$ gives the remainder of n/N and T_n is given by(4.4.18). In the frequency domain, the output of the linear filter, $E_{out}(\omega)$, is the product of the input signal, $E_{in}(\omega)$, and the frequency response, $H(\omega)$,

$$E_{out}(\omega) = H(\omega) E_{in}(\omega), \tag{4.5.8}$$

where E_{in} and are E_{out} complex amplitudes of the input and output electric field spectra, respectively. Furthermore, it should be noted that $E_{in}(\omega)$, $E_{out}(\omega)$ and $H(\omega)$ and $e_{in}(t)$, $e_{out}(t)$ and $h(t)$ are, respectively, Fourier transform pairs which are defined as

$$e(t) = \frac{1}{2\pi} \int_{-\infty}^{\infty} E(\omega) e^{-i\omega t} d\omega, \qquad E(\omega) = \int_{-\infty}^{\infty} e(t) e^{i\omega t} dt, \tag{4.5.9}$$

$$h(t) = \frac{1}{2\pi} \int_{-\infty}^{\infty} H(\Omega) e^{-i\Omega t} d\Omega, \qquad H(\Omega) = \int_{-\infty}^{\infty} h(t) e^{i\Omega t} dt. \tag{4.5.10}$$

$H(\omega)$ can also be called the effective frequency LC-SLM, $M_{eff}(\omega)$, which is related to the physical LC-SLM [132] by

$$H(\omega) = M_{eff}(\omega) = \int dx\, M(x) g(x, \omega). \tag{4.5.11}$$

The effective frequency filter is given by the complex transmittance of the physical mask, $M(x)$, convolved with the spatial intensity profile of the impingent beam, $g(x)$, which for example, can be defined as

$$g(x, \omega) = \left(\frac{2}{\pi w_0^2}\right)^{1/2} e^{-2(x-\alpha\omega)^2/w_0^2} \tag{4.5.12}$$

for a Gaussian shape, and

$$w_0 = \frac{f\lambda \cos\theta_{in}}{\pi w_{in} \cos\theta_d} \tag{4.5.13}$$

is the radius of the focused spot at the masking plane, where θ_{in} is the light incident angle, and w_{in} is the spot size before the grating. Combining the results of Eqs (4.4.18), (4.5.1), (4.5.8), (4.5.9), (4.5.11) and (4.5.12) and solving the system by the simulated–annealing (SA) computer program [211] it could be find the pulse shaping due to the mask on the twist nematic with cholesteric mixture and with homeotropic boundaries. For calculations, consider mask pattern giving the pixel number dependence of Mauguin parameter $u(n)$ shown in Fig. 1. This kind of TNCM SLM mask pattern generates the waveform shown in Fig. 2. The input pulse was assumed to be a 21 fs sech^2 pulse with unit intensity. The simulated waveform obtained by SA calculation has a high peak at 132 fs at the positive time direction. There remains, however, a peak at time zero with a comparable intensity, and several small peaks are also apparent at the negative times of $-$ 132fs, $-$ 264fs and $-$ 396fs. These peaks appear due to the coupling between the amplitude and phase of the shaping procedure.

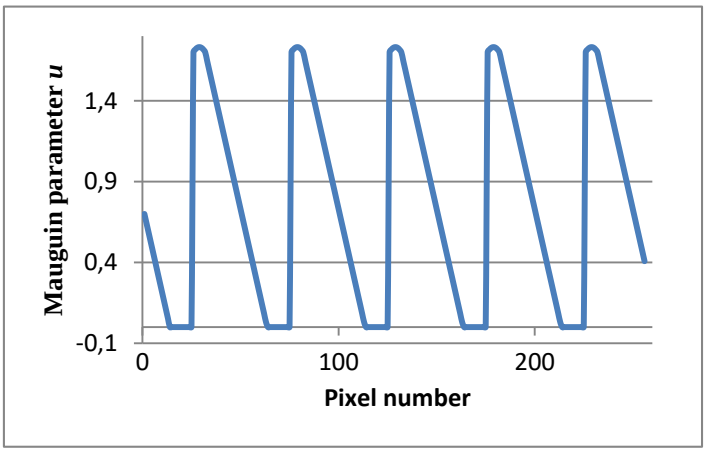

Fig. 4.5.1. *SLM mask pattern which generates the waveform. The vertical axis shows the Mauguin parameter u of each pixel.*

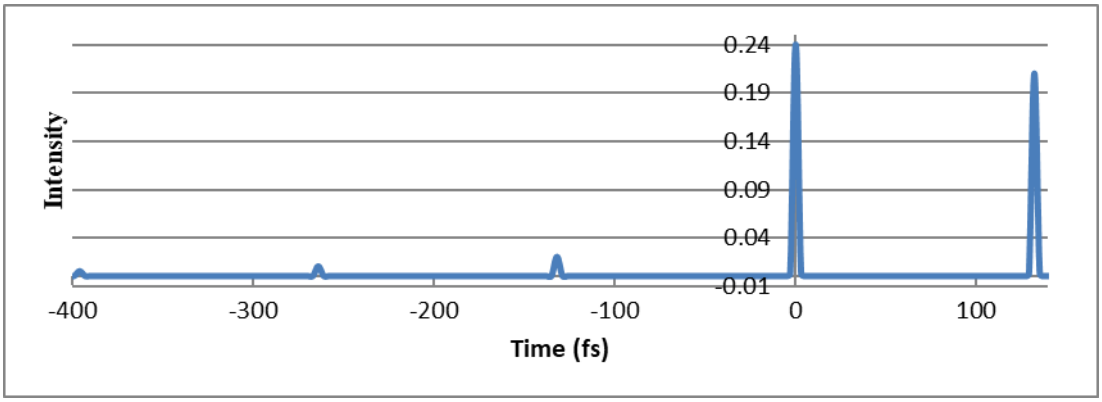

Fig. 4.5.2. *Waveform with a single pulse at 132 fs in the positive time region obtained by a simulated annealing calculation. The peak intensity of the input pulse is normalized to unity.*

Let us note some pixilation effects. Before voltage is applied on each pixel, all the liquid crystal molecules are aligned in the plane parallel to the cell walls, except those who are in the vicinity of the glass plates. This is because rigid homeotropic conditions on the walls. When the voltage is applied the whole molecules are exactly align homeotropically and parallel to the field. If an exact pulse shape is desired the inhomogeneous distribution of molecules in the absence of electric field will brings to the observable imperfections between the desired and the measured shape.

§4.6. Conclusion to the chapter 4

In this chapter we developed the relevant mode extraction method for the calculation of mask patterns which can generate multiple pulse sequences with arbitrary relative amplitudes and phases. We used SLM on the base of twist nematic with cholesteric mixture and with homeotropic boundary conditions. By the choosing relevant distribution of the electric field voltages (~ 0.1V) across the mask with SLM we get very different pulse shaping. Let us note, that this approach allows to control of the relative amplitudes of different pulse within pulse train. By varying the

modulation depth (by altering the amplitude of the electric field voltages distribution), we generate different number of pulses and intensity ratio of them. Electric field used energy could be make much lower by mixing ferroelectric nanoparticles with liquid crystal. It is well known that ferroelectric nanoparticles could produce enhanced changes in the physical properties of liquid crystal host. Electrical Fréedericksz transition in twist nematic with cholesteric mixture doped with spherical ferroelectric nanoparticles has very low threshold because they strongly increase the electric field in the medium.

SUMMARY

Thus, some new peculiarities of spectral compression and self-compression of regular and randomly modulated pulses are studied numerically. The new effective approach of pulse compression is offered. In addition, it is proposed new shaping method of receiving different form of regular and random pulses needed for compression.

The following main results were obtained in the thesis:

1. The physical pattern of soliton spectral self-compression process is studied. The process is realized in the fiber with negative dispersion when the impact of dispersion exceeds the nonlinearity in the SMF (dispersive length is shorter than the nonlinearity length in the fiber).
2. Our research shows that there is an analogue between soliton self-compression and soliton spectral self-compression processes. However, there is no strict periodicity for soliton spectral self-compression process because of incomplete cancellation of the chirp. The frequency dependence on the nonlinearity parameter is studied.
3. Our studies for soliton spectral self-compression processes are carried out for the Gaussian, secant-hyperbolic, and super-Gaussian pulses. The soliton spectral self-compression ratio is approximately 30 times in the range of parameters $R=0.25 \div 1$ and $\zeta \approx 1 \div 20000$. During numerical investigation of soliton spectral self-compression, the research shows that in the case of small values of nonlinearity parameter and the large lengths of fiber, the shape of spectrum is maintained, but the size is not. The changes in the spectrum slow down for fiber lengths of ≈ 11000: because of pulse broadening (≈ 6000 times), the peak of the pulse drops so much that self-phase

modulation is practically absent. It is also shown that the quality coefficient of compression reduces as the length of fiber increases. This is caused by the incomplete cancelation of the phase.

4. We study the effects preventing the effective pulse compression and offer an opportunity to improve the process efficiency. The results show that the impact of third-order dispersion in a fiber and dispersive delay line can be compensated by initial pulse asymmetry since the phase obtained due to the self-phase modulation in the fiber is conditioned by the pulse shape.

5. The pulse compression by asymmetric pulses at the system input gives opportunity to increase the process efficiency to the point where the pulse compression ratio equals to the spectral broadening factor (spectral compression ratio is ≈ 10 for 10 spectral broadening). Pulse compression ratio equaling to ≈ 20 in the case of 26 times spectral broadening is also obtained.

6. We demonstrate the results of detailed numerical studies for spectral compression and spectral self-compression for randomly modulated pulses. The spectral compression efficiency dependence on the coherency of initial pulses is presented. The study shows that the maximum value of spectral self-compression of randomly modulated pulse is ≈ 3 for fiber lengths less than 100.

7. We developed the relevant mode extraction method for the calculation of mask patterns which can generate multiple pulse sequences with arbitrary relative amplitudes and phases. As the mask we used liquid crystal spatial light modulator based on the cell with twist structure of nematic and cholesteric mixture and with homeotropic boundary conditions on the walls.

8. By the choosing relevant distribution of the electric field voltages (≈ 0.1V) across the mask with spatial light modulator we get very different pulse shaping. This approach allows to control of the relative amplitudes of different pulse within pulse train.

ACKNOWLEDGEMENTS

First of all, it is my pleasant duty to express my gratitude to my scientific supervisor R.S. Hakobyan for his guidance and supervision of my graduate research, in the formation of my dissertation objectives, in the effective discussion of scientific results, and in other aspects as well.

I am also very grateful to my previous supervisor G.L.Yesayan for his contribution and fruitful discussion during my work.

In addition to thanking the scientific director of the Ultrafast Optics Laboratory L. Kh. Mouradian, I would also like to thank all its members, especially, A. Kutuzyan for her assistance throughout my research.

I am grateful to the head of Optics Chair of Physics Department, YSU R.B.Alaverdyan and all the members of Chair since without their help this dissertation would not have been possible.

LIST OF ABBREVIATIONS

DDL	dispersive delay line
GVD	group-velocity dispersion
HCW	hollow core waveguide
ITO	indium tin oxide
LC	liquid crystal
LC-SLM	liquid crystal spatial light modulator
NLC	nematic liquid crystal
PC	pulse compression
PCF	photonic crystal fibers
self-SC	spectral self-compression
SC	spectral compression
SLM	spatial light modulator
SPM	self-phase-modulation
SMF	single mode fiber
TNCM	twist nematic with cholesteric mixture
TOD	third-order dispersion

MAIN DESIGNATIONS

The slowly varying complex amplitude of the field	$\psi(\zeta,\eta)$
The running time	η
The dimensionless propagation distance	ζ
The nonlinearity parameter	R

The nonlinearity length	L_{NL}
The dispersive length	L_D
The coefficient of second - order dispersion	k_2
The Kerr index of silica	n_2
The initial pulse duration	τ_0
Describes the impact of the third dispersion	μ_{TOD}
The dimensionless frequency	Ω
The central frequency	ω_0

REFERENCES

1. С.А.Ахманов, В.А.Выслоух, А.С.Чиркин. Оптика фемтосекундных лазерных импульсов. Москва, Наука, 1988.
2. G.P. Agrawal. Nonlinear Fiber Optics. 4th Edition, Boston, Academic Press, 2007.
3. I. Cristiani, R. Tediosi, L. Tartara , V. Degiorgio. Dispersive wave generation by solitons in microstructured optical fibers. Opt. Express, **12**(1), p. 124-135, (2004).
4. G.Yesayan. Nonlinear-Dispersive Similaritons and their applications in Ultrafast Optics. Dissertation, (2013).
5. С.А. Ахманов, В.А. Выслоух, А.С Чиркин. Самовоздействие волновых пакетов в нелинейной среде и генерация фемтосекундных лазерных импульсов. Успехи физических наук, **149**, с.450-509, 1986.
6. K. Tai, A. Tomita .1100x Optical Fiber Pulse Compression Using Grating Pair and Soliton Effect at 1.319um. Appl. Phys. Lett., **48**(5), p. 1033-1035, (1986).
7. W.H. Knox, R.L. Fork, M.C. Downer, R.H. Stolen, C.V. Shank, J.A. Valdmanis. Optical Pulse Compression to 8fs at 5kHz Repetition Rate. Appl.Phys.Lett., **46**(12), p.1120-1121, (1985).
8. C.H. Brito-Cruz, R.L. Fork, C.V. Shank. Compression of Optical Pulses to 6fs Using Cubic Phase Distortion Compensation. Conference on lasers and electro- optics and XV International conference on quantum electronics, Technical Digest, p.26, (1987).

9. J.M. Dudley, C. Finot, G. Millot, D.J. Richardson. Self-similarity and scaling phenomena in nonlinear ultrafast optics. Nat. Phys., **3**, p.597-603, (2007).
10. A. Zeytunyan. Nonlinear-spectronic similariton of Single-Mode Fiber. dissertation, (2010).
11. G.I. Barenblatt. Scaling, Self-Similarity, and Intermediate Asymptotics. Cambridge University Press, (1996).
12. V.I. Kruglov, D. Méchin, and J.D. Harvey. High compression of similariton pulses under the influence of higher-order effects. J. Opt. Soc. Am. B, **24**(4), p. 833–838, (2007).
13. K. Palanjyan, A. Muradyan, A. S. Zeytunyan, G. L. Yesayan, L. Kh. Mouradian. Pulse compression down to 17 femtoseconds by generating broadband similariton. Proc. SPIE, 7998, (2011).
14. L.Kh. Mouradian, et al. (2000) Applications of temporal Kerr lensing to signal manipulation and analysis. CLEO-Europe'2000, Conf. Digest 39, CTuH6.
15. L. Mouradian, A. Barthélémy. Nonlinear-Dispersive Similaritons of Passive Fibers: Applications in Ultrafast Optics. Shaping Light in Nonlinear Optical Fibers, p. 147-198, (2017).
16. N.L. Markaryan, L.K. Muradyan, T.A. Papazyan. Spectral compression of ultrashort laser pulses. Soviet Journal of Quantum Electronics, **21**(7), p. 783-785, (1991).
17. M. Oberthaler, R.A. Hopfel. Special narrowing of ultrashort laser pulses by self-phase modulation in optical fibers. Applied Physics Letter, **63**, p. 1017–1019 (1993).
18. G. Yesayan. Spectral self-compression of ultrashort pulses. J. Contemp. Phys., 47(5), p.225-227, 2012.
19. H. Toneyan, A. Zeytunyan, R. Zadoyan, L. Mouradian. Classic, all-fiber, and similaritonic techniques of spectral compression. J. Physics: Conf. Ser., **672**, (2016).
20. A.P.Grigoryan, G.L.Yesayan, A.A.Kutuzyan, L.Kh. Mouradian. Spectral domain soliton-effect self-compression. Journal of Physics: Conference Series, **672**, (2016).
21. A.Grigoryan, A. Kutuzyan, G.Yesayan. Soliton-effect Spectral Self-compression for Different Initial Pulses. Progress in Physics, **14**(1), p.35-37, (2018).
22. L.Kh.Mouradian, A.Grigoryan, A.Kutuzyan, G.Yesayan, M.Sukiasyan, H.Toneyan, A.Zeytunyan, R.Zadoyan, and A.Barthelemy "Spectral Analogue of the Soliton Effect Compression: Spectral Self-Compression" oral presentation at Frontiers in Optics / Laser

Science Conference (FiO/LS), in San Jose, California, USA, Oct. 18 – 22, 2015, paper FW3F.3.

23. A.Grigoryan, H.Toneyan, A.Zeytunyan, A.Kutuzyan, G.Yesayan, L.Mouradian. Spectral self-compression of Femtosecond pulses. Optics-2014, 2nd Int. Symposium Optics & Its Applications, 1-5 Sept., 2014, p.131, Yerevan-Ashtarak, Armenia.
24. A.Grigoryan, A.Kutuzyan, G. Yesayan, L.Mouradian. Spectral self-compression of chirped laser pulses. Int. Conf. Laser Physics 2013, 18-11 Oct.,2013, p.9, Ashtarak, Armenia.
25. A.Grigoryan, A.Kutuzyan, G.Yesayan, L.Mouradian. Spectral compression of ultrashort laser pulses in the negative dispersion fiber. Int. Conf. IONS-Armenia, 11-14 Sept., 2013, p.56, Yerevan-Ashtarak, Armenia.
26. A.Grigoryan, G.Yesayan, A.Zeytunyan, L.Mouradian. Optimization of femtosecond pulse compression by pulse asymmetry management. Int. J. Modern Phys.: Conf. Series, **15**, World Sci. Pub. Co, p.179-183, (2012).
27. A.Grigoryan, G.Yesayan, A.Zeytunyan, L.Mouradian. Femtosecond Pulse Compression: Managing and Optimization of the Pulse Asymmetry. Int. Conf. Laser Physics 2011, 11-14 Oct., 2011, P4-6, p.57, Ashtarak, Armenia.
28. A.Grigoryan, G.Yesayan, A.Zeytunyan, L.Mouradian. Optimizing femtosecond pulse compression: compensation of third order dispersion by controlling initial pulse asymmetry. Int. Simp. Optics & its Applications, 5-9 Sept., 2011, p.116-117, Yerevan-Ashtarak, Armenia.
29. A.P.Grigoryan. Impact of coherency on the process of spectral compression of randomly modulated pulses. Proc. of the YSU, Phys. and Mathem. Sci., (2), p. 53-56, (2015).
30. A.P.Grigoryan. Spectral self-compression of randomly modulated pulses. Armenian journal of physics, **10**(4), 144-147 (2017).
31. A.Grigoryan, A.Kutuzyan, G.Yesayan, L.Mouradian. Spectral compression of randomly modulated pulses. Optics-2014, 2nd Int. Symp. Optics & Its Applications, 1-5 Sept., 2014, p.141, Yerevan-Ashtarak, Armenia.
32. A.P. Grigoryan, M.R.Hakobyan, R.S. Hakobyan. Femtosecond pulse shaping with spatial–light modulator based on twist nematic with homeotropic boundary conditions. Armenian journal of physics, **10**(4), 185-191 (2017).

33. A.P. Grigoryan, R.S. Hakobyan. Femtosecond Pulse Shaping with Spatial-Light Modulator Based on Cholesteric with Homeotropic Boundary Conditions. Int. Conf. Laser Physics 2017, 19-22 Sept., 2017, p. 52, Ashtarak, Armenia.
34. A.P. Grigoryan, M.R.Hakobyan, R.S. Hakobyan. Ultrashort Pulse Shaping with Spatial–Light Modulator Based on Choleteric Liquid Crystal with Homeotropic Boundary Conditions. Second Panarmenian Scentific Forum, 6-8 Nov., 2017, Yerevan, Armenia.
35. M. Kalashyan. Novel nonlinear-optic methods for signal processing and delivery on femtosecond timescale. Dissertation, (2012).
36. W.R Zipfel, R.M. Williams, W.W. Webb. Nonlinear magic: multiphoton microscopy in the biosciences. Nat. Biotechnol. **21**(11), p.1369-1377, (2003).
37. B.A. Flusberg, E.D. Cocker, W. Piyawattanametha, J.C. Jung, E.L. Cheung, M.J. Schnitzer. Fiberoptic fluorescence imaging. Nat. Methods, **2**(12), p. 941-950, (2005).
38. F. Kong,* Ch. Dunn, J. Parsons, M. T. Kalichevsky-Dong, Th. W. Hawkins, M. Jones, L. Dong. Large-mode-area fibers operating near singlemode regime. Opt. Express, **24**(10), p. 10295-10301, (2016).
39. S. Ramachandran, M.F. Yan, J. Jasapara, P. Wisk, S. Ghalmi, E. Monberg, F.V. Dimarcello. High-energy (nanojoule) femtosecond pulse delivery with record dispersion higher-order mode fiber. Opt. Lett., **30**(23), p. 3225-3227 (2005).
40. F. Luan, J.C. Knight, P.St.J. Russell, S. Campbell, D. Xiao, D.T. Reid, B.J. Mangan, D.P. Williams, P.J. Roberts. Femtosecond soliton pulse delivery at 800nm wavelength in hollowcore photonic bandgap fibers. Opt. Express, **12**(5), p. 835–840, (2004).
41. J.S. Skibina, R. Iliew, J. Bethge, M. Brock, D. Fischer, V.I. Beloglasov, R. Wedell, G. Steinmeyer. A chirped photonic-crystal fiber. Nat. Photonics, **2**(11), p. 679–683, (2008).
42. T. A. Birks, J. C. Knight, and P. St. J. Russell. Endlessly single-mode photonic crystal fiber. Opt. Letters, **22**(13), p.961-963, (1997).
43. F. Helmchen, D.W. Tank, W. Denk. Enhanced Two-Photon Excitation Through Optical Fiber by Single-Mode Propagation in a Large Core. Appl. Opt., **41**(15), p. 2930-2934, (2002).
44. L. Fu, X. Gan, M. Gu. Use of a single-mode fiber coupler for second-harmonic-generation microscopy. Opt. Lett., **30**(4), p. 385-387, (2005).

45. W. Göbel, A. Nimmerjahn, F. Helmchen. Distortion-free delivery of nanojoule femtosecond pulses from a Ti:sapphire laser through a hollow-core photonic crystal fiber. Opt. Lett., **29**(11), p. 1285-1287, (2004).

46. S. Ramachandran, M.F. Yan, J. Jasapara, P. Wisk, S. Ghalmi, E. Monberg, F.V. Dimarcello. High-energy (nanojoule) femtosecond pulse delivery with record dispersion higher-order mode fiber. Opt. Lett., **30**(23), p. 3225-3227, (2005).

47. A.M. Larson, A.T. Yeh. Delivery of sub-10-fs pulses for nonlinear optical microscopy by polarization-maintaining single mode optical fiber. Opt. Express, **16** (19), p.14723-14730, (2008).

48. J.C. Knight, P.St.J. Russell. New Ways to Guide Light. Science, **296**(5566), p. 276-277, (2002).

49. J. Limpert, T. Schreiber, S. Nolte, H. Zellmer, A. Tunnermann, R. Iliew, F. Lederer, J. Broeng, G. Vienne, A. Petersson, C. Jakobsen. High-power air-clad large-mode-area photonic crystal fiber laser. Opt. Express, **11**(7), p. 818-823, (2003).

50. L. Fu, X. Gan, M. Gu. Nonlinear optical microscopy based on double-clad photonic crystal fibers. Opt. Express, **13**(14), p. 5528-5534, (2005).

51. H. Wang, T.B. Huff, J.X. Cheng. Coherent anti-Stokes Raman scattering imaging with a laser source delivered by a photonic crystal fiber. Opt. Lett., **31**(10), p.1417–1419, (2006).

52. S.A. Planas, N.L. Pires Mansur, G.H. Brito Cruz, H.L. Fragnito. Spectral Narrowing in the Propagation of Chirped Pulses in Single-mode Fibers. Opt. Lett., **18**(90), p. 699-701, (1993).

53. Н.Л.Маркарян, Л.Х.Мурадян, Т.А.Папазян. Спектральная компрессия лазерных УКИ. Квант. электрон., **18**(7), с. 865-867, (1991).

54. M. Oberthaler, R.A. Hopfel. Spectral Narrowing of Ultrashort Laser Pulses by Self-Phase Modulation in Optical Fibers. Appl. Opt., **63**(8), p. 1017-1019, (1993).

55. L.Kh. Mouradian, F. Louradour, V. Messager, A. Barthélémy, C. Froehly. Spectrotemporal imaging of femtosecond events. IEEE J. Quantum Electron., **36**(7), p. 795-801, (2000).

56. А.В.Зограбян, Л.Х.Мурадян. Сжатие спектра пикосекундного лазерного излучения. Квант. электрон., **22**(11), с. 1076-1078, (1995).

57. А.В.Зограбян, В.Ж.Ниноян, А.А.Кутузян, Л.Х.Мурадян. Спектральная компрессия пикосекундных импульсов в процессе фазовой кросс-модуляции. Изв. НАН Армении, физика, **33**(5), с. 225-230, (1998).

58. B. R. Washburn, J. A. Buck, S. E. Ralph. Transform-limited spectral compression due to self-phase modulation in fibers. Opt. Lett., **25** (7), p. 445-447, (2000).

59. L. Guo, Ch. Zhou. Spectral narrowing of negatively chirped femtosecond pulse by cross-phase modulation in a single-mode optical fiber. Opt. Commun., **260** (1), 140-143 (2006).

60. T. Mansuryan, A. Zeytunyan, M. Kalashyan, G. Yesayan, L. Mouradian, F. Louradour, A. Barthélémy. Parabolic temporal lensing and spectrotemporal imaging: a femtosecond optical oscilloscope. J. Opt. Soc. Am., B, **25**, A101-A110 (2008).

61. L.Kh.Mouradian, A.V.Zohrabyan, A.Villeneuve, A.Yavrian, G.Rousseau, M.Piche, C.Froehly, F.Louradour, A.Barthélémy. Applications of temporal Kerr lensing to signal manipulation and analysis. in Conference on Lasers and Electro-Optics (CLEO*)*, Postconference Digest, Vol. 39, OSA Trends in Optics and Photonics, paper CTuH6. (OSA 2000).

62. Н.Л. Маркарян, Л.Х. Мурадян, Т.А. Папазян, А.В. Зограбян. Подавление шумов лазерного излучения в спектральном компрессоре. Изв. НАН Армении, Физика, **27**(3), с. 128-134, (1992).

63. Н.Л.Маркарян, Л.Х.Мурадян. Определение временной огибающей УКИ с помощью техники волоконно-оптической компрессии. Квант. электрон., **22**(7), с. 695-697, (1995).

64. A.A.Kutuzyan, T.G.Mansuryan, A.A.Kirakosyan, L.Kh.Mouradian. Self-forming of temporal dark soliton in spectral compressor. Proc. SPIE **5135**, p.156-160, (2003).

65. H. Toneyan, A. Zeytunyan, R. Zadoyan, L. Mouradian. Classic, all-fiber, and similaritonic techniques of spectral compression. Journal of Physics: Conference Series, **672**, (2016).

66. G. Yesayan. Spectral self-compression of ultrashort pulses. J. Contemp. Phys., **47**(5), p. 225-227, (2012).

67. E.B.Treacy. Compression of Picosecond Light Pulses. Phys.Lett. A, **28**, p.34-35, (1968).

68. E.B.Treacy. Optical Pulse Compression with. Diffraction Gratings. IEEE J. of Quantum Electron, QE-**5**(9), p.454-458, (1969).

69. H. Nakatsuka, D. Grishkowsky, A.C. Balant. Nonlinear Picosecond Pulse Propagation through Optical Fibers with Positive Group Velocity Dispersion. Phys.Rev.Lett. , **47**, p.910-913, (1991).

70. D. Grishkowsky, A.C. Balant. Optical Pulse Compression Based on Enhanced Frequency Chirping. Appl. Phys. Lett., **41**, p.1-3, (1982).

71. B. Nicolaus, D. Grishkowsky. 12x Pulse Compression Using Optical Fibers. Appl. Phys. Lett., **42**, p.1-3, (1983).

72. C.V. Shank, R.L. Fork, R. Yen, R.H. Stolen, W.J. Tomlinson. Compression of Femtosecond Optical Pulses. Appl. Phys. Lett., **40**(9), p. 761-763, (1982).

73. С.А. Ахманов, В.А. Выслоух, Л.Х. Мурадян, СМ. Першин, А.А. Подшивалов. Перестраиваемый генератор субпикосекундных световых импульсов с компрессором на одномодовом волоконном световоде. Препринт физического факультета МГУ, **17,** (1984).

74. В.А. Выслоух, Л.Х. Мурадян, СМ. Першин, А.А. Подшивапов. Перестраиваемые генераторы субпикосекундных световых импульсов с компрессором на одномодовом волоконном световоде. Изв.АН СССР, сер.физич., **49**(3), с.573-577, (1985).

75. O.E. Martinez. Grating and Prism Compressors in Case of Finite Beam Size. J. Opt. Soc. Am. B, **3**(7), p.929-934, (1986).

76. M. Piche, P. Ouellete. Compression of Mode-locked Pulses Using Nonlinear Fabry-Perot Interferometers. Opt. Lett., **11**(1), p. 15-17, (1986).

77. В.Е.Захаров, А.Б.Шабат. Полная теория двумерной самофокусировки и одномерной автомодуляции волн в нелинейных средах. ЖЭТФ, **61**, с.118-134, (1971).

78. A.Hasegawa, F.Tappert. Transmission of Stationary Nonlinear Optical Pulses in the Dispersive Dielectric Fibers. I. Anomalous Dispersion. Appl. Phys. Lett., **23**, p.142-144, (1973).

79. D.M. Bloom, L.F. Kollenauer, C. Lin, D.W. Tailor, A.M. Del Gaudio. Direct Demonstration of Distortionless Picosecond-pulse Propagation in Kilometer-length Optical Fibers. Opt. Lett., **4**(9), p.297-299, (1979).

80. L.F.Mollenauer, R.H.Stolen, J.P.Gordon. Experimental Observation of Picosecond Pulse Narrowing and Soliton in Optical Fibers. Phys. Rev. Lett., **45**, p.1095-1098 (1980).

81. L.F. Mollenauer, R. H. Stolen. Soliton in Optical Fibers. Laser Focus, 18, p.193-198, (1982).
82. R.H. Stolen, L.F. Mollenauer, W.J. Tomlinson. Observation, of Pulse Restoration at the Soliton Period in Optical Fibers. Opt. Lett., **8**(3), p.186-188, (1983).
83. D. Anderson, M. Lisak. Nonlinear Asymmetric Self-phase Modulation and Self-steepening of Pulses in Long Optical Waveguides. Phys. Rev. A, **27** (3), p.1393-1398, (1983).
84. A.E. Kaplan. Bistable Solitons. Phys. Rev. Lett., **55**(12), p. 1291-1294, (1985).
85. S.R. Menyuk, H.H. Chen, Y.C. Lee. Amplification and Reshaping of Solitons in Optical Fibers with Suppression of Dispersive Waves. Opt. Lett., **10** (9), p. 451-453, (1985).
86. K.J. Blow, D. Wood. The Evolution of Soliton from non-transform Limited Pulses. Opt. Commun., **58**(5), p.349-354, (1986).
87. K.Tajima. Compensation of Soliton Broadening in Nonlinear Optical Fibers with Loss. Opt. Lett., **12**(1), p. 54-56, (1987).
88. R.R. Alfano, S.L. Shapiro. Observation of Self-phase Modulation and Small ScaliFilaments in Crystals and Glasses. Phys.Rev.Lett., **24**, p.592-594, (1970).
89. R. Fork, C. Shank, G. Hirliman, R. Yen. Femtosecond White-light Continuum Pulses. Opt.Lett., **8**, p. 1-3, (1983).
90. T.K. Gustavson, J. Taran, P. Keller, R. Chiao. Self-modulation of Picosecond Pulse in Electro-optical Crystal. Opt.Commun., **2**, p.17-21, (1970).
91. R.R. Alfano, S.L. Shapiro. Direct Distortion of Electronic Clouds of Rare-gas Atoms in Intense Electric Pield. Phys.Rev.Lett., **24**, p.1217-1220, (1970).
92. Р. Твдекен. Волоконная оптика и ее применение. Мир, 1975.
93. С.Э. Миллер, Э.А.ДЖ. Маркатили, Т. Ли. Исследование световодных систем связи. ТИИЭР, **61**(12), (1973).
94. Q.Z. Wang, Q.D Lui, D. Lui, P.P. Ho, R.R. Alfano. High-resolution spectra of self-phase modulation in optical fibers. J. Opt. Soc. Am. B, **11**, 1084-1089 (1994).
95. Q.Z. Wang, Q.D. Liu, P.P. Ho, E.K. Walge, R.R.Alfano. High-resolution spectra of cross-phase modulation in optical fibers. Opt. Lett., **19** (20), p.1636-1638, (1994).

96. G.R.Boyer, M.A.Franco, M.Lachgar, B.Grèzes-Besset, A.Alexandrou . Femtosecond pulse-shaping scheme for cross-phase modulation in single-mode optical fibers. J. Opt. Soc. Am. B, **11**(8), p.1451-1455 (1994).

97. C. Finot, J.M. Dudley, B. Kibler, D.J. Richardson, G. Millot. Optical parabolic pulse generation and applications. IEEE Journal of Quantum Electronics, **45**(11), p. 1482-1489, (2009).

98. D. Anderson, M. Desaix, M. Karlson, M. Lisak, M.L. Quiroga-Teixeiro. Wave-breaking-free pulses in nonlinear optical fibers. J. Opt. Soc. Am. B, **10**(7), p.1185-1190, (1993).

99. K. Tamura, M. Nakazawa. Pulse compression by nonlinear pulse evolution with reduced optical wave breaking in erbium-doped fiber amplifiers. Opt. Lett., **21**(1), p. 68-70 (1996).

100. A. Grigoryan, G. Yesayan, A. Zeytunyan, AND L. Mouradian. Optimization of femtosecond pulse compression by pulse asymmetry management. International Journal of Modern Physics: Conference Series, **15**, p. 179–183, (2012).

101. S. Zhou, L. Kuznetsova, A. Chong, F.W. Wise. Compensation of nonlinear phase shifts with third-order dispersion in short-pulse fiber amplifiers. Opt. Express, **13** (13), p. 4869–4877, (2005).

102. L. Shah, Z. Liu, I. Hartl, G. Imeshev, G.C. Cho, M.E. Fermann. High energy femtosecond Yb cubicon fiber amplifier. Opt. Express, **13**(12), p. 4717–4722, (2005).

103. T. Binhammer, E. Rittweger, R. Ell, F. X. Kärtner, U. Morgner. Prism-based pulse shaper for octave spanning spectra. IEEE Journal of Quantum Electronics, **41**(12), 1552–1557, (2005).

104. K. Yamane, T. Kito, R. Morita, M. Yamashita. 2.8-fs clean single transform-limited optical-pulse generation and characterization. In Utrafast Phenomena XIV, Optical Society of America, p. 13–15. (2005).

105. N. Karasawa, L. Li, A. Suguro, H. Shigekawa, R. Morita, M. Yamashita. Optical pulse compression to 5.0 fs by use of only a spatial light modulator for phase compensation. J. Opt. Soc. Am. B, **18** (11), p. 1742-1746, (2001).

106. M. Aeschlimann, M. Bauer, D. Bayer, T. Brixner, F. J. Garcia de Abajo, W. Pfeiffer, M. Rohmer, C. Spindler, F. Steeb. Adaptive subwavelength control of nano-optical fields. Nature, **446**(7133), p. 301–304, (2007).

107. D. Goswami. Optical pulse shaping approaches to coherent control. Physics Reports - Review Section of Physics Letters, **374**(6), p. 385–481, (2003).
108. S. Rice, M. Zhao. Optical Control of Molecular Dynamics. John Wiley and Sons, New York, 2000.
109. M. Shapiro, P. Brumer. Principles of the Quantum Control of Molecular Processes. Wiley-Interscience, New Jersey, 2003.
110. P. Forquin, J.-L. Zinszner. A pulse-shaping technique to investigate the behaviour of brittle materials subjected to plate-impact tests. **375**(2085), p. 333-339 (2017).
111. H. Saradesai, C.-C. Chang, A. Weiner. A Femtosecond Code-Division Multiple-Access Communication System Test Bed. L. Lightwave Technol. **16**, p. 1953-1964(1998).
112. F. Huang, W. Yang, W. Warren. Quadrature spectral interferometric detection and pulse shaping., Opt. Lett. **26**, p. 362-364 (2001).
113. Y. Silberberg. Quantum Coherent Control for Nonlinear Spectroscopy and Microscopy. Annual Review of Physical Chemistry, **60**, p. 277–292, (2009).
114. M. H. Brenner, D. Cai, J. A. Swanson, J. P. Ogilvie. Two photon imaging of multiple fluorescent proteins by phase-shaping and linear inmixing with a single broadband laser. Opt. Express, **21**(14), p. 17256–17264, (2013).
115. N. Dudovich, D. Oron, Y. Silberberg. Single-pulse coherently controlled nonlinear Raman spectroscopy and microscopy. Nature **418**, p. 512-514 (2002).
116. M. Aeschlimann, T. Brixner, A. Fischer, C. Kramer, P. Melchior, W. Pfeiffer, C. Schneider, C. Strueber, P. Tuchscherer, D. V. Voronine. Coherent Two-Dimensional Nanoscopy. Science, **333**(6050), p. 1723–1726, (2011).
117. S.-H. Shim, M. T. Zanni. How to turn your pump-probe instrument into a multidimensional spectrometer: 2D IR and Vis spectroscopies via pulse shaping. Physical Chemistry Chemical Physics, **11**(5), p. 748–761, (2009).
118. M. Wefers, K. Nelson. Analysis of programmable ultrashort waveform generation using liquid-crystal spatial light modulators. J. Opt. Soc. Am. B **12**, p. 1343-1362 (1995).
119. A.M. Weiner, D.E. Leaird, J.S. Patel, J.R. Wullert. Programmable shaping of femtosecond optical pulses by use of 128-element liquid crystal phase modulator. IEEE Journal of Quantum Electronics, **28**(4), p. 908–920, (1992).

120. A. Monmayrant, B. Chatel. New phase and amplitude high resolution pulse shaper. Review of Scientific Instruments, **75**(8), p. 2668–2671, (2004).
121. T. Brixner, G. Gerber. Femtosecond polarization pulse shaping. Optics Letters, **26**(8), p. 557–559, (2001).
122. E. Zeek, K. Maginnis, S. Backus, U. Russek, M. Murnane, G. Mourou, H. Kapteyn, G. Vdovin. Pulse compression by use of deformable mirrors. Opt. Lett. **24**, p. 493-495, (1999).
123. D. Leaird, A. Weiner. Femtosecond optical packet generation by a direct space-time pulse shaper. Opt. Lett. **24**, p. 853-855, (1999).
124. C. Florian, T. Cappello, D. Niessen, R. P. Paganelli, S. Schafer, Z.Popović. Efficient Programmable Pulse Shaping for X -Band GaN MMIC Radar Power Amplifiers. IEEE Transactions on Microwave Theory and Techniques, **65**(3), p. 881-891, (2017).
125. K. Hill, K. Purchase, D. Brady. Pulsed-image generation and detection. Opt. Lett. **290**, p. 1201-1203, (1995).
126. T. L. Cocker, R. Huber. Ultrafast pulse shaping: A new twist on terahertz pulses. Nature Photonics **7**, p. 678–679, (2013).
127. M. Nie, Q. Liu, E. Ji, X. Cao, X. Fu, M. Gong. Active pulse shaping for end-pumped Nd:YVO4 amplifier with high gain. Optics Letters, **42**(6), p. 1051-1054, (2017).
128. T. P. Horikis, İ. Bakırtaş. N. Antar. Pulse shaping mechanism in mode-locked lasers. Journal of Optics, **18**(6), p. 1-6, (2016).
129. E. Rahimi. K. Şendur. Femtosecond pulse shaping by ultrathin plasmonic metasurfaces. JOSA B, **33**(2), A1-A7 (2016).
130. Y. Yin, A. Chew, X. Ren, J. Li, Y. Wang, Yi Wu, Z. Chang. Towards Terawatt Sub-Cycle Long-Wave Infrared Pulses via Chirped Optical Parametric Amplification and Indirect Pulse Shaping. Sci Rep., **7:**45794, p. 1-10, (2017).
131. F. Verluise, V. Laude, J. Huignard, P. Tournois. Arbitrary dispersion control of ultrashort optical pulses with acoustic waves. J. Opt. Soc. Am. B **17**, p.138 -145, (2000).
132. A.M. Weiner. Femtosecond pulse shaping using spatial light modulators. Review of Scientific Instruments, **71**, p.1929-1960, (2000).

133. A. M. Weiner, D. E. Leaird, J. S. Patel, J. R. Wullert. Programmable femtosecond pulse shaping by use of a multielement liquid-crystal phase modulator. Optics Letters, **15**(6), p.326–328, (1990).
134. A. M. Weiner. Ultrafast optical pulse shaping: A tutorial review. Optics Communications, **284**(15, SI), p. 3669–3692, (2011).
135. L. Wittenbecher. Compression and Shaping of Femtosecond Laser Pulses for Coherent Two-Dimensional Nanoscopy. MS thesis, Lund University, 2016.
136. A. Monmayrant, S. Weber B. Chatel. A newcomer's guide to ultrashort pulse shaping and characterization. Journal of Physics B – Atomic Molecular and Optical Physics, **43**(10), p. 1-34 (2010).
137. T. Quast. Spectroscopic investigation of charge-transfer processes and polarization pulse shaping in the visible spectral range. PhD thesis, Julius-Maximilians-Universität Würzburg, 2012.
138. A. M. Weiner, J. P. Heritage, E. M. Kirschner. High-resolution femtosecond pulse shaping. J. Opt. Soc. Am. B **5**, p. 1563-1572 (1988).
139. A. M. Weiner, J. P. Heritage, J. A. Salehi. Encoding and decoding of femtosecond pulse Opt. Lett. **13**, p.300-302, (1988).
140. H. P. Sardesai, C.-C. Chang, A. M. Weiner. A Femtosecond Code-Division Multiple-Access Communication System Test Bed. J. Lightwave Technol. **16**, 1953 (1998).
141. A. M. Weiner and D. E. Leaird. Generation of terahertz-rate trains of femtosecond pulses by phase-only filtering. Opt. Lett. **15**, p. 51-53, (1990).
142. A. M. Weiner, S. Oudin, D. E. Leaird, and D. H. Reitze. Shaping of femtosecond pulses using phase-only filters designed by simulated annealing. J. Opt. Soc. Am. A **10**, p.1112-1120, (1993).
143. S. Shen, A. M. Weiner. Complete Dispersion Compensation for 400-fs Pulse Transmission over 10-km Fiber Link Using Dispersion Compensating Fiber and Spectral Phase Equalizer IEEE Photonics Technol. Lett., **11**, 827-829, (1999).
144. A. Efimov, C. Schaffer, D. H. Reitze. Programmable shaping of ultrabroad-bandwidth pulses from a Ti: sapphire laser. J. Opt. Soc. Am. B **12**, 1968-1980, (1995).

145. M. C. Wefers, K. A. Nelson. Programmable phase and amplitude femtosecond pulse shaping. Opt. Lett. **18**, p. 2032-2034, (1993).
146. M. M. Wefers and K. A. Nelson. Generation of high-fidelity programmable ultrafast optical waveforms. Opt. Lett., **20**, p. 1047-1049, (1995).
147. H. Kawashima, M. M. Wefers, K. A. Nelson. Femtosecond pulse shaping, multiple-pulse spectroscopy, and optical control. Annu. Rev. Phys. Chem. **46**, p. 627-656, (1995).
148. C. Dorrer, F. Salin, F. Verluise, and J. P. Huignard. Programmable phase control of femtosecond pulses by use of a nonpixelated spatial light modulator. Opt. Lett. **23**, p. 709-711, (1998).
149. C. Dorrer, C. Le Blanc, F. Salin, presented at the CLEO Europe, Glasgow, Scotland, 1998.
150. Y. Igasaki, N. Yoshida, H. Toyoda, Y. Kobayashi, N. Mukohzaka, T. Hara. High speed parallel aligned liquid crystal spatial light modulator operated at 180 Hz. Opt. Rev. **4**, p. 167-169, (1997).
151. T. Feurer, J. C. Vaughan, R. M. Koehl, K. A. Nelson. Multidimensional control of femtosecond pulses by use of a programmable liquid-crystal matrix. Optics letters, **27(**8), p. 652-654, (2002).
152. A. Prakelt, M. Wollenhaupt, A. Assion, Ch. Horn, C. Sarpe-Tudoran, M. Winter, T. Baumerta. Compact, robust, and flexible setup for femtosecond pulse shaping. Rev. Sci. Instrum., **74**(11), p. 4950-4953, (2003).
153. A. Monmayrant, B. Chatel. New phase and amplitude high resolution pulse shaper. Rev. Sci. Instrum., **75**(8), p. 2668-2671, (2004).
154. J. Thornes, P. Poon, M. E. Anderson. Single-iteration compression of femtosecond laser pulses. J. Opt. Soc. Am., B **21**(7), p. 1387-1390, (2004).
155. J. Capmany, I. Gasulla, D. Pérez. Microwave photonics: The programmable processor. Nature Photonics, **10**, p.6–8, (2016).
156. O. Samek, V. Hommes, R. Hergenröder, S. V. Kukhlevsky. Femtosecond pulse shaping using a liquid–crystal display: Applications to depth profiling analysis. Rev. Sci. Instrum., **76**, 086104-1-3, (2005).

157. J. C. Vaughan, T. Feurer, K.W. Stone, K. A. Nelson. Analysis of replica pulses in femtosecond pulse shaping with pixelated devices. Opt. Express, **14**(3), p.1314-1328, (2006).
158. C. G. Slater, D. E. Leaird, A. M. Weiner. Programmable polarization-independent spectral phase compensation and pulse shaping by use of a single-layer liquid-crystal modulator. Applied optics, **45**(20), p.4858-4863, (2006).
159. J. J. Field, T. A. Planchon, W. Amir, C. G. Durfee, J. A. Squier. Characterization of a high efficiency, ultrashort pulse shaper incorporating a reflective 4096-element spatial light modulator. Optics Communications, **278**, p.368–376, (2007).
160. E. Frumker, Y. Silberberg. Femtosecond pulse shaping using a two-dimensional liquid-crystal spatial light modulator. Optics letters, **32**(11), p.1384-1386, (2007).
161. E. Frumkera, Y. Silberberg. Two-dimensional phase-only spatial light modulators for dynamic phase and amplitude pulse shaping. Journal of Modern Optics, **56**(18-19), p.2049–2054, (2009).
162. J. W. Wilson, P. Schlup, R. A. Bartels. Ultrafast phase and amplitude pulse shaping with a single, one-dimensional, high-resolution phase mask. Opt. Express, **15**(14), p.8979-8987, (2007).
163. A. Monmayrant, S. Weber, B. Chatel. A newcomer's guide to ultrashort pulse shaping and characterization. J. Phys. B: At. Mol. Opt. Phys., **43**, p.103001-103034, (2010).
164. W. Hänsel, H. Hoogland, M. Giunta, S. Schmid, T. Steinmetz, R. Doubek, P. Mayer, S. Dobner, C. Cleff, M. Fischer, R. Holzwarth. All polarization-maintaining fiber laser architecture for robust femtosecond pulse generation. Appl. Phys. B, **123**:41, p.1-6, (2017).
165. H. Ma, Pu Zhou, X. Wang, Y. Ma, F. Xi, X. Xu, Z. Liu. Near-diffraction-limited annular flattop beam shaping with dual phase only liquid crystal spatial light modulators. Opt. Express, **18**(8), p.8251-8260, (2010).
166. B. Döpkea, J. C. Balzera, M. R. Hofmann. In-situ calibration of spatial light modulators in femtosecond pulse shapers. Proc. of SPIE, **9004**, 90040D-1-6, (2014).
167. B. Döpke, J.C. Balzer, M.R. Hofmann. Phase and amplitude calibration of dual mask spatial light modulator for high resolution femtosecond pulse shaping. Electronics letters, **51**(8), p.642–644, (2015).

168. B. Sun, P. S. Salter, M. J. Booth. Pulse front adaptive optics: a new method for control of ultrashort laser pulses. Opt. Express, **23**(15), p.19348-19357, (2015).
169. Mouradian L, Zohrabyan A, Villeneuve A, Yavrian A, Rousseau G, Piche M, Froehly C, Louradour F and Barthélémy A 2000 CLEO / Europe'2000, Conference Digest, CTuH6 39
170. A.S. Akhmanov, V. A.Vysloukh, A.S. Chirkin.Optics of Femtosecond Laser Pulses. New York: AIP, 1992.
171. G. P. Agrawal. Nonlinear Fiber Optics. Academic, third ed., 2001.
172. A. Kutuzyan, T. Mansuryan, A. Kirakosian, L. Mouradian. Self-forming of temporal dark soliton in spectral compressor. Proc. SPIE **5135**, p.156-160, (2003).
173. L. Mollenauer, R. Stolen, J. Gordon. Experimental Observation of Picosecond Pulse Narrowing and Soliton in Optical Fibers. Phys. Rev. Lett. **45,** 1045, (1980).
174. L. Mollenauer, R. Stolen, J. Gordon. Opt. Lett. **11**, 289, (1986).
175. M. Tognetti, H. Crespo, J. Opt. Soc. Am. B, **24**, p. 1410-1415, (2007).
176. A. Amorim, M. Tognetti, P. Oliveira, J. Silva, L. Bernardo, F. Kärtner, H. Crespo. Sub-two-cycle pulses by soliton self-compression in highly nonlinear photonic crystal fibers. Opt. Lett., **34**, p. 3851-3853, (2009).
177. A. Salem, R. Cherif , M. Zghal. Opt. Expr. **19**, 19995, 2011.
178. В.А. Выслоух. Эксперименты с оптическими солитонами.УФН, **136**(3), с.519-531, (1982).
179. И. Шеен. Электрострикция, оптический эффект Керра и самофокусировка лазерных-лучей. В кн.: Действия лазерного излучения. М.: Мир, с.210, (1968).
180. R.G. Smith. Optical Power Handing Capacity of Low-loss Optical Fibers as Determined by Stimulated Raman and Brillouin Scattering. Appl. Opt., **11**(6), p. 2489-2494, (1972).
181. Е.М. Дианов, А.Я. Карасик, П.В. Мамышев, Г.И. Онищуков, А.М. Прохоров, М.Ф. Стельмах, А.А. Фомичев. Пикосекундная структура импульса накачки при ВКР в одно-модовом волоконном световоде. Письма в ЖЭТФ, **39**(12), с.564-566, (1984).
182. В.Е. Захаров, СВ. Манаков, СП. Новиков, Л.П. Питаевский. Теория солитонов: метод обратной задачи. М.: Наука, с. 319, (1980).

183. T.R. Taha, H.J. Albowitz. Analytical and Numerical Aspects of Certain Nonlinear Evolution Equations. II Numerical, Nonlinear Schrödinger Equation. J. Comput. Phys, **55**, p.203- 230, (1984).
184. R.H.Hardin, F.D. Tappert. Applications of the split-step Fourier method to the ...coefficient wave equations. SIAM Rev.Cronicle, **15**, p.423, (1973).
185. R.A.Fisher, W.K.Bischel. The role of linear dispersion in plane-wave self-phase modulation. Appl.Phys.Lett., **23**, p.661, (1973).
186. Г.И. Марчук. Методы вычислительной математики. М.: Наука, с. 536, (1960).
187. L. F. Mollenauer, R. H. Stolen, J. P. Gordon, W. J. Tomlinson. Extreme picosecond pulse narrowing by means of soliton effect in single-mode optical fibers. Optics Lett., **8**, p.289-291, (1983).
188. E. Gershgoren, R.A. Bartels, J.T. Fourkas, R. Tobey, M.M. Murnane, H.C. Kapteyn. Simplified setup for high-resolution spectroscopy that uses ultrashort pulses. Opt. Letters, **28** (5), p. 361-363, (2003).
189. A. S. Zeytunyan, G. L. Yesayan, L. Kh. Mouradian, P. Kockaert, P. Emplit, F. Louradour, A. Barthélémy. Nonlinear-dispersive similariton of passive fiber. J. Europ. Opt. Soc. Rap. Public. 09009, **4** (2009).
190. L. Muradyan, N. Markaryan, T. Papazyan, A. Ohanyan. Digest of International Conference on Lasers and Electro-Optics. USA, CTUH32, p. 120, (1990).
191. L. Muradyan, N. Markaryan, T. Papazyan, A. Ohanyan. Spectral Compression of Ultrashort Laser Pulses. Sov. J. Quantum Electron, **21**, p. 783–784, (1991).
192. M. Oberthaler, R. Hopfel. Special Narrowing of Ultrashort Laser Pulses By Self–Phase Modulation in Optical Fibers. Appl. Phys. Lett., **63**, p. 1017–1019, (1993).
193. L. Mouradian, A. Zohrabyan, A.Villeneuve, A. Yavrian, G. Rousseau, M. Piche, C. Froehly, F. Louradour, A. Barthélémy. CLEO/Europe'00. Conference Digest. France, Nice, CTuH6, p.79, (2000).
194. N. Markaryan, L. Muradyan. Determination of the Temporal Profiles of Ultrashort Pulses by a Fibre-Optic Compression Technique. Sov. J. Quantum Electron, **25**, p. 668–670, (1995).

195. L. Mouradian, F. Louradour, V. Messager, A. Barthélémy, C. Froehly. Spectro-Temporal Imaging of Femtosecond Events. IEEE J. Quantum Electron, **36**, p. 795–801, (2000).
196. T. Mansuryan, A. Zeytunyan, M. Kalashyan, G. Yesayan, L. Mouradian, F. Louradour, A. Barthélémy. Parabolic Temporal Lensing and Spectrotemporal Imaging: A Femtosecond Optical Oscilloscope. J. Opt. Soc. Am., **25**, p. 101, (2008).
197. A. Kutuzyan, T. Mansuryan, A. Kirakosian, L. Mouradian. Self-Forming of Temporal Dark Soliton in Spectral Compressor. Proc. SPIE, **5135**, p. 156, (2003).
198. F. Louradour, E. Lopez-Lago, V. Couderc, V. Messager, A. Barthélémy. Dispersive-Scan Measurement of the Fast Component of the Third-Order Nonlinearity of Bulk Materials and Waveguides. /Opt. Lett., **24**, p. 1361, (1999).
199. S. Boscolo, S. Turitsyn, Ch. Finot. Amplifier Similariton Fiber Laser with Nonlinear Spectral Compression. Opt. Lett., **37**(21), p. 4531, (2012).
200. S. Clark, F. Ilday, F. Wise. Fiber Delivery of Femtosecond Pulses from a Ti:sapphire Laser. Opt. Lett., **26**, p. 1320, (2001).
201. E. Andresen, J. Dudley, D. Oron, Ch. Finot, H. Rigneault. Transform-Limited Spectral Compression by Self-Phase Modulation of Amplitude-Shaped Pulses with Negative Chirp. Opt. Lett., **36**, p. 707, (2011).
202. M. Oberthaler, R. Hopfel. Special Narrowing of Ultrashort Laser Pulses By Self–Phase Modulation in Optical Fibers. Appl. Phys. Lett., **63**, p. 1017–1019, (1993).
203. M.R.Hakobyan, R.S.Hakobyan. Liquid-Crystal Devices and Waveplates for light controlling. Armenian Journal of Physics, **7**(2), p. 59-68, (2014).
204. T.Hattori, K.Kabuki, Y.Kawashima, M.Daikoku, H.Nakatsuka. Femtosecond pulse shaping with twisted-nematic liquid-crystal spatial-light modulators. Jpn. J. Appl. Phys., **38**, p. 5898-5904, (1999).
205. R.S.Akopyan, R.B.Alaverdyan, V.V.Saakyan, Yu.S.Chilingaryan. Light induced transformation in homeotropically oriented cholesteric liquid crystals. Kristallografiya, **30**(4), p.746-749, (1985).
206. R.S.Akopyan, R.B.Alaverdyan, Yu.S.Chilingaryan. Optical anisotropy of a cholesteric liquid crystal with homeotropic orientation on the walls. Sov. Journ. Contemp. Phys. (Arm. Ac. Sc.), **21**(4), p. 77-80, (1986).

207. O. E. Martinez. Grating and prism compressors in the case of finite beam size. J. Opt. Soc. Am. B **3**, p. 929-934, (1986).

208. O. E. Martinez. 3000 times grating compressor with positive group velocity dispersion: Application to fiber compensation in 1.3-1.6 μm region. IEEE J. Quantum Electron. QE-**23**, p.59-64, (1987).

209. B.Ya.Zeldovich, N.V.Tabiryan. Equilibrium structure of a cholesteric with homeotropic orientation on the walls. Sov. Phys. JETP, **56**(3), p.563, (1982).

210. P.Yeh, C.Gu. Optics of Liquid Crystal Displays. John Wiley & Sons, Inc., Hoboken, New Jersey, USA, 2010.

211. W. H. Press, S. A. Teukolsky, W. T. Vettering and B. P. Flannery: Numerical Recipes (Cambridge University Press, Cambridge, 1992), Chap. 10.